AN EFFICIENT NONLINEAR STRUCTURAL DYNAMICS SOLVER FOR USE IN COMPUTATIONAL AEROELASTIC ANALYSIS

A Thesis

by

BRIAN ANDREW FRENO

Submitted to the Office of Graduate Studies of
Texas A&M University
in partial fulfillment of the requirements for the degree of

MASTER OF SCIENCE

May 2010

Major Subject: Aerospace Engineering

AN EFFICIENT NONLINEAR STRUCTURAL DYNAMICS SOLVER FOR USE IN COMPUTATIONAL AEROELASTIC ANALYSIS

A Thesis

by

BRIAN ANDREW FRENO

Submitted to the Office of Graduate Studies of
Texas A&M University
in partial fulfillment of the requirements for the degree of

MASTER OF SCIENCE

Approved by:

Chair of Committee,	Paul G. A. Cizmas
Committee Members,	Raytcho D. Lazarov
	Thomas W. Strganac
	Theofanis Strouboulis
Head of Department,	Dimitris C. Lagoudas

May 2010

Major Subject: Aerospace Engineering

ABSTRACT

An Efficient Nonlinear Structural Dynamics Solver
for Use in Computational Aeroelastic Analysis. (May 2010)
Brian Andrew Freno, B.S., Texas A&M University
Chair of Advisory Committee: Dr. Paul G. A. Cizmas

Aerospace structures with large aspect ratio, such as airplane wings, rotorcraft blades, wind turbine blades, and jet engine fan and compressor blades, are particularly susceptible to aeroelastic phenomena. Finite element analysis provides an effective and generalized method to model these structures; however, it is computationally expensive. Fortunately, these structures have a length appreciably larger than the largest cross-sectional diameter. This characteristic is exploitable as these potential aeroelastically unstable structures can be modeled as cantilevered beams, drastically reducing computational time.

In this thesis, the nonlinear equations of motion are derived for an inextensional, non-uniform cantilevered beam with a straight elastic axis. Along the elastic axis, the cross-sectional center of mass can be offset in both dimensions, and the principal bending and centroidal axes can each be rotated uniquely. The Galerkin method is used, permitting arbitrary and abrupt variations along the length that require no knowledge of the spatial derivatives of the beam properties. Additionally, these equations consistently retain all third-order nonlinearities that account for flexural-flexural-torsional coupling and extend the validity of the equations for large deformations.

Furthermore, linearly independent shape functions are substituted into these equations, providing an efficient method to determine the natural frequencies and

mode shapes of the beam and to solve for time-varying deformation.

This method is validated using finite element analysis and is extended to swept wings. The importance of retaining cubic terms, in addition to quadratic terms, for nonlinear analysis is demonstrated for several examples. Ultimately, these equations are coupled with a fluid dynamics solver to provide a structurally efficient aeroelastic program.

ACKNOWLEDGMENTS

I would like to thank my advisor, Dr. Paul Cizmas as well as the members of my committee. I was fortunate to have Dr. Raytcho Lazarov as my instructor for a calculus course my freshman year. Dr. Thomas Strganac was the teacher for my first aerospace engineering course and ignited my interest in aeroelasticity in his aeroelasticity course. Dr. Theofanis Strouboulis's numerical simulation and finite element courses confirmed my interest in computational mechanics, and he subsequently provided me with opportunities to refine my teaching skills as a grader and as a teaching assistant. I am especially grateful to Dr. John Hurtado for substituting for Dr. Strouboulis during my thesis defense and for his valuable insight.

Additionally, I would like to extend my gratitude to Dr. Glenn Gebert in the Aerodynamics Department at Lockheed Martin Missiles and Fire Control in Orlando, Florida for my two summer internships. The work was rewarding and motivated me to continue my studies beyond the undergraduate level.

Finally, I would like to thank my parents and the rest of my family for their unconditional and unending support. They are the reason for my success.

TABLE OF CONTENTS

Page

CHAPTER Page

CHAPTER Page

LIST OF TABLES

TABLE Page

LIST OF FIGURES

FIGURE Page

FIGURE Page

FIGURE Page

NOMENCLATURE

Roman Letters

A	Cross-sectional area
a	Non-dimensional distance of elastic axis aft of semichord for thin airfoils
$\mathcal{B}$	Cross-section fixed coordinate system
b	Semichord
C	Damping matrix
c	Chord
c	Cosine
$C(k)$	Theodorsen's function
e_η	Offset of centroidal axis above elastic axis along η-axis
e_ζ	Offset of centroidal axis aft of elastic axis along ζ-axis
D	Stiffness
E	Young's modulus
$\mathbf{F}$	Forcing vector
f	Natural frequency
G	Modulus of rigidity
$H_n^{(2)}$	Hankel function of the second kind
I	Identity matrix
i	$\sqrt{-1}$
I_n	Modified Bessel function of the first kind
j	Cross-sectional mass moment of inertia
J_n	Bessel function of the first kind
K	Stiffness matrix or torsion constant
k	Reduced frequency

K_n	Modified Bessel function of the second kind
L	Length
$\mathcal{L}$	Lagrangian
l	Cross-sectional Lagrangian or number of z-direction bending shape functions
L_A	Sectional lift
M	Mass matrix
m	Cross-sectional mass or number of y-direction bending shape functions
M_A	Sectional aerodynamic moment about the elastic axis
$\mathcal{N}$	Inertial reference coordinate system
$\mathbb{N}_1$	The set of natural numbers consisting of positive integers
n	Number of torsional shape functions
Q	Generalized non-conservative sectional force
q	Generalized direction
s	Position along elastic axis of beam
s	Sine
T	Cross-sectional kinetic energy
$\mathcal{T}$	Kinetic energy
t	Time
u	Displacement in x-direction
V	Cross-sectional potential energy
$\mathbf{V}$	Inertial velocity of each cross section
$\mathcal{V}$	Potential energy
v	Displacement in y-direction

v_i y-direction displacement time coefficient for i^{th} bending shape function

V_∞ Magnitude of freestream velocity

$\mathcal{W}$ Virtual work resulting from forces

w Displacement in z-direction

$\mathcal{W}_b$ $\mathcal{W}_{nc}$ at boundaries ($s = 0$ and $s = L$)

$\mathcal{W}_c$ Virtual work resulting from conservative forces

W_i i^{th} bending shape function

w_i z-direction displacement time coefficient for i^{th} bending shape function

$\mathcal{W}_{nc}$ Virtual work resulting from non-conservative forces

x Inertial axis in lengthwise direction

y Inertial axis along plane of fixed end

Y_n Bessel function of the second kind

z Inertial axis along plane of fixed end

Greek Letters

α Angle of attack

δ Variational operator

ζ Cross-section fixed axis along plane of cross section

η Cross-section fixed axis along plane of cross section

θ Second Euler angle rotation about y_1-axis

Λ Sweep angle

λ Lagrange multiplier

ξ Cross-section fixed axis tangent to elastic axis

ρ Mass density

$\boldsymbol{\rho}$	Curvature vector
τ	Distance traveled in semichords
ϕ	Third Euler angle rotation about ξ-axis
ϕ	Torsional displacement
$\Phi(\tau)$	Wagner's function
Φ_i	i^{th} torsional shape function
ϕ_i	Torsional displacement time coefficient for i^{th} torsional shape function
ψ	First Euler angle rotation about z-axis
ω	Circular frequency
$\boldsymbol{\omega}$	Angular velocity of the cross-sectional frame, relative to the inertial frame

Primes denote differentiation with respect to s, while over-dots indicate differentiation with respect to time.

CHAPTER I

INTRODUCTION

A. Motivation

Aeroelasticity is generally considered to be the field of study that accounts for the interaction of aerodynamic, elastic, and inertial forces on an aerospace structure [1, pp. 1-2],[2, pp. 1-2]. Static and dynamic aeroelastic instabilities are typically the phenomena of concern in aeroelastic analysis. These instabilities are introduced when the aerodynamic forces exceed the elastic restoring forces. Divergence is a static aeroelastic instability in which inertial forces are negligible, whereas flutter is a dynamic aeroelastic instability occurring when inertial forces are significant [3, p. 1].

Aerospace structures with large aspect ratio, such as airplane wings, rotorcraft blades, wind turbine blades, and jet engine fan and compressor blades, are particularly susceptible to aeroelastic phenomena. Finite element analysis provides an effective and generalized method to model these structures; however, it is computationally expensive. Fortunately, these structures have a length appreciably larger than the largest cross-sectional diameter. This characteristic is exploitable as these potential aeroelastically unstable structures can be modeled as cantilevered beams, drastically reducing computational time.

B. Literature Review

This observation has led to the use of beam models to approximate the aeroelastic response of wings for several decades. Earlier implementations, however, largely fo-

---

This thesis follows the style of the *Journal of Computational Physics*.

cused on the planar bending of uniform beams and only provided for linear coupling between bending and torsional motion [1, pp. 67-129], [3, pp. 193-198].

In 1978, Crespo da Silva and Glynn [4] derived the nonlinear flexural-flexural-torsional equations of motion for an inextensional uniform beam, consistently retaining third-order nonlinearities. A decade later, Crespo da Silva removed the inextensionality and uniformity constraints and demonstrated the validity of the inextensional assumption [5]. Additionally, around this time, Hodges formulated multiple nonlinear inextensional beam equations, accounting for second-order nonlinearities to model helicopter blades [6, 7].

The use of uncoupled mode shapes satisfying the boundary conditions and linear equations of motion for a uniform cantilevered beam is a classical method used in vibrational analysis that expedites calculation of the deformed shape by reducing the partial differential equations in time and space into a set of ordinary differential equations in time [1, pp. 114-164], [2, pp. 30-70]. In 2005, Strganac et al. [8] used the uncoupled mode shapes to evaluate the deformation of a wing approximated by a uniform beam. The beam model retained a majority of the nonlinear terms accounted for by Crespo da Silva as well as the linear contribution of mass-offset from the elastic axis along the chord-wise principal axis [9]. Integration was done explicitly, and several of the nonlinear structural terms were grouped into a forcing vector that lagged by a time step.

C. Objective and Scope

In this thesis, the nonlinear equations of motion are derived for an inextensional, non-uniform cantilevered beam with a straight elastic axis. Along the elastic axis, the cross-sectional center of mass can be offset in both dimensions, and the principal bend-

ing and centroidal axes can each be rotated uniquely. The Galerkin method is used, permitting arbitrary and abrupt variations along the length that require no knowledge of the spatial derivatives of the beam properties. Additionally, these equations consistently retain all third-order nonlinearities that account for flexural-flexural-torsional coupling and extend the validity of the equations for large deformations.

Furthermore, linearly independent shape functions are substituted into these equations, providing an efficient method to determine the natural frequencies and mode shapes of the beam and to solve for time-varying deformation.

This method is validated using finite element analysis and is extended to swept wings. The importance of retaining cubic terms, in addition to quadratic terms, for nonlinear analysis is demonstrated for several examples. Ultimately, these equations are coupled with a fluid dynamics solver to provide a structurally efficient aeroelastic program.

D. Novel Aspects of this Thesis

Though some facets of the method and model presented herein have been used previously, there are several features worth noting that distinguish this work.

Compared to Crespo da Silva and Glynn [4], this method offers improvement by accounting for a non-uniform beam with the center of mass of each cross section offset from the elastic axis. Relative to Crespo da Silva's later work [5], this approach additionally permits rotation of the centroidal axes along the length of the undeformed beam and uses the Galerkin method to numerically address abrupt lengthwise variations.

This work improves upon that of Hodges [6, 7] by extending the order of the nonlinear terms retained to the third order. Additionally, comparisons are made

between the results of linear, quadratic, and cubic beam models.

Compared to Strganac et al. [8] and Kim [9], the method presented herein yields several additional features. The improved features are: (1) beam non-uniformity, (2) the ability to account for the nonlinear contribution of mass-offset, (3) mass-offset in both dimensions, (4) principal bending and stiffness axes that vary mutually and along the length of the beam, (5) abrupt lengthwise property changes, (6) the consistent retention of all third-order nonlinearities, and (7) a reduction of the explicitness of the time integration of nonlinear terms.

CHAPTER II

DERIVATION OF THE NONLINEAR EQUATIONS OF MOTION

A. Preliminaries

In this chapter, the third-order nonlinear flexural-flexural-torsional equations of motion are derived for a beam with a straight elastic axis, along which the cross sections can vary arbitrarily and abruptly. The cross sections of the undeformed beam can have a center of mass offset from the elastic axis and the principal centroidal and bending axes variably and uniquely rotated about the elastic axis. Finally, due to the consistent retention of nonlinear terms, the equations are valid for large deformations, provided the elasticity limit is not exceeded.

B. Definition of Parameters

The beam is assumed to have an elastic axis that is straight when undeformed. The inertial reference coordinate system, $\mathcal{N}(x, y, z)$, is located at the fixed end of the beam, where the x-axis is coincident with the undeformed elastic axis and positive in the direction of the free end. The cross-sectional coordinate system, $\mathcal{B}(\xi, \eta, \zeta)$, is fixed to each cross section during deformation, and the origin is located where the elastic axis intersects the cross section. When the beam is undeformed, the cross-sectional coordinate system is parallel to the reference coordinate system, and the ξ-axis is collinear with the x-axis. Figure 1 illustrates the two coordinate systems.

To describe the orientation of the cross-sectional coordinate system relative to the reference coordinate system, three Euler angle rotations are invoked as shown in Figure 2. The inertial frame is rotated an angle ψ about the z-axis, θ about the first

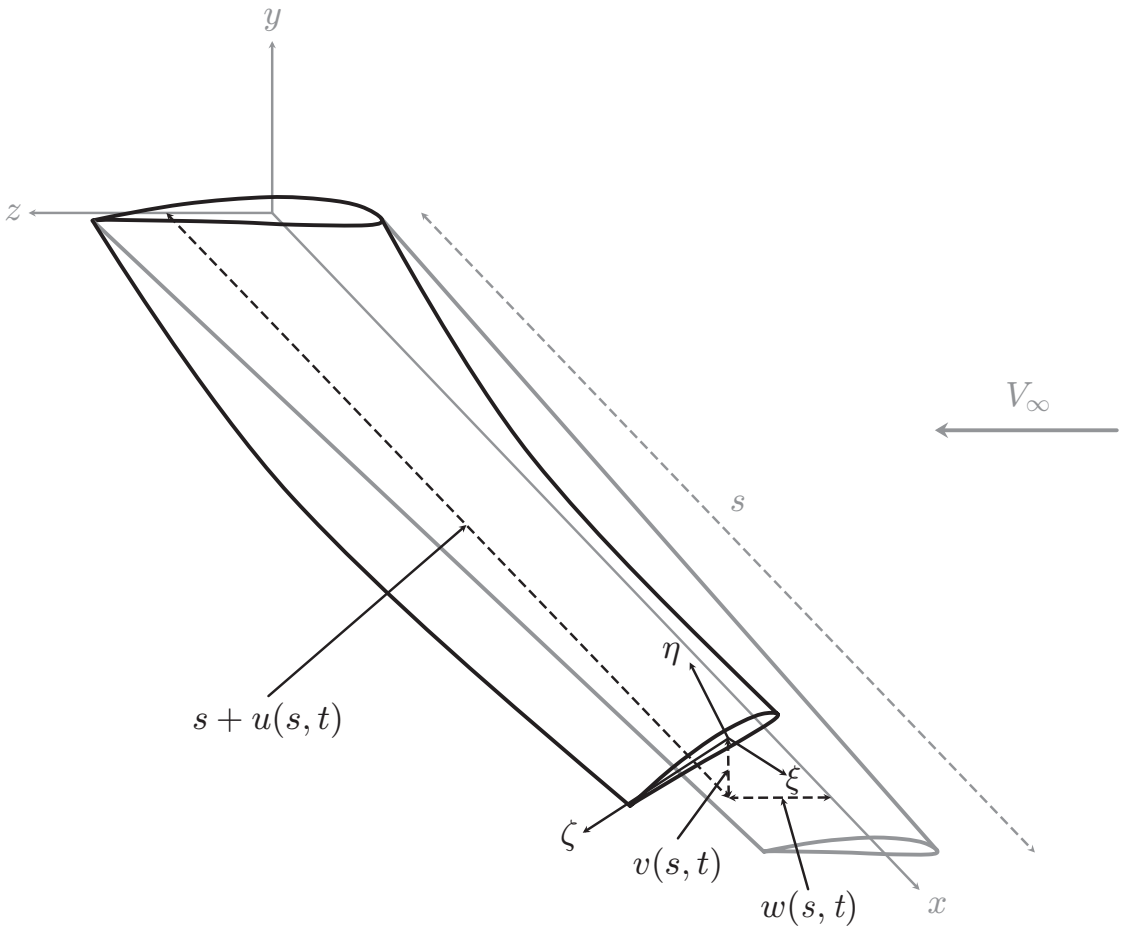

Figure 1. Diagram of deformed beam.

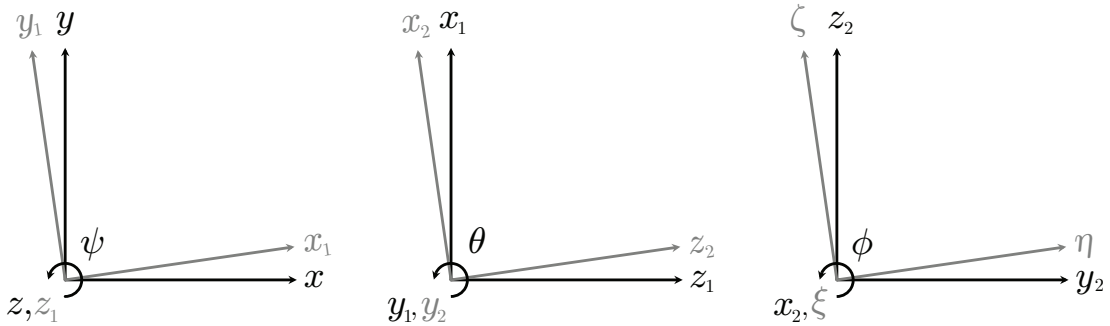

Figure 2. The three successive Euler angle rotations.

intermediate y-axis, and ϕ about the second intermediate x-axis, which is in turn the ξ-axis. The Euler angle rotations are expressed by the following matrices:

$$
\begin{aligned}
E_3(\psi) &= \begin{bmatrix} \cos\psi & \sin\psi & 0 \\ -\sin\psi & \cos\psi & 0 \\ 0 & 0 & 1 \end{bmatrix}, \\
E_2(\theta) &= \begin{bmatrix} \cos\theta & 0 & -\sin\theta \\ 0 & 1 & 0 \\ \sin\theta & 0 & \cos\theta \end{bmatrix}, \\
E_1(\phi) &= \begin{bmatrix} 1 & 0 & 0 \\ 0 & \cos\phi & \sin\phi \\ 0 & -\sin\phi & \cos\phi \end{bmatrix},
\end{aligned}
$$

leading to

$$
\begin{Bmatrix} \xi \\ \eta \\ \zeta \end{Bmatrix}_{\mathcal{B}} = E_1(\phi)E_2(\theta)E_3(\psi) \begin{Bmatrix} x \\ y \\ z \end{Bmatrix}_{\mathcal{N}}
$$

or

$$
\begin{Bmatrix} \xi \\ \eta \\ \zeta \end{Bmatrix}_{\mathcal{B}} = \begin{bmatrix} \mathrm{c}\psi\mathrm{c}\theta & \mathrm{c}\theta\mathrm{s}\psi & -\mathrm{s}\theta \\ -\mathrm{c}\phi\mathrm{s}\psi + \mathrm{c}\psi\mathrm{s}\phi\mathrm{s}\theta & \mathrm{c}\phi\mathrm{c}\psi + \mathrm{s}\phi\mathrm{s}\psi\mathrm{s}\theta & \mathrm{c}\theta s\phi \\ \mathrm{s}\phi\mathrm{s}\psi + \mathrm{c}\phi\mathrm{c}\psi\mathrm{s}\theta & -\mathrm{c}\psi\mathrm{s}\phi + \mathrm{c}\phi\mathrm{s}\psi\mathrm{s}\theta & \mathrm{c}\phi\mathrm{c}\theta \end{bmatrix} \begin{Bmatrix} x \\ y \\ z \end{Bmatrix}_{\mathcal{N}}. \tag{2.1}
$$

Each of these angles is a function of time, t, and position, s, along the deformed elastic axis. These coordinate systems and transformations are similar to those used by Crespo da Silva and Glynn [4], the main difference arising from $\mathcal{B}(\xi, \eta, \zeta)$ being located at the intersection of the cross section with the elastic axis instead of with the centroidal axis.

To characterize the beam, the following parameters are used [5]:

$$
\begin{aligned}
m(s) &= \iint_A \rho \, d\eta \, d\zeta, && \text{(2.2a)}\\
j_\xi(s) &= \iint_A \rho \left(\eta^2 + \zeta^2\right) d\eta \, d\zeta, && \text{(2.2b)}\\
j_\eta(s) &= \iint_A \rho \, \zeta^2 d\eta \, d\zeta, && \text{(2.2c)}\\
j_\zeta(s) &= \iint_A \rho \, \eta^2 d\eta \, d\zeta, && \text{(2.2d)}\\
j_{\eta\zeta}(s) &= -\iint_A \rho \, \eta \, \zeta \, d\eta \, d\zeta, && \text{(2.2e)}\\
D_\xi(s) &= GK, && \text{(2.2f)}\\
D_\eta(s) &= \iint_A E \, \zeta^2 \, d\eta \, d\zeta, && \text{(2.2g)}\\
D_\zeta(s) &= \iint_A E \, \eta^2 \, d\eta \, d\zeta, && \text{(2.2h)}\\
D_{\eta\zeta}(s) &= -\iint_A E \, \eta \, \zeta \, d\eta \, d\zeta. && \text{(2.2i)}
\end{aligned}
$$

Additionally, e_η and e_ζ respectively describe the distance between the center of mass and the elastic axis along the η and ζ axes. The sign of e_η and e_ζ is positive when the center of mass has η and ζ coordinates exceeding those of the elastic axis.

The torsion constant K in (2.2f) satisfies

$$\phi = \frac{\tau L}{GK},$$

where τ is the twisting moment and ϕ is expressed in radians. For circular cross sections, K is exactly the polar moment of inertia, while for other cross sections, K is obtained through approximation and is less than the polar moment of inertia as a result of warping [10, pp. 382-383].

In this thesis, nonlinearities are described by an order that indicates the number of factors of the displacements v, w, and ϕ that comprise a term. These factors may include spatial and/or time derivatives of the displacements. As an example, $j_\zeta v'^2 \ddot{v}'$

is a cubic term.

C. The Lagrangian

The equations of motion in this chapter are derived using Lagrangian mechanics. Therefore, an expression for the Lagrangian, which is the difference between the kinetic and potential energy of the beam, is required to describe the beam dynamics.

1. Kinetic Energy

The kinetic energy of each cross section of the beam is given by

$$T = \frac{1}{2} \iint_A \rho \, \mathbf{V} \cdot \mathbf{V} \, d\eta \, d\zeta. \tag{2.3}$$

One of the fundamental assumptions of the beam model is that planar cross sections perpendicular to the elastic axis remain planar and perpendicular to the elastic axis without deforming. The inertial velocity of each point on a cross section of the beam can be decomposed into the sum of the inertial velocity of the cross-sectional coordinate system, relative to the inertial coordinate system, and the inertial velocity of a point on the cross section, relative to the origin of the cross-sectional coordinate system. The velocity of each point on the beam is then

$$\mathbf{V} = \left\{ \begin{array}{c} \dot{u} \\ \dot{v} \\ \dot{w} \end{array} \right\}_{\mathcal{N}} + \boldsymbol{\omega} \times \left\{ \begin{array}{c} 0 \\ \eta \\ \zeta \end{array} \right\}_{\mathcal{B}}. \tag{2.4}$$

The angular velocity of the cross-sectional frame relative to the inertial frame is

$$\boldsymbol{\omega} = \dot{\phi} \, \hat{\xi} + \dot{\theta} \, \hat{y}_1 + \dot{\psi} \, \hat{z},$$

which, when expressed in the cross-sectional frame, leads to

$$\boldsymbol{\omega} = \left\{ \begin{array}{c} \dot{\phi} - \dot{\psi}\sin\theta \\ \dot{\psi}\cos\theta\sin\phi + \dot{\theta}\cos\phi \\ \dot{\psi}\cos\theta\cos\phi - \dot{\theta}\sin\phi) \end{array} \right\}_{\mathcal{B}} = \left\{ \begin{array}{c} \omega_\xi \\ \omega_\eta \\ \omega_\zeta \end{array} \right\}_{\mathcal{B}}.$$

Resolving (2.4) into the inertial frame provides

$$\mathbf{V} = \left\{ \begin{array}{c} (\zeta\omega_\eta - \eta\omega_\zeta)\,\mathrm{c}\psi\mathrm{c}\theta + \eta\omega_\xi\,(\mathrm{s}\phi\mathrm{s}\psi + \mathrm{c}\phi\mathrm{c}\psi\mathrm{s}\theta) + \zeta\omega_\xi\,(\mathrm{c}\phi\mathrm{s}\psi - \mathrm{c}\psi\mathrm{s}\phi\mathrm{s}\theta) + \dot{u} \\ (\zeta\omega_\eta - \eta\omega_\zeta)\,\mathrm{s}\psi\mathrm{c}\theta - \eta\omega_\xi\,(\mathrm{s}\phi\mathrm{c}\psi - \mathrm{c}\phi\mathrm{s}\psi\mathrm{s}\theta) - \zeta\omega_\xi\,(\mathrm{c}\phi\mathrm{c}\psi + \mathrm{s}\psi\mathrm{s}\phi\mathrm{s}\theta) + \dot{v} \\ -(\zeta\omega_\eta - \eta\omega_\zeta)\,\mathrm{s}\theta + \eta\omega_\xi\mathrm{c}\phi\mathrm{c}\theta - \zeta\omega_\xi\mathrm{s}\phi\mathrm{c}\theta + \dot{w} \end{array} \right\}_{\mathcal{N}}. \tag{2.5}$$

Substituting (2.5) into (2.3) yields

$$\begin{aligned} T = {} & \frac{1}{2}m\left(\dot{u}^2 + \dot{v}^2 + \dot{w}^2\right) + \frac{1}{2}\left(j_\xi\omega_\xi^2 + j_\eta\omega_\eta^2 + j_\zeta\omega_\zeta^2\right) + j_{\eta\zeta}\omega_\eta\omega_\zeta \\ & + me_\zeta\omega_\xi\left[(\mathrm{c}\phi\mathrm{s}\psi - \mathrm{s}\phi\mathrm{c}\psi\mathrm{s}\theta)\,\dot{u} - (\mathrm{s}\phi\mathrm{s}\psi\mathrm{s}\theta + \mathrm{c}\phi\mathrm{c}\psi)\,\dot{v} - \mathrm{s}\phi\mathrm{c}\theta\dot{w}\right] \\ & + me_\zeta\omega_\eta\left[\mathrm{c}\psi\mathrm{c}\theta\dot{u} + \mathrm{c}\theta\mathrm{s}\psi\dot{v} - \mathrm{s}\theta\dot{w}\right] \\ & + me_\eta\omega_\xi\left[(\mathrm{s}\phi\mathrm{s}\psi + \mathrm{c}\phi\mathrm{c}\psi\mathrm{s}\theta)\,\dot{u} + (\mathrm{c}\phi\mathrm{s}\psi\mathrm{s}\theta - \mathrm{s}\phi\mathrm{c}\psi)\,\dot{v} + \mathrm{c}\phi\mathrm{c}\theta\dot{w}\right] \\ & - me_\eta\omega_\zeta\left[\mathrm{c}\psi\mathrm{c}\theta\dot{u} + \mathrm{c}\theta\mathrm{s}\psi\dot{v} - \mathrm{s}\theta\dot{w}\right]. \end{aligned}$$

2. Potential Energy

Assuming infinitesimal strain, the potential energy of each cross section is the strain energy [4]:

$$V = \frac{1}{2}\left(D_\xi\rho_\xi^2 + D_\eta\rho_\eta^2 + D_\zeta\rho_\zeta^2\right) + D_{\eta\zeta}\rho_\eta\rho_\zeta.$$

In his analogy, Love [11, pp. 51-53] shows that the curvature vector can be calculated in a manner similar to that of the angular velocity vector, replacing temporal

differentiation with spatial differentiation:

$$\boldsymbol{\rho}(s,t) = \left\{ \begin{array}{c} \phi' - \psi' \sin\theta \\ \psi' \cos\theta \sin\phi + \theta' \cos\phi) \\ \psi' \cos\theta \cos\phi - \theta' \sin\phi) \end{array} \right\}_{\mathcal{B}} = \left\{ \begin{array}{c} \rho_\xi \\ \rho_\eta \\ \rho_\zeta \end{array} \right\}_{\mathcal{B}}.$$

With the kinetic and potential energy for each cross section known, the cross-sectional Lagrangian is simply

$$l = T - V.$$

D. Inextensionality Constraint and Dependent Euler Angles

It is assumed that the length of the beam, specifically the length of the elastic axis, remains constant during deformation. For an infinitesimal segment of the elastic axis of length ds, the coordinates of the endpoints in the inertial frame are $(s + u(s), v(s), w(s))$ and $(s + ds + u(s + ds), v(s + ds), w(s + ds))$. Letting

$$du = u(s + ds) - u(s),$$
$$dv = v(s + ds) - v(s),$$
$$dw = w(s + ds) - w(s),$$

and requiring that the distance between the endpoints remains ds, the Pythagorean theorem yields

$$(ds)^2 = (dv)^2 + (dw)^2 + (ds + du)^2. \tag{2.6}$$

Taking the limit as $ds \to 0$, the inextensionality constraint (2.6) becomes

$$1 = v'^2 + w'^2 + (1 + u')^2. \tag{2.7}$$

Additionally, from (2.1), the relationship between the infinitesimal segment of length ds, which is tangent to the ξ-axis, and the distance between coordinates of the endpoints in the inertial frame is

$$\left\{ \begin{array}{c} ds \\ 0 \\ 0 \end{array} \right\}_{\mathcal{B}} = \left[\begin{array}{ccc} \mathrm{c}\psi\mathrm{c}\theta & \mathrm{c}\theta\mathrm{s}\psi & -\mathrm{s}\theta \\ -\mathrm{c}\phi\mathrm{s}\psi + \mathrm{c}\psi\mathrm{s}\phi\mathrm{s}\theta & \mathrm{c}\phi\mathrm{c}\psi + \mathrm{s}\phi\mathrm{s}\psi\mathrm{s}\theta & \mathrm{c}\theta s\phi \\ \mathrm{s}\phi\mathrm{s}\psi + \mathrm{c}\phi\mathrm{c}\psi\mathrm{s}\theta & -\mathrm{c}\psi\mathrm{s}\phi + \mathrm{c}\phi\mathrm{s}\psi\mathrm{s}\theta & \mathrm{c}\phi\mathrm{c}\theta \end{array} \right] \left\{ \begin{array}{c} ds + du \\ dv \\ dw \end{array} \right\}_{\mathcal{N}} . \tag{2.8}$$

Multiplying both sides of (2.8) by the inverse of the transformation matrix and taking the limit as $ds \to 0$ leads to

$$\cos\psi\cos\theta = 1 + u',$$
$$\cos\theta\sin\psi = v',$$
$$\sin\theta = -w',$$

permitting ψ and θ to be expressed in terms of the derivatives of the displacements:

$$\psi = \tan^{-1}\frac{v'}{1+u'},$$
$$\theta = \tan^{-1}\frac{-w'}{\sqrt{(1+u')^2 + v'^2}}.$$

As a result, for each cross section, there are three independent degrees of freedom: v, w, and ϕ.

E. Hamilton's Principle

With the Lagrangian known for each cross section and multiplying the inextensionality constraint by a Lagrange multiplier, the extended form of Hamilton's principle provides the governing equations of motion associated with the variations δu, δv, δw,

and $\delta\phi$ [4],[12, pp. 42-46]. These are derived in Appendix A and result in

$$G'_u = \left[A_\psi \frac{\partial \psi}{\partial u'} + A_\theta \frac{\partial \theta}{\partial u'} + \lambda\left(1 + u'\right)\right]' = \frac{\partial^2 l}{\partial t \partial \dot{u}} - Q_u, \tag{2.9}$$

$$G'_v = \left[A_\psi \frac{\partial \psi}{\partial v'} + A_\theta \frac{\partial \theta}{\partial v'} + \lambda v'\right]' = \frac{\partial^2 l}{\partial t \partial \dot{v}} - Q_v, \tag{2.10}$$

$$G'_w = \left[A_\theta \frac{\partial \theta}{\partial w'} + \lambda w'\right]' = \frac{\partial^2 l}{\partial t \partial \dot{w}} - Q_w, \tag{2.11}$$

$$A_\phi = Q_\phi, \tag{2.12}$$

where

$$A_\alpha = \frac{\partial^2 l}{\partial t \partial \dot{\alpha}} + \frac{\partial^2 l}{\partial s \partial \alpha'} - \frac{\partial l}{\partial \alpha} \qquad (\alpha = \psi, \theta, \phi).$$

Equations (2.9)-(2.12) are simplified using the following Taylor series expansions that are derived in Appendix B:

$$\begin{aligned}
\psi &\approx v'\left(1 + \frac{v'^2}{6} + \frac{w'^2}{2}\right), \\
\frac{\partial \psi}{\partial u'} &\approx -v', \\
\frac{\partial \psi}{\partial v'} &\approx 1 - \frac{v'^2}{2} + \frac{w'^2}{2},
\end{aligned}$$

$$\begin{aligned}
\theta &\approx -w'\left(1 + \frac{w'^2}{6}\right), \\
\frac{\partial \theta}{\partial u'} &\approx w', \\
\frac{\partial \theta}{\partial v'} &\approx v'w', \\
\frac{\partial \theta}{\partial w'} &\approx -1 + \frac{w'^2}{2},
\end{aligned}$$

$$u' \approx -\frac{1}{2}\left(v'^2 + w'^2\right),$$

$$u \approx -\frac{1}{2}\int_0^s \left(v'^2 + w'^2\right) d\hat{s}.$$

The terms in the extensional equation (2.9) are expanded in Taylor series to quadratic order, and the terms in the bending and torsional equations (2.10)-(2.12) are expanded to cubic order. The extensional equation only requires quadratic order as it is used to determine λ, which only appears when multiplied by a spatial derivative of a displacement in the bending equations.

F. Application of the Galerkin Method

Invoking the Galerkin method facilitates discretization of the beam, particularly with regard to abrupt property changes along the length. The method consists of multiplying the equations of motion by a set of test functions and integrating the product over the length of the beam. These test functions satisfy the homogeneous boundary conditions of the equation of interest [13, pp. 267-268]. Furthermore, by invoking integration by parts, the spatial derivatives of the parameters are eliminated by distributing the differentiation into the test function.

1. Bending Equations of Motion

For a cantilevered beam, the boundary conditions of the variables describing transverse displacement, v and w, are [2, pp. 46-51]

$$v(0,t) = w(0,t) = 0, \tag{2.13}$$

$$v'(0,t) = w'(0,t) = 0, \tag{2.14}$$

$$v''(L,t) = w''(L,t) = 0, \tag{2.15}$$

$$v'''(L,t) = w'''(L,t) = 0. \tag{2.16}$$

Equations (2.13) and (2.14) are a consequence of the geometric, fixed-end boundary condition, which provides for no deflection and no slope. Equations (2.15) and (2.16) are associated with the natural, free-end boundary condition and indicate that there is no bending moment and no shear.

Given these boundary conditions, a set of test functions, $W_i(s)$, where $i \in \mathbb{N}_1$, is selected that satisfy $W_i(0) = W_i'(0) = W_i''(L) = W_i'''(L) = 0$. Multiplying (2.10) and (2.11) by W_i, expanding the rightmost side, integrating over the length of the beam, and performing integration by parts yields

$$\begin{aligned}
&W_i(L)\left[A_\psi\frac{\partial\psi}{\partial v'}+A_\theta\frac{\partial\theta}{\partial v'}\right]_{s=L}-\int_0^L W_i'\left(A_\psi\frac{\partial\psi}{\partial v'}+A_\theta\frac{\partial\theta}{\partial v'}\right)ds+\int_0^L W_i\left(\lambda v'\right)'ds\\
&=\int_0^L W_i\Big[m\ddot{v}-me_\eta\left(\dot{\phi}^2+\phi\ddot{\phi}+\ddot{\phi}v'w'+2\dot{\phi}w'\dot{v}'+\dot{v}'^2+2\dot{\phi}v'\dot{w}'+2\phi\dot{v}'\dot{w}'\right)\\
&-me_\eta\left(v'\ddot{v}'+\phi w'\ddot{v}'+\phi v'\ddot{w}'\right)+me_\zeta\left(\phi\dot{\phi}^2-\ddot{\phi}+\frac{1}{2}\phi^2\ddot{\phi}+\frac{1}{2}\ddot{\phi}v'^2+2\dot{\phi}v'\dot{v}'\right)\\
&+me_\zeta\left(\phi\dot{v}'^2-2\dot{v}'\dot{w}'+\phi v'\ddot{v}'-w'\ddot{v}'-v'\ddot{w}'\right)-Q_v\Big]ds
\end{aligned}\tag{2.17}$$

and

$$\begin{aligned}
&W_i(L)\left[A_\theta\frac{\partial\theta}{\partial w'}\right]_{s=L}-\int_0^L W_i'\left(A_\theta\frac{\partial\theta}{\partial w'}\right)ds+\int_0^L W_i\left(\lambda w'\right)'ds\\
&=\int_0^L W_i\Big[m\ddot{w}-me_\eta\left(\phi\dot{\phi}^2-\ddot{\phi}+\frac{1}{2}\phi^2\ddot{\phi}+\frac{1}{2}\ddot{\phi}w'^2+2\dot{\phi}w'\dot{w}'\right)\\
&-me_\eta\left(\phi\dot{w}'^2+\phi w'\ddot{w}'\right)-me_\zeta\left(\dot{\phi}^2+\phi\ddot{\phi}+\dot{w}'^2+w'\ddot{w}'\right)-Q_w\Big]ds.
\end{aligned}\tag{2.18}$$

2. Torsional Equation of Motion

A cantilevered beam experiencing torsional motion cannot rotate at the fixed end and does not undergo a twisting moment at the free end. As a result, a set of functions, Φ_i, is chosen such that $\Phi_i(0) = \Phi_i'(L) = 0$.

Analogous to the bending equations, (2.12) is multiplied by Φ_i and integrated

over the length of the beam, providing

$$\int_0^L A_\phi \Phi_i ds = \int_0^L Q_\phi \Phi_i ds.$$

G. The Lagrange Multiplier

In (2.17) and (2.18), the terms containing the Lagrange multiplier, $\int_0^L W_i \left(\lambda v'\right)' ds$ and $\int_0^L W_i \left(\lambda w'\right)' ds$, must be determined. The Lagrange multiplier is calculated from the extensional equation (2.9), which can be written as

$$G_u' = \left[A_u + \lambda \left(1 + u'\right)\right]' = \frac{\partial^2 l}{\partial t \partial \dot{u}} - Q_u, \tag{2.19}$$

where

$$A_u(s,t) = A_\psi \frac{\partial \psi}{\partial u'} + A_\theta \frac{\partial \theta}{\partial u'}.$$

Equation (2.19) is integrated from the free end of the beam to s:

$$\int_L^s G_u' d\hat{s} = \int_L^s \left[A_u + \lambda \left(1 + u'\right)\right]' d\hat{s} = \int_L^s \left[\frac{\partial^2 l}{\partial t \partial \dot{u}} - Q_u\right] d\hat{s}.$$

Knowing that $G_u(L,t) = 0$ [5, 14],

$$\lambda(s,t) = \frac{1}{1 + u'(s,t)} \left[-A_u(s,t) + \int_L^s \left[\frac{\partial^2 l}{\partial t \partial \dot{u}} - Q_u\right] d\hat{s}\right].$$

The quadratic expansions of $A_u(s,t)$ and $\dfrac{\partial^2 l}{\partial t \partial \dot{u}}$ are

$$\begin{aligned} A_u(s,t) = & j_{\eta\zeta}\left(\ddot{v}'w' + v'\ddot{w}'\right) - j_\zeta v'\ddot{v}' - j_\eta w'\ddot{w}' \\ & + D'_\zeta v'v'' + D'_\eta w'w'' + D_\zeta v'v''' + D_\eta w'w''' \\ & - D'_{\eta\zeta}\left(w'v'' + v'w''\right) - D_{\eta\zeta}\left(w'v''' + v'w'''\right), \end{aligned} \tag{2.20}$$

$$\begin{aligned} \frac{\partial^2 l}{\partial t \partial \dot{u}} = & - m\int_0^s \left(\dot{v}'^2 + v'\ddot{v}' + \dot{w}'^2 + w'\ddot{w}'\right) d\hat{s} \\ & + me_\eta\left(-\ddot{\phi}w' - 2\dot{\phi}\dot{w}' - \ddot{v}' - \phi\ddot{w}'\right) \\ & + me_\zeta\left(\ddot{\phi}v' + 2\dot{\phi}\dot{v}' + \phi\ddot{v}' - \ddot{w}'\right). \end{aligned} \tag{2.21}$$

Equations (2.20) and (2.21) contain no zero-order terms. Additionally, Q_u must be small for the inextensionality constraint to be valid [5]. Therefore, $(1+u')^{-1}$ is expanded using a first-order Taylor series:

$$\frac{1}{1+u'} = \frac{1}{\sqrt{1-v'^2-w'^2}} \approx 1.$$

This leads to the quadratic expression for λ:

$$\begin{aligned} \lambda(s,t) = -A_u(s,t) + \int_L^s \Bigg[& - m\int_0^{\hat{s}} \left(\dot{v}'^2 + v'\ddot{v}' + \dot{w}'^2 + w'\ddot{w}'\right) d\tilde{s} \\ & + me_\eta\left(-\ddot{\phi}w' - 2\dot{\phi}\dot{w}' - \ddot{v}' - \phi\ddot{w}'\right) \\ & + me_\zeta\left(\ddot{\phi}v' + 2\dot{\phi}\dot{v}' + \phi\ddot{v}' - \ddot{w}'\right) - Q_u \Bigg] d\hat{s}, \end{aligned}$$

and at L,

$$\lambda(L,t) = \left[-j_{\eta\zeta}\left(\ddot{v}'w' + v'\ddot{w}'\right) + j_\zeta v'\ddot{v}' + j_\eta w'\ddot{w}'\right]_{s=L}.$$

With λ known, $\int_0^L W_i \left(\lambda v'\right)' ds$ and $\int_0^L W_i \left(\lambda w'\right)' ds$ are determinable. Integration by parts of the former yields

$$\int_0^L W_i \left(\lambda v'\right)' ds = -\int_0^L W_i' v' \lambda ds + W_i(L,t)\lambda(L,t)v'(L,t),$$

which is expanded as

$$\begin{aligned}
\int_0^L W_i \left(\lambda v'\right)' ds = &\int_0^L W_i' v' A_u(s,t) ds \\
&- \int_0^L W_i' v' \int_L^s \Big\{ -m \int_0^{\hat{s}} \left(\dot{v}'^2 + v'\ddot{v}' + \dot{w}'^2 + w'\ddot{w}'\right) d\tilde{s} \\
&+ m e_\eta \left(-\ddot{\phi} w' - 2\dot{\phi}\dot{w}' - \ddot{v}' - \phi\ddot{w}'\right) \\
&+ m e_\zeta \left(\ddot{\phi} v' + 2\dot{\phi}\dot{v}' + \phi\ddot{v}' - \ddot{w}'\right) - Q_u \Big\} d\hat{s} ds \\
&+ W_i(L,t)\lambda(L,t)v'(L,t).
\end{aligned}$$

A_u contains derivatives of the spatially dependent parameters, which are eliminated by further integrating by parts, ultimately resulting in

$$\begin{aligned}
\int_0^L W_i \left(\lambda v'\right)' ds = &- \int_0^L \Big\{ D_\zeta \left(v' v''^2 W_i' + v'^2 v''' W_i' + v'^2 v'' W_i'' + v' v''^2 W_i' \right) \\
&+ D_\eta \left(v' w''^2 W_i' + v' w' w''' W_i' + v' w' w'' W_i'' + v'' w' w'' W_i' \right) \\
&- D_{\eta\zeta} \left(v''^2 w' W_i' + v' v''' w' W_i' + v' v'' w' W_i'' \right) \\
&- D_{\eta\zeta} \left(3 v' v'' w'' W_i' + v'^2 w''' W_i' + v'^2 w'' W_i'' \right) \Big\} ds \\
&+ \int_0^L W_i' v' \Big\{ j_{\eta\zeta} \left(\ddot{v}' w' + v' \ddot{w}' \right) - j_\zeta v' \ddot{v}' - j_\eta w' \ddot{w}' \\
&+ D_\zeta v' v''' + D_\eta w' w''' - D_{\eta\zeta} \left(w' v''' + v' w''' \right) \Big\} ds \\
&- \int_0^L W_i' v' \int_L^s \Big\{ - m \int_0^{\hat{s}} \left(\dot{v}'^2 + v' \ddot{v}' + \dot{w}'^2 + w' \ddot{w}' \right) d\tilde{s} \\
&+ m e_\eta \left(-\ddot{\phi} w' - 2 \dot{\phi} \dot{w}' - \ddot{v}' - \phi \ddot{w}' \right) \\
&+ m e_\zeta \left(\ddot{\phi} v' + 2 \dot{\phi} \dot{v}' + \phi \ddot{v}' - \ddot{w}' \right) - Q_u \Big\} d\hat{s} ds \\
&+ W_i \left[-j_{\eta\zeta} \left(v' \ddot{v}' w' + v'^2 \ddot{w}' \right) + j_\zeta v'^2 \ddot{v}' + j_\eta v' w' \ddot{w}' \right]_{s=L}
\end{aligned}$$

and similarly

$$\begin{aligned}
\int_0^L W_i\left(\lambda w'\right)' ds = &- \int_0^L \Big\{ D_\zeta \left(w' v''^2 W_i' + w' v' v''' W_i' + w' v' v'' W_i'' + v' v'' w'' W_i' \right) \\
&+ D_\eta \left(w' w''^2 W_i' + w'^2 w''' W_i' + w'^2 w'' W_i'' + w' w''^2 W_i' \right) \\
&- D_{\eta\zeta} \left(v' w''^2 W_i' + v' w' w''' W_i' + v' w' w'' W_i'' \right) \\
&- D_{\eta\zeta} \left(3 v'' w' w'' W_i' + v''' w'^2 W_i' + w'^2 v'' W_i'' \right) \Big\} ds \\
&+ \int_0^L W_i' w' \Big\{ j_{\eta\zeta} \left(\ddot{v}' w' + v' \ddot{w}' \right) - j_\zeta v' \ddot{v}' - j_\eta w' \ddot{w}' \\
&+ D_\zeta v' v''' + D_\eta w' w''' - D_{\eta\zeta} \left(w' v''' + v' w''' \right) \Big\} ds \\
&- \int_0^L W_i' w' \int_L^s \Big\{ - m \int_0^{\hat{s}} \left(\dot{v}'^2 + v' \ddot{v}' + \dot{w}'^2 + w' \ddot{w}' \right) d\tilde{s} \\
&+ m e_\eta \left(-\ddot{\phi} w' - 2 \dot{\phi} \dot{w}' - \ddot{v}' - \phi \ddot{w}' \right) \\
&+ m e_\zeta \left(\ddot{\phi} v' + 2 \dot{\phi} \dot{v}' + \phi \ddot{v}' - \ddot{w}' \right) - Q_u \Big\} d\hat{s} ds \\
&+ W_i \left[-j_{\eta\zeta} \left(\ddot{v}' w'^2 + v' w' \ddot{w}' \right) + j_\zeta v' \ddot{v}' w' + j_\eta w'^2 \ddot{w}' \right]_{s=L}.
\end{aligned}$$

H. The Equations of Motion

At this point, everything can be determined. Remaining terms containing derivatives of the spatially dependent parameters are integrated by parts to distribute the derivative into the cofactors.

Consequently, the equation of motion in the y-direction for each i^{th} test function is

$$
\begin{aligned}
W_i(L)\Bigg[& \left(me_\eta - me_\zeta\phi\right)\int_0^s \left(\dot{v}'^2 + v'\ddot{v}' + \dot{w}'^2 + w'\ddot{w}'\right)d\hat{s} + me_\eta\left(-\ddot{v}v' - \phi\ddot{v}w'\right) \\
& + me_\zeta\left(\phi\ddot{v}v' - \ddot{v}w'\right) + j_\xi\left(\ddot{\phi}w' + \dot{\phi}\dot{w}' + 2w'\dot{v}'\dot{w}' + w'^2\ddot{v}'\right) + j_\eta\left(-\dot{\phi}\dot{w}' + \phi^2\ddot{v}'\right) \\
& + j_\eta\left(-\phi\ddot{w}' + 2\phi\dot{\phi}\dot{v}'\right) + j_\zeta\left(-2\phi\dot{\phi}\dot{v}' + v'\dot{v}'^2 + \dot{\phi}\dot{w}' + v'\dot{w}'^2 + \ddot{v}' - \phi^2\ddot{v}'\right) \\
& + j_\zeta\left(v'^2\ddot{v}' + \phi\ddot{w}' + v'w'\ddot{w}'\right) + j_{\eta\zeta}\left(2\dot{\phi}\dot{v}' + 4\phi\dot{\phi}\dot{w}' + 2\phi\ddot{v}' - \ddot{w}' + 2\phi^2\ddot{w}'\right) \\
& - \frac{1}{2}j_{\eta\zeta}\left(v'^2\ddot{w}' + w'^2\ddot{w}'\right) - D_\xi w'\phi''\Bigg]_{s=L} \\
& - \int_0^L \Bigg\{ W_i'\Bigg[\left(me_\eta - me_\zeta\phi\right)\int_0^s \left(\dot{v}'^2 + v'\ddot{v}' + \dot{w}'^2 + w'\ddot{w}'\right)d\hat{s} \\
& + me_\eta\left(-\ddot{v}v' - \phi\ddot{v}w'\right) + me_\zeta\left(\phi\ddot{v}v' - \ddot{v}w'\right) + j_\xi\left(\ddot{\phi}w' + \dot{\phi}\dot{w}' + 2w'\dot{v}'\dot{w}' + w'^2\ddot{v}'\right) \\
& + j_\eta\left(-\dot{\phi}\dot{w}' + \phi^2\ddot{v}' - \phi\ddot{w}' + 2\phi\dot{\phi}\dot{v}'\right) + j_\zeta\left(-2\phi\dot{\phi}\dot{v}' + v'\dot{v}'^2 + \dot{\phi}\dot{w}' + v'\dot{w}'^2 + \ddot{v}'\right) \\
& + j_\zeta\left(-\phi^2\ddot{v}' + v'^2\ddot{v}' + \phi\ddot{w}' + v'w'\ddot{w}'\right) + j_{\eta\zeta}\left(2\dot{\phi}\dot{v}' + 4\phi\dot{\phi}\dot{w}' + 2\phi\ddot{v}' - \ddot{w}'\right) \\
& + j_{\eta\zeta}\left(2\phi^2\ddot{w}' - \frac{1}{2}v'^2\ddot{w}' - \frac{1}{2}w'^2\ddot{w}'\right) + D_\zeta\left(v'v''^2 + v''w'w''\right) \\
& + D_{\eta\zeta}\left(-v'v''w'' + w'w''^2\right) + v'\int_L^s -m\int_0^{\hat{s}}\left(\dot{v}'^2 + v'\ddot{v}' + \dot{w}'^2 + w'\ddot{w}'\right)d\tilde{s} \\
& + me_\eta\left(-\ddot{\phi}w' - 2\dot{\phi}\dot{w}' - \ddot{v}' - \phi\ddot{w}'\right) + me_\zeta\left(\ddot{\phi}v' + 2\dot{\phi}\dot{v}' + \phi\ddot{v}' - \ddot{w}'\right) - Q_u d\hat{s}\Bigg] \\
& + W_i''\Bigg[D_\xi\left(\phi'w' + w'^2v''\right) + D_\eta\left(\phi^2v'' - \phi w''\right) + D_\zeta\left(v'' - \phi^2v'' + v'^2v''\right) \\
& + D_\zeta\left(\phi w'' + v'w'w''\right) + D_{\eta\zeta}\left(2\phi v'' - w'' + 2\phi^2w'' - \frac{1}{2}v'^2w'' - \frac{1}{2}w'^2w''\right)\Bigg]\Bigg\}ds \\
= & \int_0^L W_i\Big(m\ddot{v} - me_\eta\left(\dot{\phi}^2 + \phi\ddot{\phi} + \ddot{\phi}v'w' + 2\dot{\phi}w'\dot{v}' + \dot{v}'^2 + 2\dot{\phi}v'\dot{w}' + 2\phi\dot{v}'\dot{w}'\right) \\
& - me_\eta\left(+v'\ddot{v}' + \phi w'\ddot{v}' + \phi v'\ddot{w}'\right) + me_\zeta\left(\phi\dot{\phi}^2 - \ddot{\phi} + \frac{1}{2}\phi^2\ddot{\phi} + \frac{1}{2}\ddot{\phi}v'^2\right) \\
& + me_\zeta\left(2\dot{\phi}v'\dot{v}' + \phi\dot{v}'^2 - 2\dot{v}'\dot{w}' + \phi v'\ddot{v}' - w'\ddot{v}' - v'\ddot{w}'\right) - Q_v\Big)ds. \quad (2.22)
\end{aligned}
$$

Additionally, the equation of motion in the z-direction is

$$
\begin{aligned}
W_i(L)\Big[& \left(me_\eta\phi + me_\zeta\right)\int_0^s \left(\dot{v}'^2 + v'\ddot{v}' + \dot{w}'^2 + w'\ddot{w}'\right) d\hat{s} - me_\eta\left(\phi\ddot{v}v' + \phi\ddot{w}w'\right) \\
& + me_\zeta\left(-\ddot{v}v' - \ddot{w}w'\right) - j_\xi\left(\dot{\phi}\dot{v}' + w'\dot{v}'^2\right) + j_\eta\left(-\dot{\phi}\dot{v}' - 2\phi\dot{\phi}\dot{w}' - \phi\ddot{v}' + \ddot{w}'\right) \\
& + j_\eta\left(-\phi^2\ddot{w}' + w'\dot{w}'^2 + w'^2\ddot{w}'\right) + j_\zeta\left(\dot{\phi}\dot{v}' + w'\dot{v}'^2 + 2\phi\dot{\phi}\dot{w}' + \phi\ddot{v}' + \phi^2\ddot{w}'\right) \\
& + j_\zeta v'w'\ddot{v}' - j_{\eta\zeta}\left(-4\phi\dot{\phi}\dot{v}' + v'\dot{v}'^2 + 2\dot{\phi}\dot{w}' + 2w'\dot{v}'\dot{w}' + v'\dot{w}'^2 + \ddot{v}' - 2\phi^2\ddot{v}'\right) \\
& - j_{\eta\zeta}\left(\frac{1}{2}v'^2\ddot{v}' + \frac{1}{2}w'^2\ddot{v}' + 2\phi\ddot{w}' + 2v'w'\ddot{w}'\right)\Big]_{s=L} \\
& - \int_0^L \Big\{ W_i'\Big[\left(me_\eta\phi + me_\zeta\right)\int_0^s \left(\dot{v}'^2 + v'\ddot{v}' + \dot{w}'^2 + w'\ddot{w}'\right) d\hat{s} \\
& - me_\eta\left(\phi\ddot{v}v' + \phi\ddot{w}w'\right) + me_\zeta\left(-\ddot{v}v' - \ddot{w}w'\right) - j_\xi\left(\dot{\phi}\dot{v}' + w'\dot{v}'^2\right) - j_\eta\dot{\phi}\dot{v}' \\
& + j_\eta\left(-2\phi\dot{\phi}\dot{w}' - \phi\ddot{v}' + \ddot{w}' - \phi^2\ddot{w}' + w'^2\ddot{w}' + w'\dot{w}'^2\right) + j_\zeta\left(\dot{\phi}\dot{v}' + w'\dot{v}'^2\right) \\
& + j_\zeta\left(2\phi\dot{\phi}\dot{w}' + \phi\ddot{v}' + \phi^2\ddot{w}' + v'\ddot{v}'w'\right) - j_{\eta\zeta}\left(-4\phi\dot{\phi}\dot{v}' + v'\dot{v}'^2 + 2\dot{\phi}\dot{w}'\right) \\
& - j_{\eta\zeta}\left(2w'\dot{v}'\dot{w}' + v'\dot{w}'^2 + \ddot{v}' - 2\phi^2\ddot{v}' + \frac{1}{2}v'^2\ddot{v}' + \frac{1}{2}w'^2\ddot{v}' + 2\phi\ddot{w}' + 2v'w'\ddot{w}'\right) \\
& + D_\xi\left(\phi'v'' + w'v''^2\right) + D_\eta w'w''^2 + D_\zeta v'v''w'' - D_{\eta\zeta}\left(v''w'w'' + v'w''^2\right) \\
& + w'\int_L^s -m\int_0^{\hat{s}} \left(\dot{v}'^2 + v'\ddot{v}' + \dot{w}'^2 + w'\ddot{w}'\right) d\tilde{s} - me_\eta\ddot{\phi}w' \\
& + me_\eta\left(-2\dot{\phi}\dot{w}' - \ddot{v}' - \phi\ddot{w}'\right) + me_\zeta\left(\ddot{\phi}v' + 2\dot{\phi}\dot{v}' + \phi\ddot{v}' - \ddot{w}'\right) - Q_u d\hat{s}\Big] \\
& + W_i''\Big[D_\eta\left(-\phi v'' + w'' - \phi^2 w'' + w'^2 w''\right) + D_\zeta\left(\phi v'' + \phi^2 w'' + v'v''w'\right) \\
& + D_{\eta\zeta}\left(-v'' + 2\phi^2 v'' - \frac{1}{2}v'^2 v'' - \frac{1}{2}w'^2 v'' - 2\phi w'' - 2v'w'w''\right)\Big]\Big\} ds \\
& = \int_0^L W_i\Big(m\ddot{w} - me_\eta\left(\phi\dot{\phi}^2 - \ddot{\phi} + \frac{1}{2}\phi^2\ddot{\phi} + \frac{1}{2}\ddot{\phi}w'^2 + 2\dot{\phi}w'\dot{w}'\right) \\
& - me_\eta\left(\phi\dot{w}'^2 + \phi w'\ddot{w}'\right) - me_\zeta\left(\dot{\phi}^2 + \phi\ddot{\phi} + \dot{w}'^2 + w'\ddot{w}'\right) - Q_w\Big) ds. \qquad (2.23)
\end{aligned}
$$

Finally, the torsional equation of motion is

$$\int_0^L \Bigg\{ \Phi_i \Bigg[\left(me_\eta w' - me_\varsigma v'\right) \int_0^s \left(\dot{v}'^2 + v'\ddot{v}' + \dot{w}'^2 + w'\ddot{w}'\right) d\hat{s} + me_\eta \left(-\phi\ddot{v} + \ddot{w} - \frac{1}{2}\phi^2\ddot{w} - \ddot{v}v'w' - \frac{1}{2}\ddot{w}w'^2\right) + me_\varsigma \left(-\ddot{v} + \frac{1}{2}\phi^2\ddot{v} - \phi\ddot{w} + \frac{1}{2}\ddot{v}v'^2\right) + j_\xi \left(\ddot{\phi} + \dot{v}'\dot{w}' + w'\ddot{v}'\right) + j_\eta \left(-\phi\dot{v}'^2 + \dot{v}'\dot{w}' + \phi\dot{w}'^2\right) + j_\varsigma \left(\phi\dot{v}'^2 - \phi\dot{w}'^2 - \dot{v}'\dot{w}'\right) - j_{\eta\varsigma} \left(\dot{v}'^2 - \dot{w}'^2 + 4\phi\dot{v}'\dot{w}'\right) + D_\eta \left(\phi v''^2 - v''w'' - \phi w''^2\right) + D_\varsigma \left(-\phi v''^2 + v''w'' + \phi w''^2\right) + D_{\eta\varsigma} \left(v''^2 + 4\phi v''w'' - w''^2\right) \Bigg] + \Phi_i' D_\xi \left(\phi' + v''w'\right) \Bigg\} ds = \int_0^L Q_\phi \Phi_i ds. \tag{2.24}$$

With the equations of motion known, a method is needed to provide an efficient and accurate solution.

CHAPTER III

THE USE OF SHAPE FUNCTIONS IN THE SOLUTION TO THE EQUATIONS OF MOTION

A. Introduction

The equations of motion (2.22)-(2.24) are nonlinear, coupled partial differential equations in time and space. As mentioned previously, the boundary conditions are known. Therefore, it is possible to represent the deformations as an infinite sum of the product of spatially dependent, linearly independent shape functions and time-dependent coefficients.

B. Shape Function Selection

1. Bending Motion

For the case of a uniform beam undergoing planar bending along the x-z plane, the simplified linear equation of motion in which the mass moment of inertia and mass offset are neglected is

$$D_\eta w'''' + m\ddot{w} = 0. \tag{3.1}$$

The boundary conditions are given in (2.13)-(2.16). Assuming this partial differential equation is separable in time and space, w is expressed as

$$w(s,t) = w(t)W(s). \tag{3.2}$$

Substituting (3.2) into (3.1) results in

$$\frac{W''''(s)}{W(s)} = -\frac{m}{D_\zeta}\frac{\ddot{w}(t)}{w(t)} = \lambda,$$

where λ is a constant. The spatial contribution to the equation is therefore

$$W''''(s) - \lambda W(s) = 0, \tag{3.3}$$

and (2.13)-(2.16) lead to $W(0) = W'(0) = W''(L) = W'''(L) = 0$. The sign of λ is determined by applying the Galerkin method to the spatial equation (3.3), integrating by parts, and applying the boundary conditions:

$$\int_0^L W''''(s)W(s)ds = \lambda \int_0^L W^2(s)ds,$$
$$\int_0^L W''(s)W''(s)ds = \lambda \int_0^L W^2(s)ds.$$

This confirms that λ must be positive for a nontrivial solution to exist. The solution to (3.3) is of the form

$$W(s) = A\cosh\left(\sqrt[4]{\lambda}\, s\right) + B\sinh\left(\sqrt[4]{\lambda}\, s\right) + C\cos\left(\sqrt[4]{\lambda}\, s\right) + D\sin\left(\sqrt[4]{\lambda}\, s\right).$$

Since $W(0) = W'(0) = 0$,

$$W(s) = A\left[\cosh\left(\sqrt[4]{\lambda}\, s\right) - \cos\left(\sqrt[4]{\lambda}\, s\right)\right] + B\left[\sinh\left(\sqrt[4]{\lambda}\, s\right) - \sin\left(\sqrt[4]{\lambda}\, s\right)\right].$$

A and B are determined from the remaining two boundary conditions, which require that

$$W''(L) = A\sqrt{\lambda}\left[\cosh\left(\sqrt[4]{\lambda}\, L\right) + \cos\left(\sqrt[4]{\lambda}\, L\right)\right]$$
$$+ B\sqrt{\lambda}\left[\sinh\left(\sqrt[4]{\lambda}\, L\right) + \sin\left(\sqrt[4]{\lambda}\, L\right)\right] = 0$$

and

$$W'''(L) = A\lambda^{3/4}\left[\sinh\left(\sqrt[4]{\lambda}\,L\right) - \sin\left(\sqrt[4]{\lambda}\,L\right)\right] + B\lambda^{3/4}\left[\cosh\left(\sqrt[4]{\lambda}\,L\right) + \cos\left(\sqrt[4]{\lambda}\,L\right)\right] = 0,$$

or equivalently:

$$\begin{bmatrix} \cosh\left(\sqrt[4]{\lambda}\,L\right) + \cos\left(\sqrt[4]{\lambda}\,L\right) & \sinh\left(\sqrt[4]{\lambda}\,L\right) + \sin\left(\sqrt[4]{\lambda}\,L\right) \\ \sinh\left(\sqrt[4]{\lambda}\,L\right) - \sin\left(\sqrt[4]{\lambda}\,L\right) & \cosh\left(\sqrt[4]{\lambda}\,L\right) + \cos\left(\sqrt[4]{\lambda}\,L\right) \end{bmatrix} \begin{Bmatrix} A \\ B \end{Bmatrix} = \begin{Bmatrix} 0 \\ 0 \end{Bmatrix}. \quad (3.4)$$

For a nontrivial solution to A and B, the determinant of the coefficient matrix in (3.4) must be zero, which, when simplified, yields

$$\cosh\left(\sqrt[4]{\lambda}\,L\right)\cos\left(\sqrt[4]{\lambda}\,L\right) + 1 = 0.$$

Letting $\beta = \sqrt[4]{\lambda}\,L$, the spatial contribution to (3.1) is

$$W_i(s) = \cosh\left(\frac{\beta_i s}{L}\right) - \cos\left(\frac{\beta_i s}{L}\right) - \sigma_i\left[\sinh\left(\frac{\beta_i s}{L}\right) - \sin\left(\frac{\beta_i s}{L}\right)\right],$$

where

$$\sigma_i = \frac{\cosh\beta_i + \cos\beta_i}{\sinh\beta_i + \sin\beta_i},$$

$$\cosh\beta_i\cos\beta_i + 1 = 0.$$

Table I lists the first five values of β and σ.

The functions $W_i(s)$ are the mode shapes of the simple beam described at the beginning of the section and are only approximate mode shapes for beams of greater complexity. Nonetheless, this set of functions provides a systematic method of generating linearly independent functions that satisfy the boundary conditions for transverse displacements. Therefore, these functions are used as shape functions to be

Table I. Values of the parameters in the bending shape function.

i	β_i	σ_i
1	1.87510	0.734096
2	4.69409	1.01847
3	7.85476	0.999224
4	10.9955	1.00003
5	14.1372	0.999999

multiplied by time coefficients and summed to provide the displacement. The fidelity of the solution is preserved by using a sufficient amount of functions to accurately model the solution. These shape functions are additionally used to comprise the associated set of test functions used for the Galerkin method in the previous chapter. Figure 3 contains a plot of the first five bending shape functions.

2. Torsional Motion

For the case of a uniform beam undergoing pure torsional motion about the x-axis, the simplified linear equation of motion in which the mass offset is neglected is

$$D_\xi \phi'' = j_\xi \ddot{\phi}. \tag{3.5}$$

As explained in the previous chapter, the boundary conditions are $\phi(0,t) = \phi'(L,t) = 0$. Assuming this partial differential equation is also separable in time and space, ϕ is expressed as

$$\phi(s,t) = \phi(t)\Phi(s). \tag{3.6}$$

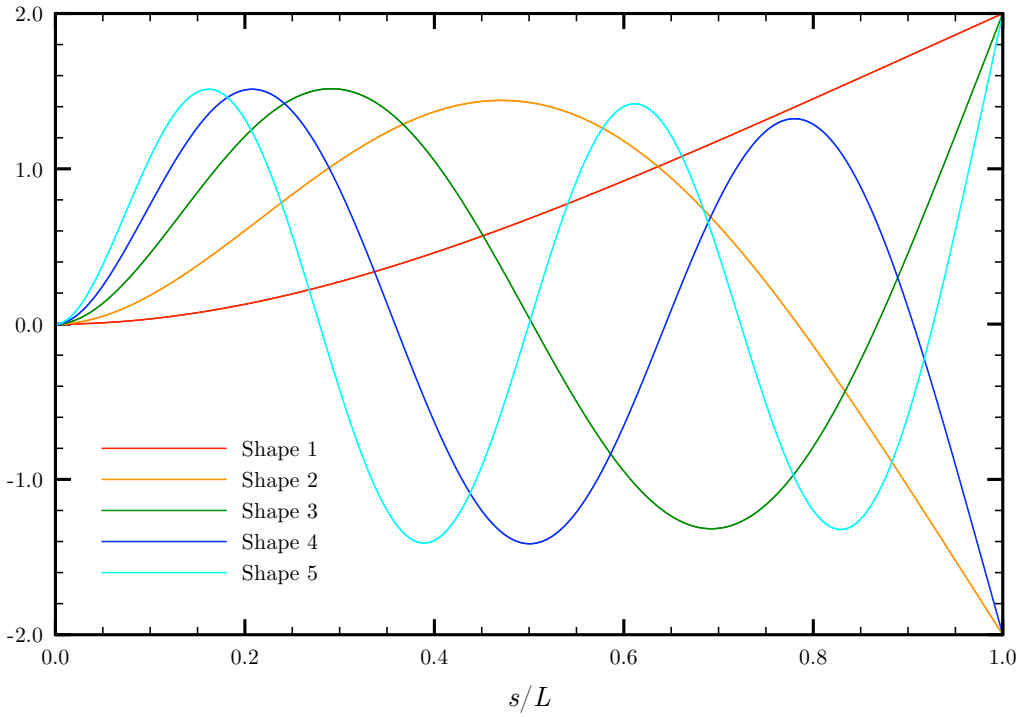

Figure 3. The first five bending shape functions.

Substituting (3.6) into (3.5) results in

$$\frac{\Phi''(s)}{\Phi(s)} = \frac{j_\xi}{D_\xi}\frac{\ddot{\phi}(t)}{\phi(t)} = -\lambda,$$

where λ is a constant. The spatial contribution to the equation is therefore

$$\Phi''(s) + \lambda\Phi(s) = 0, \tag{3.7}$$

and the boundary conditions lead to $\Phi(0) = \Phi'(L) = 0$. The sign of λ is determined by applying the Galerkin method to the spatial equation (3.7), integrating by parts,

and applying the boundary conditions:

$$\int_0^L \Phi''(s)\Phi(s)ds = -\lambda \int_0^L \Phi^2(s)ds,$$
$$\int_0^L \Phi'(s)\Phi'(s)ds = \lambda \int_0^L \Phi^2(s)ds.$$

This confirms that λ must be positive for a nontrivial solution to exist. The solution to (3.7) is of the form

$$\Phi(s) = A\cos\left(\sqrt{\lambda}\,s\right) + B\sin\left(\sqrt{\lambda}\,s\right).$$

Since $\Phi(0) = 0$,

$$\Phi(s) = B\sin\left(\sqrt{\lambda}\,s\right).$$

B is determined from $\Phi'(L) = 0$:

$$\Phi'(L) = B\sqrt{\lambda}\cos\left(\sqrt{\lambda}\,L\right) = 0.$$

For a nontrivial solution, B cannot be zero; therefore,

$$\cos\left(\sqrt{\lambda}\,L\right) = 0,$$

or

$$\sqrt{\lambda_i}\,L = \frac{(2i-1)\,\pi}{2} \quad \text{for } i \in \mathbb{N}_1.$$

Letting $\gamma_i = \sqrt{\lambda_i}\,L$, the spatial contribution to (3.5) can be written as

$$\Phi_i(s) = \sqrt{2}\sin\frac{\gamma_i s}{L},$$

where

$$\gamma_i = \frac{(2i-1)\,\pi}{2}.$$

As with the bending shape functions, this set of functions provides a systematic method of generating linearly independent functions that satisfy the boundary conditions for torsional motion. Analogously, these functions are used as shape functions for the solution of the torsional displacement in the nonlinear, non-uniform equations. The fidelity of the solution is preserved by using a sufficient amount of shape functions, and these functions also comprise the corresponding test functions used in the Galerkin method. The first three torsional shape functions are plotted in Figure 4.

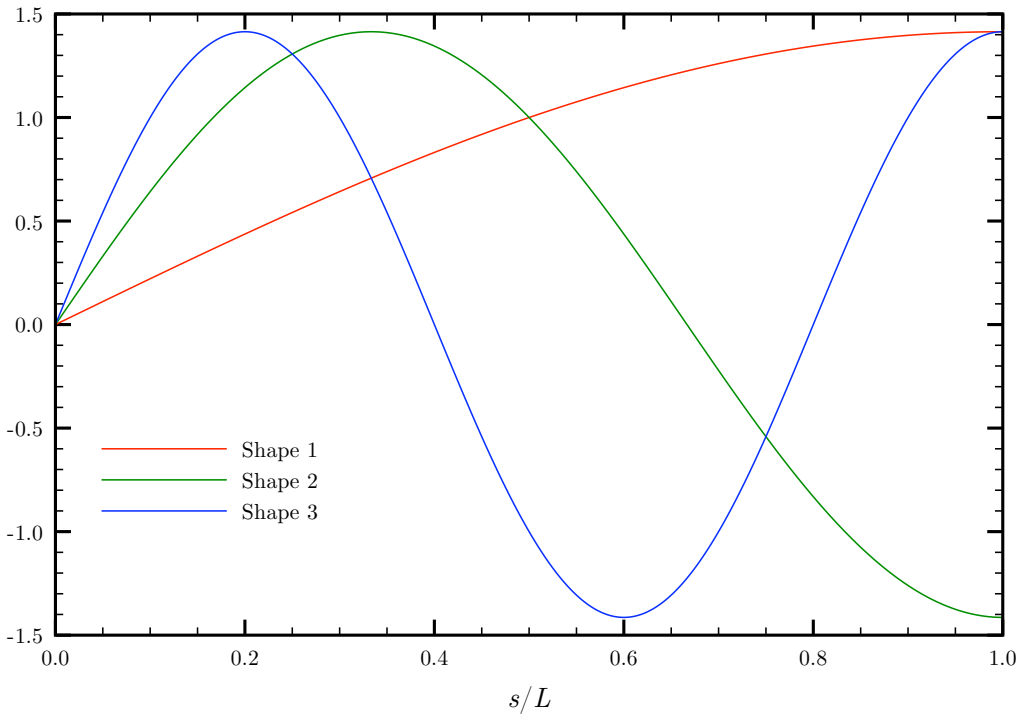

Figure 4. The first three torsional shape functions.

C. Ordinary Differential Equation Form

Using these shape functions, the displacements can be approximated by

$$w = \sum_{i=1}^{l} w_i(t)W_i(s), \quad v = \sum_{i=1}^{m} v_i(t)W_i(s), \quad \phi = \sum_{i=1}^{n} \phi_i(t)\Phi_i(s).$$

Upon invoking this representation, the partial differential equations reduce to a system of ordinary differential equations in time, for which the time coefficients are the unknown quantities. Therefore, the equations of motion are written in the following manner using linear and non-linear arrays:

$$[M_L + M_{NL}] \begin{Bmatrix} \ddot{\mathbf{w}} \\ \ddot{\mathbf{v}} \\ \ddot{\boldsymbol{\phi}} \end{Bmatrix} + [C_L + C_{NL}] \begin{Bmatrix} \dot{\mathbf{w}} \\ \dot{\mathbf{v}} \\ \dot{\boldsymbol{\phi}} \end{Bmatrix} + [K_L + K_{NL}] \begin{Bmatrix} \mathbf{w} \\ \mathbf{v} \\ \boldsymbol{\phi} \end{Bmatrix} = \mathbf{F_L} + \mathbf{F_{NL}}, \quad (3.8)$$

where $\mathbf{w}$, $\mathbf{v}$, and $\boldsymbol{\phi}$ each represent vectors containing the time coefficients: $\{w_1, ..., w_l\}^T$, $\{v_1, ..., v_m\}^T$, and $\{\phi_1, ..., \phi_n\}^T$.

Each of the matrices is $(l + m + n) \times (l + m + n)$ and can be expressed as the concatenation of 9 submatrices with the following dimensions:

$$\begin{bmatrix} [l \times l] & [l \times m] & [l \times n] \\ [m \times l] & [m \times m] & [m \times n] \\ [n \times l] & [n \times m] & [n \times n] \end{bmatrix}.$$

D. Linear Matrices

1. Linear Mass Matrix

The submatrices of the linear mass matrix are defined as follows:

$$
\begin{aligned}
[M_L]_{i,j} &= \int_0^L \left(W_i m W_j + W_i' j_\eta W_j'\right) ds - \left[W_i j_\eta W_j'\right]_{s=L}, \\
[M_L]_{i,l+j} &= -\int_0^L W_i' j_{\eta\zeta} W_j' ds + \left[W_i j_{\eta\zeta} W_j'\right]_{s=L}, \\
[M_L]_{i,l+m+j} &= \int_0^L W_i m e_\eta \Phi_j ds, \\
[M_L]_{l+i,j} &= -\int_0^L W_i' j_{\eta\zeta} W_j' ds + \left[W_i j_{\eta\zeta} W_j'\right]_{s=L}, \\
[M_L]_{l+i,l+j} &= \int_0^L \left(W_i m W_j + W_i' j_\zeta W_j'\right) ds - \left[W_i j_\zeta W_j'\right]_{s=L}, \\
[M_L]_{l+i,l+m+j} &= -\int_0^L W_i m e_\zeta \Phi_j ds, \\
[M_L]_{l+m+i,j} &= \int_0^L \Phi_i m e_\eta W_j ds, \\
[M_L]_{l+m+i,l+j} &= -\int_0^L \Phi_i m e_\zeta W_j ds, \\
[M_L]_{l+m+i,l+m+j} &= \int_0^L \Phi_i j_\xi \Phi_j ds.
\end{aligned}
$$

2. Linear Damping Matrix

In the equations of motion, there are no linear occurrences of the first time derivative of any of the deformations as there is no energy dissipation. Therefore, the linear damping matrix is zero:

$$[C_L] = 0.$$

3. Linear Stiffness Matrix

The nonzero submatrices of the linear stiffness matrix are

$$
\begin{aligned}
[K_L]_{i,j} &= \int_0^L W_i'' D_\eta W_j'' ds, \\
[K_L]_{i,l+j} &= -\int_0^L W_i'' D_{\eta\zeta} W_j'' ds, \\
[K_L]_{l+i,j} &= -\int_0^L W_i'' D_{\eta\zeta} W_j'' ds, \\
[K_L]_{l+i,l+j} &= \int_0^L W_i'' D_\zeta W_j'' ds, \\
[K_L]_{l+m+i,l+m+j} &= \int_0^L \Phi_i' D_\xi \Phi_j' ds.
\end{aligned}
$$

E. Nonlinear Matrices

In determining the nonlinear matrices, there are several possibilities concerning where to assign terms from the equations of motion. This decision is done systematically such that terms containing second-order time derivatives are assigned to the mass matrix, remaining terms that contain first-order time derivatives are assigned to the damping matrix, and terms containing no time derivatives are assigned to the stiffness matrix. Furthermore, for terms containing factors that have the same-order time derivative, placement within the matrix is done such that the term with the lowest-order spatial derivative is the unknown. Finally, for instances in which the temporal and spatial derivatives of the factors are both of the same order, the spatial derivative of v is taken to be the unknown.

1. Nonlinear Mass Matrix

The nonzero submatrices of the nonlinear mass matrix are:

$$
\begin{aligned}
[M_{NL}]_{i,j} = \int_0^L \Bigg\{ & W_i' \left(me_\eta \phi + me_\zeta\right) \int_0^s w' W_j' d\hat{s} + W_i' \left[-me_\eta \phi w' - me_\zeta w'\right] W_j \\
& + W_i' w' \int_L^s \left(-me_\eta \phi - me_\zeta\right) W_j' d\hat{s} \\
& + W_i' \left(-2j_{\eta\zeta}\phi - 2j_{\eta\zeta} v' w' - j_\eta \phi^2 + j_\eta w'^2 + j_\zeta \phi^2\right) W_j' \\
& - W_i' w' \int_L^s m \int_0^{\hat{s}} w' W_j' d\tilde{s} d\hat{s} + W_i \left[-me_\eta \phi w' - me_\zeta w'\right] W_j' \Bigg\} ds \\
& - \Bigg[W_i \left(me_\eta \phi + me_\zeta\right) \int_0^s w' W_j' d\hat{s} + W_i \left[-me_\eta \phi w' - me_\zeta w'\right] W_j \\
& + W_i \left(-2j_{\eta\zeta}\phi - 2j_{\eta\zeta} v' w' + j_\eta w'^2 - j_\eta \phi^2 + j_\zeta \phi^2\right) W_j' \Bigg]_{s=L},
\end{aligned}
$$

$$
\begin{aligned}
[M_{NL}]_{i,l+j} = \int_0^L \Bigg\{ & W_i' \left(me_\eta \phi + me_\zeta\right) \int_0^s v' W_j' d\hat{s} + W_i' \left[-me_\eta \phi v' - me_\zeta v'\right] W_j \\
& + W_i' w' \int_L^s \left(-me_\eta + me_\zeta \phi\right) W_j' d\hat{s} \\
& + W_i' \left(2j_{\eta\zeta}\phi^2 - \frac{1}{2} j_{\eta\zeta} v'^2 - \frac{1}{2} j_{\eta\zeta} w'^2 - j_\eta \phi + j_\zeta \phi + j_\zeta v' w'\right) W_j' \\
& - W_i' w' \int_L^s m \int_0^{\hat{s}} v' W_j' d\tilde{s} d\hat{s} \Bigg\} ds \\
& - \Bigg[W_i \left(me_\eta \phi + me_\zeta\right) \int_0^s v' W_j' d\hat{s} + W_i \left[-me_\eta \phi v' - me_\zeta v'\right] W_j \\
& + W_i \left(2j_{\eta\zeta}\phi^2 - \frac{1}{2} j_{\eta\zeta} v'^2 - \frac{1}{2} j_{\eta\zeta} w'^2 - j_\eta \phi + j_\zeta \phi + j_\zeta v' w'\right) W_j' \Bigg]_{s=L},
\end{aligned}
$$

$$
\begin{aligned}
[M_{NL}]_{i,l+m+j} = \int_0^L \Bigg\{ & W_i' w' \int_L^s \left(-me_\eta w' + me_\zeta v'\right) \Phi_j d\hat{s} \\
& + W_i \left[-me_\eta \left(\frac{1}{2}\phi^2 + \frac{1}{2} w'^2\right) - me_\zeta \phi\right] \Phi_j \Bigg\} ds,
\end{aligned}
$$

$$
\begin{aligned}
[M_{NL}]_{l+i,j} = \int_0^L \Big\{ & W_i' \left(me_\eta - me_\zeta \phi\right) \int_0^s w' W_j' d\hat{s} \\
& + W_i' v' \int_L^s \left(-me_\eta \phi - me_\zeta\right) W_j' d\hat{s} \\
& + W_i \left[-me_\eta \phi v' - me_\zeta v'\right] W_j' - W_i' v' \int_L^s m \int_0^{\hat{s}} w' W_j' d\tilde{s} d\hat{s} \\
& + W_i' \left(2j_{\eta\zeta}\phi^2 - \frac{1}{2} j_{\eta\zeta} v'^2 - \frac{1}{2} j_{\eta\zeta} w'^2 - j_\eta \phi + j_\zeta \phi + j_\zeta v' w'\right) W_j' \Big\} ds \\
& - \Big[W_i \left(me_\eta - me_\zeta \phi\right) \int_0^s w' W_j' d\hat{s} + W_i \left[-me_\eta \phi v' - me_\zeta v'\right] W_j \\
& + W_i \left(2j_{\eta\zeta}\phi^2 - \frac{1}{2} j_{\eta\zeta} v'^2 - \frac{1}{2} j_{\eta\zeta} w'^2 - j_\eta \phi + j_\zeta \phi + j_\zeta v' w'\right) W_j' \Big]_{s=L},
\end{aligned}
$$

$$
\begin{aligned}
[M_{NL}]_{l+i,l+j} = \int_0^L \Big\{ & W_i' \left(me_\eta - me_\zeta \phi\right) \int_0^s v' W_j' d\hat{s} \\
& + W_i' \left[-me_\eta \left(v' + \phi w'\right) + me_\zeta \left(\phi v' - w'\right)\right] W_j \\
& + W_i' v' \int_L^s \left(-me_\eta + me_\zeta \phi\right) W_j' d\hat{s} \\
& + W_i \left[-me_\eta \left(v' + \phi w'\right) + me_\zeta \left(\phi v' - w'\right)\right] W_j' \\
& + W_i' \left(2j_{\eta\zeta}\phi + j_\xi w'^2 + j_\eta \phi^2 - j_\zeta \phi^2 + j_\zeta v'^2\right) W_j' \\
& - W_i' v' \int_L^s m \int_0^{\hat{s}} v' W_j' d\tilde{s} d\hat{s} \Big\} ds - \Big[W_i \left(me_\eta - me_\zeta \phi\right) \int_0^s v' W_j' d\hat{s} \\
& + W_i \left[-me_\eta \left(v' + \phi w'\right) + me_\zeta \left(\phi v' - w'\right)\right] W_j \\
& + W_i \left(2j_{\eta\zeta}\phi + j_\xi w'^2 + j_\eta \phi^2 - j_\zeta \phi^2 + j_\zeta v'^2\right) W_j' \Big]_{s=L},
\end{aligned}
$$

$$
\begin{aligned}
[M_{NL}]_{l+i,l+m+j} = \int_0^L \Big\{ & W_i' v' \int_L^s \left(-me_\eta w' + me_\zeta v'\right) \Phi_j d\hat{s} + W_i' j_\xi w' \Phi_j \\
& + W_i \left[-me_\eta \left(\phi + v' w'\right) + me_\zeta \left(\frac{1}{2}\phi^2 + \frac{1}{2} v'^2\right)\right] \Phi_j \Big\} ds \\
& - \left[W_i j_\xi w' \Phi_j\right]_{s=L},
\end{aligned}
$$

$$[M_{NL}]_{l+m+i,j} = \int_0^L \Phi_i \Bigg\{ (me_\eta w' - me_\zeta v') \int_0^s w' W_j' d\hat{s} + \left[-me_\eta \left(\frac{1}{2}\phi^2 + \frac{1}{2}w'^2 \right) - me_\zeta \phi \right] W_j \Bigg\} ds,$$

$$[M_{NL}]_{l+m+i,l+j} = \int_0^L \Phi_i \Bigg\{ (me_\eta w' - me_\zeta v') \int_0^s v' W_j' d\hat{s} + j_\xi w' W_j' + \left[-me_\eta (\phi + v'w') + me_\zeta \left(\frac{1}{2}\phi^2 + \frac{1}{2}v'^2 \right) \right] W_j \Bigg\} ds. \tag{3.9}$$

2. Nonlinear Damping Matrix

The nonzero submatrices of the nonlinear damping matrix are

$$\begin{aligned}[C_{NL}]_{i,j} = \int_0^L \Bigg\{ & W_i' (me_\eta \phi + me_\zeta) \int_0^s \dot{w}' W_j' d\hat{s} + W_i (-me_\eta \phi \dot{w}' - me_\zeta \dot{w}') W_j' \\ & + W_i' (-j_{\eta\zeta} v' \dot{w}' + j_\eta w' \dot{w}') W_j' - W_i' w' \int_L^s m \int_0^{\hat{s}} \dot{w}' W_j' d\tilde{s} d\hat{s} \Bigg\} ds \\ & - \Big[W_i (me_\eta \phi + me_\zeta) \int_0^s \dot{w}' W_j' d\hat{s} + W_i (-j_{\eta\zeta} v' \dot{w}' + j_\eta w' \dot{w}') W_j' \Big]_{s=L},\end{aligned}$$

$$\begin{aligned}[C_{NL}]_{i,l+j} = \int_0^L \Bigg\{ & W_i' (me_\eta \phi + me_\zeta) \int_0^s \dot{v}' W_j' d\hat{s} \\ & + W_i' (-j_{\eta\zeta} v' \dot{v}' - 2 j_{\eta\zeta} w' \dot{w}' - j_\xi w' \dot{v}' + j_\zeta \dot{v}' w') W_j' \\ & - W_i' w' \int_L^s m \int_0^{\hat{s}} \dot{v}' W_j' d\tilde{s} d\hat{s} \Bigg\} ds \\ & - \Big[W_i (me_\eta \phi + me_\zeta) \int_0^s \dot{v}' W_j' d\hat{s} \\ & + W_i (-j_{\eta\zeta} v' \dot{v}' - 2 j_{\eta\zeta} w' \dot{w}' - j_\xi w' \dot{v}' + j_\zeta \dot{v}' w') W_j' \Big]_{s=L},\end{aligned}$$

$$
\begin{aligned}
[C_{NL}]_{i,l+m+j} = & \int_0^L \Big\{ W_i' w' \int_L^s \left(-2me_\eta \dot{w}' + 2me_\zeta \dot{v}'\right) \Phi_j d\hat{s} \\
& + W_i \left[-me_\eta \left(\phi\dot{\phi} + 2w'\dot{w}' \right) - me_\zeta \dot{\phi} \right] \Phi_j + W_i' \left(4j_{\eta\zeta}\phi\dot{v}' - 2j_{\eta\zeta}\dot{w}'\right)\Phi_j \\
& + W_i' \left(-j_\xi \dot{v}' - j_\eta \dot{v}' - 2j_\eta \phi \dot{w}' + j_\zeta \dot{v}' + 2j_\zeta \phi \dot{w}'\right)\Phi_j \Big\} ds \\
& - \left[W_i \left(4j_{\eta\zeta}\phi\dot{v}' - 2j_{\eta\zeta}\dot{w}' - j_\xi\dot{v}' - j_\eta\dot{v}' - 2j_\eta\phi\dot{w}' + j_\zeta\dot{v}'\right)\Phi_j \right]_{s=L} \\
& - 2\left[W_i j_\zeta \phi \dot{w}' \Phi_j \right]_{s=L},
\end{aligned}
$$

$$
\begin{aligned}
[C_{NL}]_{l+i,j} = & \int_0^L \Big\{ W_i' \left(me_\eta - me_\zeta\phi\right) \int_0^s \dot{w}' W_j' d\hat{s} + W_i' j_\zeta v' \dot{w}' W_j' \\
& - W_i' v' \int_L^s m \int_0^{\hat{s}} \dot{w}' W_j' d\tilde{s} d\hat{s} \Big\} ds \\
& - \left[W_i \left(me_\eta - me_\zeta\phi\right) \int_0^s \dot{w}' W_j' d\hat{s} + W_i j_\zeta v' \dot{w}' W_j' \right]_{s=L},
\end{aligned}
$$

$$
\begin{aligned}
[C_{NL}]_{l+i,l+j} = & \int_0^L \Big\{ W_i' \left(me_\eta - me_\zeta\phi\right) \int_0^s \dot{v}' W_j' d\hat{s} \\
& + W_i \left[-me_\eta \left(\dot{v}' + 2\phi\dot{w}'\right) + me_\zeta \left(\phi\dot{v}' - 2\dot{w}'\right) \right] W_j' \\
& + W_i' \left(2j_\xi w'\dot{w}' + j_\zeta v'\dot{v}'\right) W_j' - W_i' v' \int_L^s m \int_0^{\hat{s}} \dot{v}' W_j' d\tilde{s} d\hat{s} \Big\} ds \\
& - \left[W_i \left(me_\eta - me_\zeta\phi\right) \int_0^s \dot{v}' W_j' d\hat{s} + W_i \left(2j_\xi w'\dot{w}' + j_\zeta v'\dot{v}'\right) W_j' \right]_{s=L},
\end{aligned}
$$

$$
\begin{aligned}
[C_{NL}]_{l+i,l+m+j} = & \int_0^L \Big\{ W_i' v' \int_L^s \left(-2me_\eta \dot{w}' + 2me_\zeta \dot{v}'\right) \Phi_j d\hat{s} \\
& + W_i \left[-me_\eta \left(\dot{\phi} + 2w'\dot{v}' + 2v'\dot{w}' \right) + me_\zeta \left(\phi\dot{\phi} + 2v'\dot{v}' \right) \right] \Phi_j \\
& + W_i' \left(2j_{\eta\zeta}\dot{v}' + 4j_{\eta\zeta}\phi\dot{w}' + j_\xi\dot{w}' - j_\eta\dot{w}' + 2j_\eta\phi\dot{v}' + j_\zeta\dot{w}'\right)\Phi_j \\
& - 2W_i' j_\zeta \phi \dot{v}' \Phi_j \Big\} ds - \left[W_i \left(2j_{\eta\zeta}\dot{v}' + 4j_{\eta\zeta}\phi\dot{w}' + j_\xi\dot{w}' - j_\eta\dot{w}'\right)\Phi_j \right]_{s=L} \\
& - \left[W_i \left(2j_\eta\phi\dot{v}' + j_\zeta\dot{w}' - 2j_\zeta\phi\dot{v}'\right)\Phi_j \right]_{s=L},
\end{aligned}
$$

$$[C_{NL}]_{l+m+i,j} = \int_0^L \Big\{ \Phi_i \left(m e_\eta w' - m e_\zeta v' \right) \int_0^s \dot{w}' W_j' d\hat{s} + \Phi_i \left(j_{\eta\zeta} \dot{w}' + j_\eta \phi \dot{w}' - j_\zeta \phi \dot{w}' \right) W_j' \Big\} ds,$$

$$[C_{NL}]_{l+m+i,l+j} = \int_0^L \Big\{ \Phi_i \left(m e_\eta w' - m e_\zeta v' \right) \int_0^s \dot{v}' W_j' d\hat{s} + \Phi_i \left(-j_{\eta\zeta} \dot{v}' - 4 j_{\eta\zeta} \phi \dot{w}' \right) W_j' + \Phi_i \left(j_\xi \dot{w}' - j_\eta \phi \dot{v}' + j_\eta \dot{w}' + j_\zeta \dot{v}' \phi - j_\zeta \dot{w}' \right) W_j' \Big\} ds. \tag{3.10}$$

3. Nonlinear Stiffness Matrix

The submatrices of the nonlinear stiffness matrix are

$$[K_{NL}]_{i,j} = \int_0^L \Big\{ W_i' \left(D_\xi v''^2 + D_\eta w''^2 - D_{\eta\zeta} v'' w'' \right) W_j' + W_i'' \left(D_\eta w' w'' - \frac{1}{2} D_{\eta\zeta} v'' w' \right) W_j' \Big\} ds,$$

$$[K_{NL}]_{i,l+j} = \int_0^L \Big\{ W_i' \left(D_\zeta v'' w'' - D_{\eta\zeta} w''^2 \right) W_j' + W_i'' \left(D_\zeta v'' w' - \frac{1}{2} D_{\eta\zeta} v' v'' - 2 D_{\eta\zeta} w' w'' \right) W_j' \Big\} ds,$$

$$[K_{NL}]_{i,l+m+j} = \int_0^L \Big\{ W_i' D_\xi v'' \Phi_j' + W_i'' \left(-D_\eta v'' - D_\eta \phi w'' + D_\zeta v'' + D_\zeta \phi w'' \right) \Phi_j + W_i'' \left(2 D_{\eta\zeta} \phi v'' - 2 D_{\eta\zeta} w'' \right) \Phi_j \Big\} ds,$$

$$
\begin{aligned}
[K_{NL}]_{l+i,j} &= \int_0^L \Big\{ W_i' \left(D_\zeta v'' w'' + D_{\eta\zeta} w''^2 \right) W_j' \\
&\quad + W_i'' \left(D_\xi w' v'' - \frac{1}{2} D_{\eta\zeta} w' w'' \right) W_j' \Big\} ds,
\end{aligned}
$$

$$
\begin{aligned}
[K_{NL}]_{l+i,l+j} &= \int_0^L \Big\{ W_i' \left(D_\zeta v''^2 - D_{\eta\zeta} v'' w'' \right) W_j' \\
&\quad + W_i'' \left(D_\zeta v' v'' + D_\zeta w' w'' - \frac{1}{2} D_{\eta\zeta} v' w'' \right) W_j' \Big\} ds,
\end{aligned}
$$

$$
\begin{aligned}
[K_{NL}]_{l+i,l+m+j} &= \int_0^L \Big\{ W_i'' \left(D_\eta \phi v'' - D_\eta w'' - D_\zeta \phi v'' + D_\zeta w'' + 2 D_{\eta\zeta} v'' \right) \Phi_j \\
&\quad + 2 W_i'' D_{\eta\zeta} \phi w'' \Phi_j + W_i'' D_\xi w' \Phi_j' \Big\} ds + \left[W_i D_\xi w' \Phi_j'' \right]_{s=L},
\end{aligned}
$$

$$
[K_{NL}]_{l+m+i,j} = \int_0^L \left\{ -\Phi_i D_{\eta\zeta} w'' W_j'' + \Phi_i' D_\xi v'' W_j' \right\} ds,
$$

$$
[K_{NL}]_{l+m+i,l+j} = \int_0^L \Phi_i \left(-D_\eta w'' + D_\zeta w'' + D_{\eta\zeta} v'' \right) W_j'' ds,
$$

$$
[K_{NL}]_{l+m+i,l+m+j} = \int_0^L \Phi_i \left(D_\eta v''^2 - D_\eta w''^2 - D_\zeta v''^2 + D_\zeta w''^2 + 4 D_{\eta\zeta} v'' w'' \right) \Phi_j ds. \tag{3.11}
$$

F. Forcing Vectors

1. Linear Forcing Vector

The subvectors of the linear forcing vector are

$$\{F_L\}_i = \int_0^L W_i Q_w ds,$$
$$\{F_L\}_{l+i} = \int_0^L W_i Q_v ds,$$
$$\{F_L\}_{l+m+i} = \int_0^L \Phi_i Q_\phi ds.$$

2. Nonlinear Forcing Vector

The nonzero subvectors of the nonlinear forcing vector are

$$\{F_{NL}\}_i = -\int_0^L W_i' w' \int_s^L Q_u d\hat{s} ds,$$
$$\{F_{NL}\}_{l+i} = -\int_0^L W_i' v' \int_s^L Q_u d\hat{s} ds.$$

CHAPTER IV

NUMERICAL IMPLEMENTATION

A. Overview

The shape-function based ordinary differential equation of motion (3.8) is evaluated numerically in Fortran 90 using explicit integration. Essentially, this process consists of calculating the mass, damping, and stiffness matrices and the force vectors at each time step.

B. Matrices

The time-invariant linear matrices are calculated once using Simpson's $\frac{1}{3}$ rule. The forcing vectors and nonlinear matrices are dependent upon time and consequently calculated for every time step.

From a computational perspective, the triple integrals in the nonlinear mass and damping matrices are particularly expensive. However, since the deformations are expressed in terms of separable variables, the time-dependent contribution can be extracted, enabling the spatial integrals to be computed once and accordingly multiplied by the corresponding time coefficients and summed subsequently.

For example, in the triple integral

$$-\int_0^L W_i'(s)w'(s,t)\int_L^s m(\hat{s})\int_0^{\hat{s}} \dot{v}'(\tilde{s},t)W_j'(\tilde{s})d\tilde{s}d\hat{s}ds,$$

the deformations are expanded in terms of shape functions and time coefficients:

$$\int_0^L W_i'(s)\left\{\sum_{a=1}^{l} w_a(t)W_a'(s)\right\}\int_s^L m(\hat{s})\int_0^{\hat{s}}\left\{\sum_{b=1}^{m}\dot{v}_b(t)W_b'(\tilde{s})\right\}W_j'(\tilde{s})d\tilde{s}d\hat{s}ds.$$

The time coefficients and summations are rearranged to yield

$$\sum_{a=1}^{l}\sum_{b=1}^{m}\left\{w_a(t)\dot{v}_b(t)\int_0^L W_i'(s)W_a'(s)\int_s^L m(\hat{s})\int_0^{\hat{s}} W_b'(\tilde{s})W_j'(\tilde{s})d\tilde{s}d\hat{s}ds\right\}.$$

Furthermore,

$$\int_0^{\hat{s}} W_b'(\tilde{s})W_j'(\tilde{s})d\tilde{s}$$

has a closed-form solution, ultimately reducing the calculation of the triple integral at every time step to a once-computed double integral that undergoes double summation at subsequent time steps. The remaining integrals in the nonlinear matrices are calculated in a similar manner, reducing the integrals to double summations.

C. Forcing Vectors

The forcing vectors are computed at every time step using Simpson's $\frac{1}{3}$ rule. For the case of p point loads, $\mathbf{F}_i(t)$, expressed in the inertial frame,

$$\mathbf{Q} = \begin{Bmatrix} Q_u \\ Q_v \\ Q_w \end{Bmatrix} = \sum_{i=1}^{p}\delta(s-s_i)\mathbf{F}_i,$$

where $\delta(s)$ is the Dirac delta function [13, pp. 391-392]. This is done similarly for Q_ϕ with the moment about the ξ-axis, leading to

$$\begin{aligned}
\{F_L\}_i &= \int_0^L W_i Q_w ds &&= \sum_{j=1}^{p} W_i(s_j)F_{z_j}(t), \\
\{F_L\}_{l+i} &= \int_0^L W_i Q_v ds &&= \sum_{j=1}^{p} W_i(s_j)F_{y_j}(t), \\
\{F_L\}_{l+m+i} &= \int_0^L \Phi_i Q_\phi ds &&= \sum_{k=1}^{q} \Phi_i(s_k)M_{\xi_k}(t),
\end{aligned}$$

and

$$\{F_{NL}\}_i = -\int_0^L W_i' w' \int_s^L Q_u ds = -\sum_{j=1}^{p} F_{x_j}(t) \int_0^{s_j} W_i'(s) w'(s,t) ds,$$
$$\{F_{NL}\}_{l+i} = -\int_0^L W_i' v' \int_s^L Q_u ds = -\sum_{j=1}^{p} F_{x_j}(t) \int_0^{s_j} W_i'(s) v'(s,t) ds,$$

or

$$\{F_{NL}\}_i = -\sum_{j=1}^{p} \sum_{a=1}^{l} F_{x_j}(t) w_a(t) \int_0^{s_j} W_i'(s) W_a'(s) ds,$$
$$\{F_{NL}\}_{l+i} = -\sum_{j=1}^{p} \sum_{a=1}^{m} F_{x_j}(t) v_a(t) \int_0^{s_j} W_i'(s) W_a'(s) ds,$$

where the integral has a closed-form solution.

D. Solution

Letting the time coefficients be represented by

$$\mathbf{X} = \{w_1, \ldots, w_l, v_1, \ldots, v_m, \phi_1, \ldots, \phi_n\},$$

equation (3.8) is rewritten such that

$$\frac{d}{dt}\begin{Bmatrix} \mathbf{X} \\ \dot{\mathbf{X}} \end{Bmatrix} = \begin{Bmatrix} \dot{\mathbf{X}} \\ [M_L + M_{NL}]^{-1} \left\{ \mathbf{F_L} + \mathbf{F_{NL}} - [K_L + K_{NL}]\,\mathbf{X} - [C_{NL}]\,\dot{\mathbf{X}} \right\} \end{Bmatrix}, \tag{4.1}$$

or in shorthand as

$$\dot{\mathbf{Y}} = \mathbf{F}(\mathbf{Y}, t).$$

At each point in time, (4.1) is integrated using a fourth-order Runge-Kutta method [15, pp. 340-343]:

$$\mathbf{Y}_{n+1} = \mathbf{Y}_n + \frac{1}{6}\Delta t \left(\mathbf{k}_1 + 2\mathbf{k}_2 + 2\mathbf{k}_3 + \mathbf{k}_4\right),$$

where

$$\begin{aligned}
t_{n+1} &= t_n + \Delta t, \\
\mathbf{k}_1 &= \mathbf{F}\left(\mathbf{Y}_n, t_n\right), \\
\mathbf{k}_2 &= \mathbf{F}\left(\mathbf{Y}_n + \frac{1}{2}\Delta t \mathbf{k}_1, t_n + \frac{1}{2}\Delta t\right), \\
\mathbf{k}_3 &= \mathbf{F}\left(\mathbf{Y}_n + \frac{1}{2}\Delta t \mathbf{k}_2, t_n + \frac{1}{2}\Delta t\right), \\
\mathbf{k}_4 &= \mathbf{F}\left(\mathbf{Y}_n + \Delta t \mathbf{k}_3, t_n + \Delta t\right).
\end{aligned}$$

This provides the time coefficients and the first derivatives of the time coefficients for each time step. Consequently, the deformation of the elastic axis can be calculated with respect to time by summing the product of the time coefficients and the shape functions at the position of interest. Knowing the deformed position of each point along the elastic axis as well as ϕ, the angle about ξ that the cross section coordinate system is rotated, enables the displacement of any point on the structure to be calculated.

CHAPTER V

VALIDATION

A. Method

The structural solver is validated by comparing results with those generated by Abaqus, a commercial finite element software package. Validation consists of comparing natural frequencies and displacements arising from a time-varying force applied to the beam.

B. Natural Frequencies

Three beams are used as test cases for matching natural frequencies obtained by Abaqus. In Abaqus, the natural frequencies are calculated using a linear perturbation method [16]. Each of the beams is modeled in Abaqus using quadratic three-dimensional continuum elements. Furthermore, for each case, the mesh is refined twice. The five frequencies corresponding to the first five vibrational modes are compared with those obtained by the linear contribution to the beam model.

For these comparisons, the beam model uses five shape functions for each of the three independent degrees of freedom. The linear contribution to the beam model provides a system of 15 coupled linear second-order differential equations:

$$M_L \begin{Bmatrix} \ddot{\mathbf{w}} \\ \ddot{\mathbf{v}} \\ \ddot{\boldsymbol{\phi}} \end{Bmatrix} + K_L \begin{Bmatrix} \mathbf{w} \\ \mathbf{v} \\ \boldsymbol{\phi} \end{Bmatrix} = \mathbf{0}.$$

An analytical solution is obtainable for the shape function time coefficients, and the natural frequencies are calculated by solving the characteristic equation [17, pp. 478-

483]:

$$\left|M_L^{-1}K_L - (2\pi f)^2 I\right| = 0.$$

To calculate the mode shape for each frequency, each of the shape functions is relatively weighed using the corresponding element of the eigenvector and summed. Letting X denote the matrix consisting of the eigenvectors, in which each eigenvector is a row, the shapes of the independent degrees of freedom of the i^{th} mode shape are given by

$$w_i(s) = \sum_{j=1}^{l} X_{i,j}W_j(s), \qquad v_i(s) = \sum_{j=1}^{m} X_{i,l+j}W_j(s), \qquad \phi_i(s) = \sum_{j=1}^{n} X_{i,l+m+j}\Phi_j(s).$$

1. Case 1: A Tapered Beam

The first beam used for frequency comparison is a linearly tapered, homogeneous beam composed of aluminum alloy 6061-T6. This beam choice provides a simple example of a non-uniform beam. 6061-T6 has a density of 2710 kg/m^3, a Young's modulus of 70 GPa, and a modulus of rigidity of 26 GPa [18, p. 747].

The beam is shown in Figure 5. It is 20-cm long and consists of a 2 cm $\times$ 1 cm cross section at the fixed end and a 1 cm $\times$ 1 cm cross section at the free end. The properties of the tapered beam are listed in Table II. For a rectangular cross section with dimensions $a \times b$, where a is the greater of the two, the torsion constant can be approximated as follows [10, p. 401]:

$$K = ab^3\left[\frac{1}{3} - 0.21\frac{b}{a}\left(1 - \frac{b^4}{12a^4}\right)\right]. \tag{5.1}$$

Table III shows the mesh sizes for the three finite element meshes. For each of the three meshes, the first five frequencies are tabulated in Table IV. The error is measured by taking the absolute value of the difference between the frequencies of

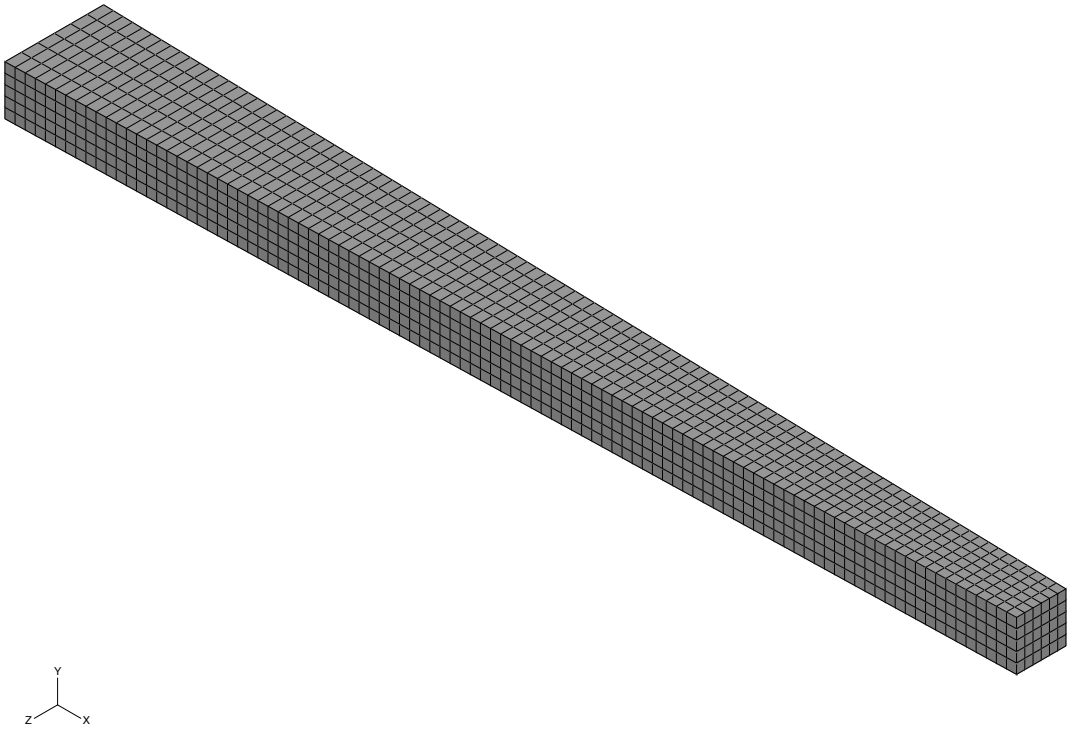

Figure 5. Tapered beam with 100×5×6 mesh.

Table II. Properties of tapered beam.

Parameter	Value
$m(s)$	$0.542 - 1.355s$ kg/m
$j_\xi(s)$	$(0.22583 - 1.4679s + 3.3875s^2 - 2.8229s^3) \times 10^{-4}$ kg m^2/m
$j_\eta(s)$	$(0.18067 - 1.3550s + 3.3875s^2 - 2.8229s^3) \times 10^{-4}$ kg m^2/m
$j_\zeta(s)$	$(0.045167 - 0.11292s) \times 10^{-4}$ kg m^2/m
$D_\xi(s)$	$173.33 + \frac{9.1\times10^{-10}}{(0.02-0.05s)^5} - \frac{1.092}{(0.02-0.05s)}$
	$-433.33s - \frac{(2.275\times10^{-9}s)}{(0.02-0.05s)^5} + \frac{(2.73s)}{(0.02-0.05s)}$ N m^2
$D_\eta(s)$	$466.67 - 3500s + 8750s^2 - 7291.7s^3$ N m^2
$D_\zeta(s)$	$116.67 - 291.67s$ N m^2

the finest finite element mesh and the beam solution and dividing by that obtained from the finite element analysis.

Table III. Finite element mesh sizes of tapered beam.

Mesh Number	Elements Along x, y, z	Total Elements
1	$50 \times 3 \times 3$	450
2	$67 \times 3 \times 5$	1005
3	$100 \times 5 \times 6$	3000

Table IV. First five frequencies of tapered beam.

Mode	Mesh 1 [Hz]	Mesh 2 [Hz]	Mesh 3 [Hz]	Beam [Hz]	% Error
1	252.75	252.71	252.64	251.89	0.297
2	445.46	445.38	445.30	446.20	0.202
3	1362.1	1361.8	1361.4	1370.8	0.686
4	2081.4	2080.8	2080.4	2130.5	2.41
5	3594.1	3593.4	3592.1	3671.3	2.16

The beam solution favorably agrees with the finite element solution, providing an error of less than 2.5%.

2. Case 2: A Twisted Beam

A twisted, homogeneous beam composed of aluminum alloy 6061-T6 is the second beam used for frequency comparison. This beam is chosen as it provides an example of a non-uniform beam for which the orientation of the principal mass and bending axes varies along the length of the beam with respect to the reference coordinate system.

The beam is shown in Figure 6. It is 10-m long and consists of a 1 m $\times$ 0.5 m cross section that is unrotated at the fixed end and linearly rotated such that it is at a 45° angle about the elastic axis at the free end. The properties of the twisted beam are presented in Table V. For a rectangular cross section with an aspect ratio of 2, the torsion constant, K, is $0.229ab^3$, where a and b are respectively the lengths of the longer and shorter sides [19, p. 173].

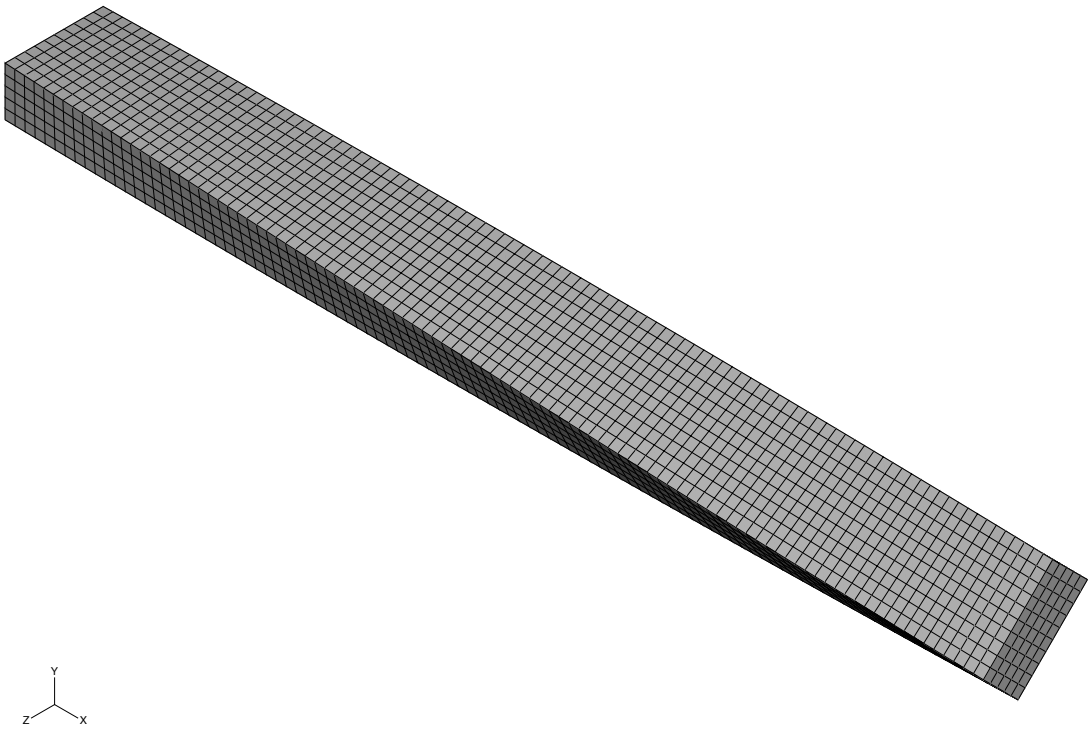

Figure 6. Twisted beam with 100×5×10 mesh.

Table V. Properties of twisted beam.

Parameter	Value
$m(s)$	1355 kg/m
$j_\xi(s)$	141.15 kg m^2/m
$j_\eta(s)$	$70.573 + 42.344\cos\frac{\pi s}{20}$ kg m^2/m
$j_\zeta(s)$	$70.573 - 42.344\cos\frac{\pi s}{20}$ kg m^2/m
$j_{\eta\zeta}(s)$	$42.344\sin\frac{\pi s}{20}$ kg m^2/m
$D_\xi(s)$	7.4425×10^8 N m^2
$D_\eta(s)$	$(1.8229 + 1.0938\cos\frac{\pi s}{20}) \times 10^9$ N m^2
$D_\zeta(s)$	$(1.8229 - 1.0938\cos\frac{\pi s}{20}) \times 10^9$ N m^2
$D_{\eta\zeta}(s)$	$1.0938\sin\frac{\pi s}{20} \times 10^9$ N m^2

As with the tapered beam, Table VI provides the mesh sizes for the three finite element meshes. For each of the three meshes, the first five frequencies and the error are tabulated in Table VII.

Table VI. Finite element mesh sizes of twisted beam.

Mesh Number	Elements Along x, y, z	Total Elements
1	$50 \times 2 \times 5$	500
2	$67 \times 3 \times 7$	1407
3	$100 \times 5 \times 10$	5000

Once more, the beam representation agrees nicely with the finite element solution, providing an error of less than 3.7%.

Table VII. First five frequencies of twisted beam.

Mode	Mesh 1 [Hz]	Mesh 2 [Hz]	Mesh 3 [Hz]	Beam [Hz]	% Error
1	4.1440	4.1423	4.1410	4.1291	0.288
2	8.0006	7.9981	7.9961	8.0229	0.335
3	26.265	26.253	26.245	26.483	0.907
4	46.756	46.737	46.723	48.425	3.64
5	58.102	58.041	58.024	57.407	1.06

3. Case 3: A Composite Beam

The final beam used for frequency analysis is a uniform composite beam consisting of aluminum alloy 6061-T6 and steel. Steel has a density of 7860 kg/m^3, a Young's modulus of 200 GPa, and a modulus of rigidity of 77.2 GPa [18, p. 747]. Three quarters of the beam are aluminum, while the remaining quarter is steel. The beam is shown in Figure 7.

This beam is selected because it provides an example of a beam for which the mass and elastic centers of each cross section are offset in both dimensions. Furthermore, the principal bending and mass axes are oriented differently with respect to each other and to the reference coordinate system.

The beam is 1-m long with a 5 cm $\times$ 3 cm cross section. The properties of the composite beam are presented in Table VIII. The torsional stiffness is approximated by multiplying an area-weighted average of the modulus of rigidity by the result of (5.1) for this cross section.

Table IX tabulates the mesh sizes for the three finite element meshes, and Table X lists the first five frequencies and the error.

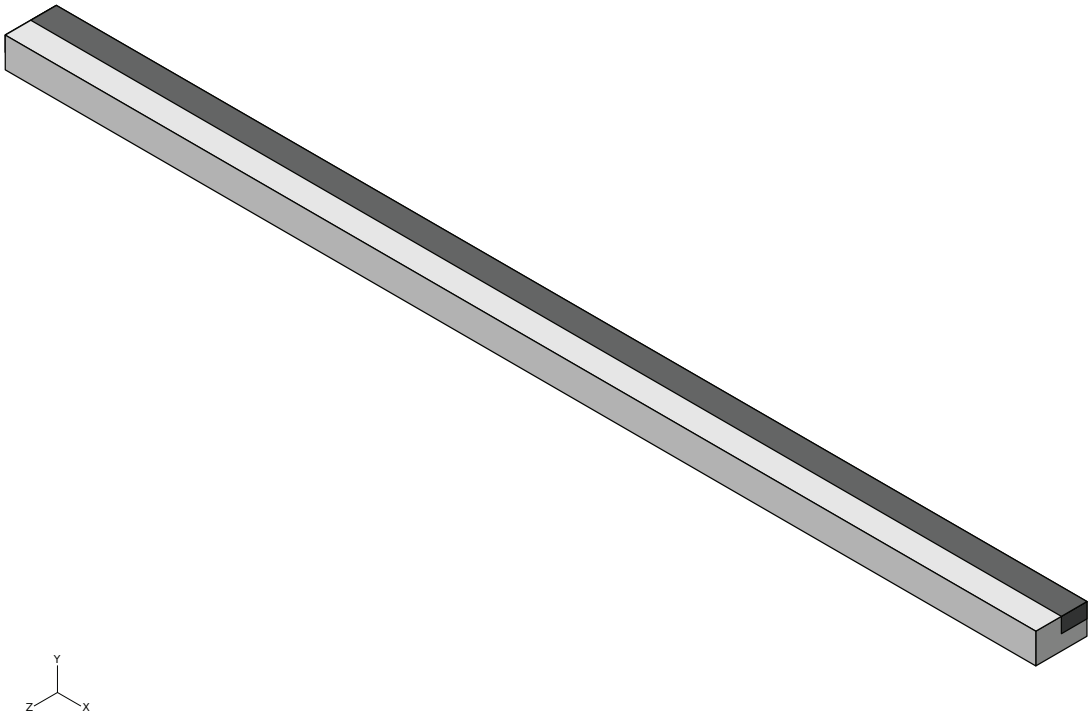

Figure 7. Aluminum-steel composite beam.

Table VIII. Properties of composite beam.

Parameter	Value
$e_\eta(s)$	3.7524×10^{-5} m
$e_\zeta(s)$	-6.2539×10^{-5} m
$m(s)$	5.9963 kg/m
$j_\xi(s)$	1.5668×10^{-3} kg m^2/m
$j_\eta(s)$	1.1521×10^{-3} kg m^2/m
$j_\zeta(s)$	0.41474×10^{-3} kg m^2/m
$j_{\eta\zeta}(s)$	0.12276×10^{-3} kg m^2/m
$D_\xi(s)$	1.0931×10^4 N m^2
$D_\eta(s)$	2.9616×10^4 N m^2
$D_\zeta(s)$	1.0662×10^4 N m^2
$D_{\eta\zeta}(s)$	0.31212×10^4 N m^2

Table IX. Finite element mesh sizes of composite beam.

Mesh Number	Elements Along x, y, z	Total Elements
1	$77 \times 2 \times 4$	616
2	$100 \times 4 \times 6$	2400
3	$143 \times 4 \times 8$	4576

Table X. First five frequencies of composite beam.

Mode	Mesh 1 [Hz]	Mesh 2 [Hz]	Mesh 3 [Hz]	Beam [Hz]	% Error
1	23.099	23.091	23.089	23.036	0.230
2	39.675	39.668	39.665	39.662	0.00756
3	144.18	144.13	144.12	144.30	0.125
4	245.73	245.68	245.66	248.21	1.04
5	401.19	401.01	400.98	403.61	0.656

The frequencies calculated by the beam model have an error of less than 1.1%, continuing to provide an accurate result that is computationally efficient.

C. Forced Response

To test the nonlinear beam model, three beams are used. At the free end of the elastic axis, a time-dependent force is applied, and the displacement is measured. For each beam, the displacement at four points along the elastic axis is compared using the linear and nonlinear versions of both Abaqus and the beam model [16].

The beam model is executed using one core of an eight-core Intel Xeon 2.26 GHz Mac Pro with 24 GB of RAM running Mac OS X Server 10.5.8. Abaqus is executed on a Windows XP Professional SP3 virtual machine running on the Mac Pro. The Abaqus simulation uses one core and has access to 2.5 GB of RAM.

1. Case 1: A Tapered Beam

The first beam used for forced-response testing is the same as that used for the first frequency comparison. This beam is discretized in Abaqus using 1920 ($80\times4\times6$) quadratic elements and is shown in Figure 8. The time-dependent force plotted in Figure 9 is applied to the node at the intersection of the elastic axis and the free end. In Abaqus, this simulation spans 0.5 seconds with 10^{-4}-second time steps.

The beam model uses five shape functions for each of the three degrees of freedom. The time step is 10^{-5} seconds, and the beam is discretized with 200 elements.

Figures 10, 11, 12, and 13 respectively plot the time history of the displacement in the y-direction of the nodes along the elastic axis at the free end, three quarters of the length, half of the length, and one quarter of the length. These plots show the results obtained from Abaqus using linear and nonlinear geometric models as well as the linear and nonlinear versions of the beam model.

In Figure 10, there is a clear difference between the amplitude of the linear and nonlinear models. This difference is due to the effect of the relatively large deforma-

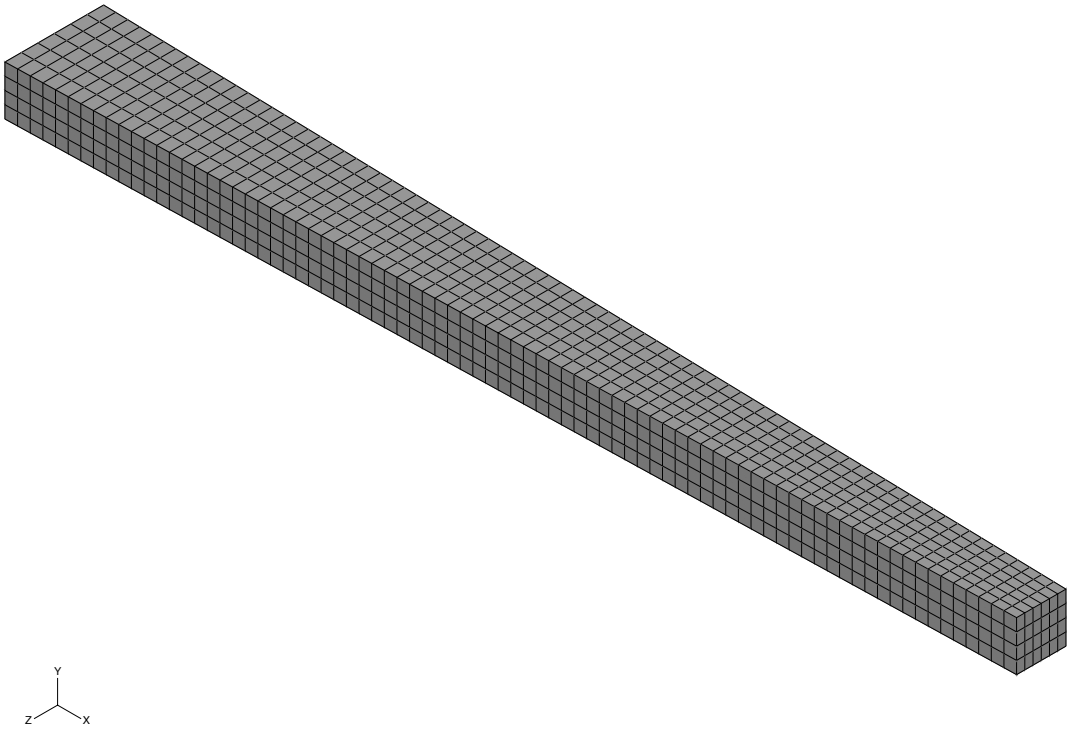

Figure 8. Tapered beam with 80×4×6 mesh.

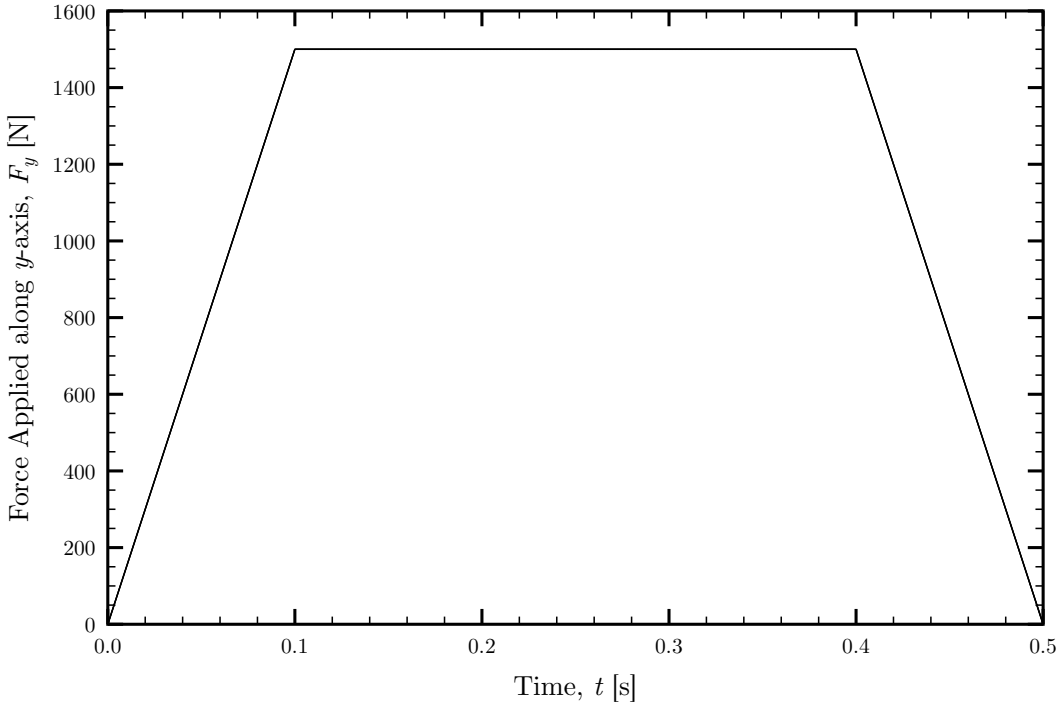

Figure 9. Force applied to tapered beam.

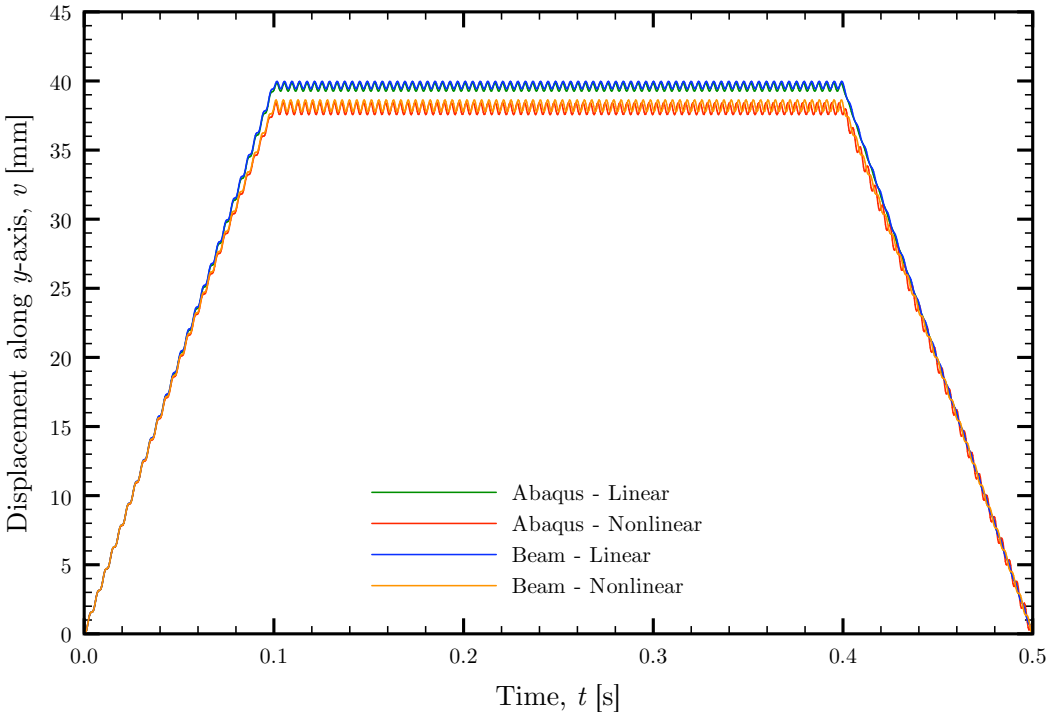

Figure 10. Tapered beam elastic axis displacement along y-axis at $s = L$.

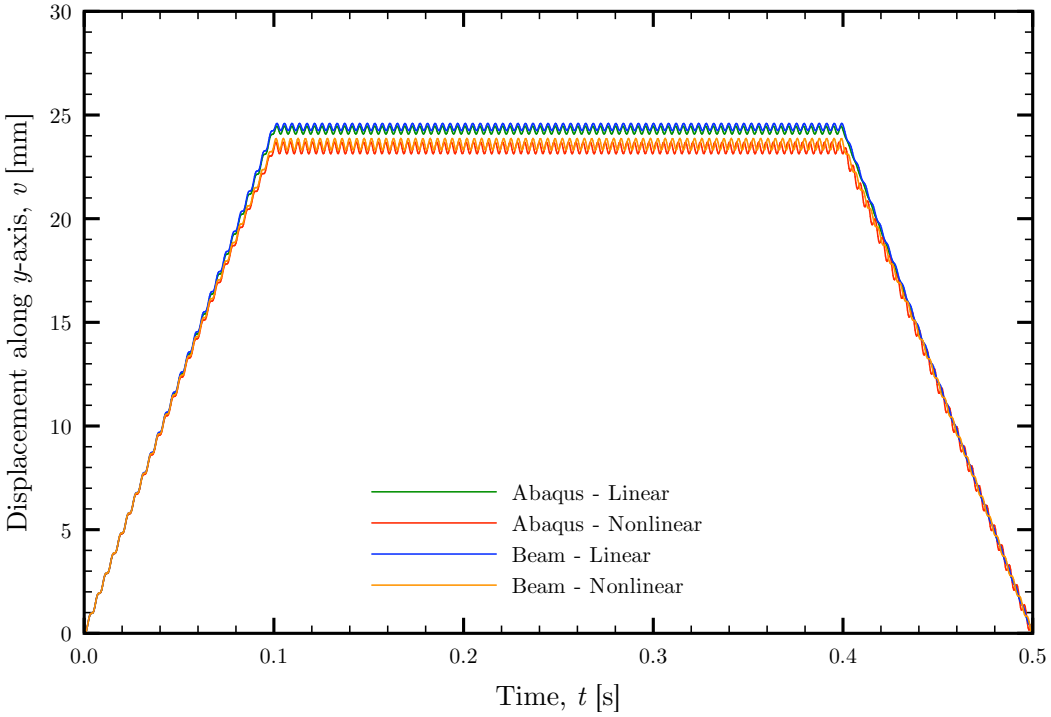

Figure 11. Tapered beam elastic axis displacement along y-axis at $s = \frac{3}{4}L$.

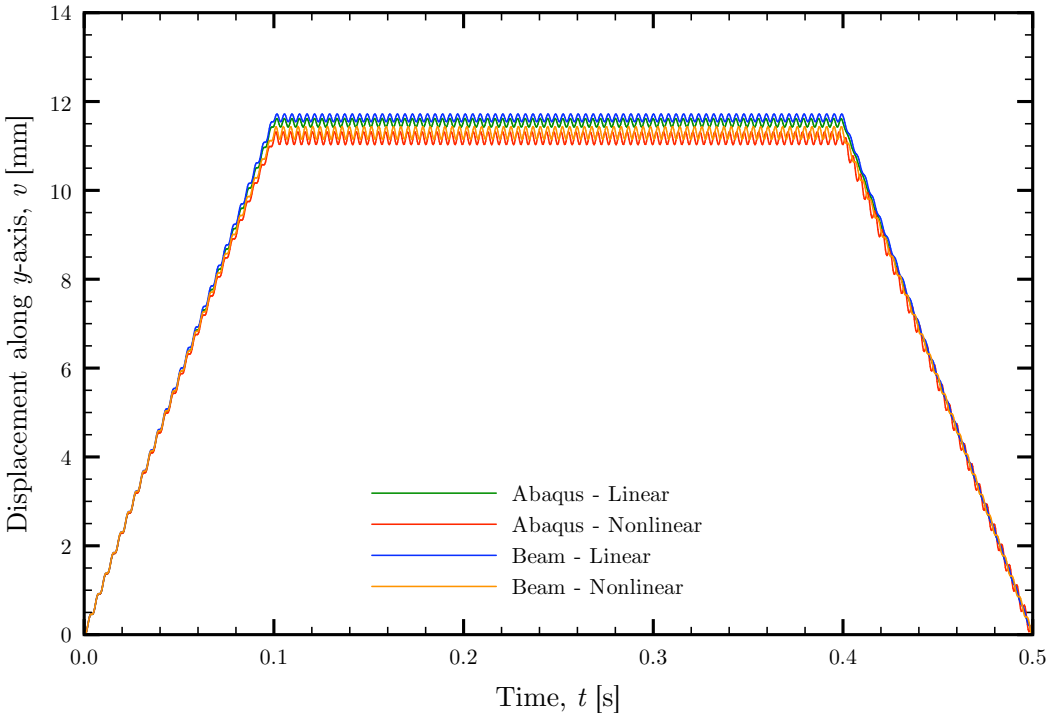

Figure 12. Tapered beam elastic axis displacement along y-axis at $s = \frac{1}{2}L$.

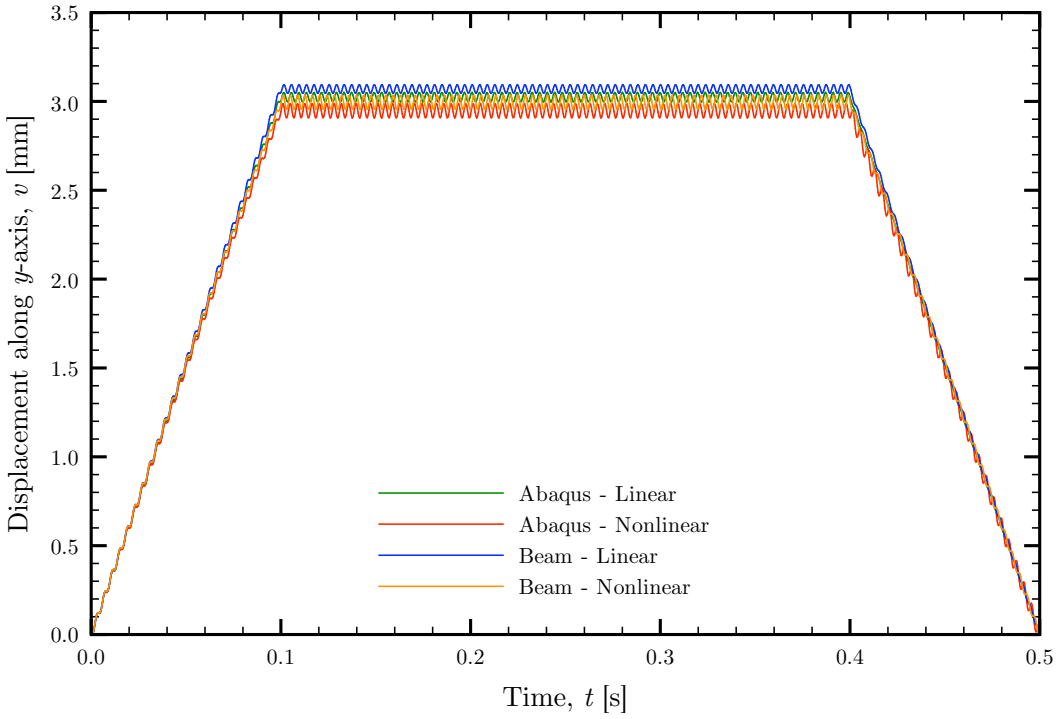

Figure 13. Tapered beam elastic axis displacement along y-axis at $s = \frac{1}{4}L$.

tion induced by the force and the consequent relevance of curvature. The frequency of the nonlinear beam model is slightly different from that of the nonlinear Abaqus simulation, resulting in a phase difference that increases in time. Nonetheless, the linear and nonlinear beam models compare favorably and distinctly with the Abaqus counterparts, especially given the computational time, which is listed in Table XI.

Table XI. Tapered beam computational time.

Method	Time
Abaqus - Linear	385 min
Abaqus - Nonlinear	437 min
Beam - Linear	8 min
Beam - Nonlinear	16 min

2. Case 2: A Twisted Beam

For the second forced-response test case, the beam is the same as that used for the second frequency comparison. This beam is discretized in Abaqus using 2688 (84×4×8) quadratic elements and is shown in Figure 14. Figure 15 shows the time-dependent force applied to the node at the intersection of the elastic axis and the free end. In Abaqus, this simulation spans 5 seconds with 5×10^{-3}-second time steps.

The beam model uses five shape functions for each of the three degrees of freedom. The time step is 10^{-4} seconds, and the beam is discretized with 200 elements.

Figures 16, 17, 18, and 19 respectively plot the time history of the displacement in the y-direction of the nodes along the elastic axis at the free end, three quarters of the length, half of the length, and one quarter of the length. These plots show the

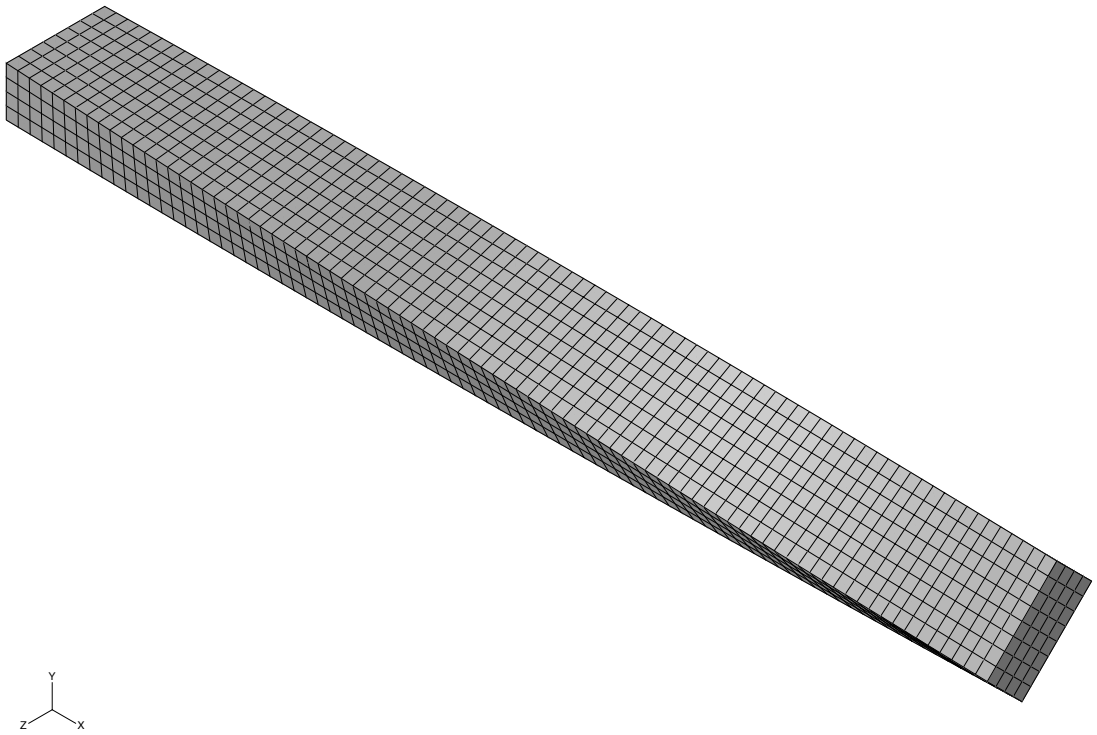

Figure 14. Twisted beam with 84×4×8 mesh.

results of Abaqus using linear and nonlinear geometric models as well as the linear and nonlinear versions of the beam model.

Similarly, Figures 20, 21, 22, and 23 respectively plot the time history of the displacement in the z-direction.

In Figures 16-23, the amplitudes of the four simulations are similar; however, there is a distinct difference between the frequencies of the linear and nonlinear models that is emphasized with the progression of time. The angle about the deformed elastic axis the cross section rotates at the free end is shown in Figure 24. Once more, the beam models compare favorably with the corresponding Abaqus simulations, and the computational time is shown in Table XII.

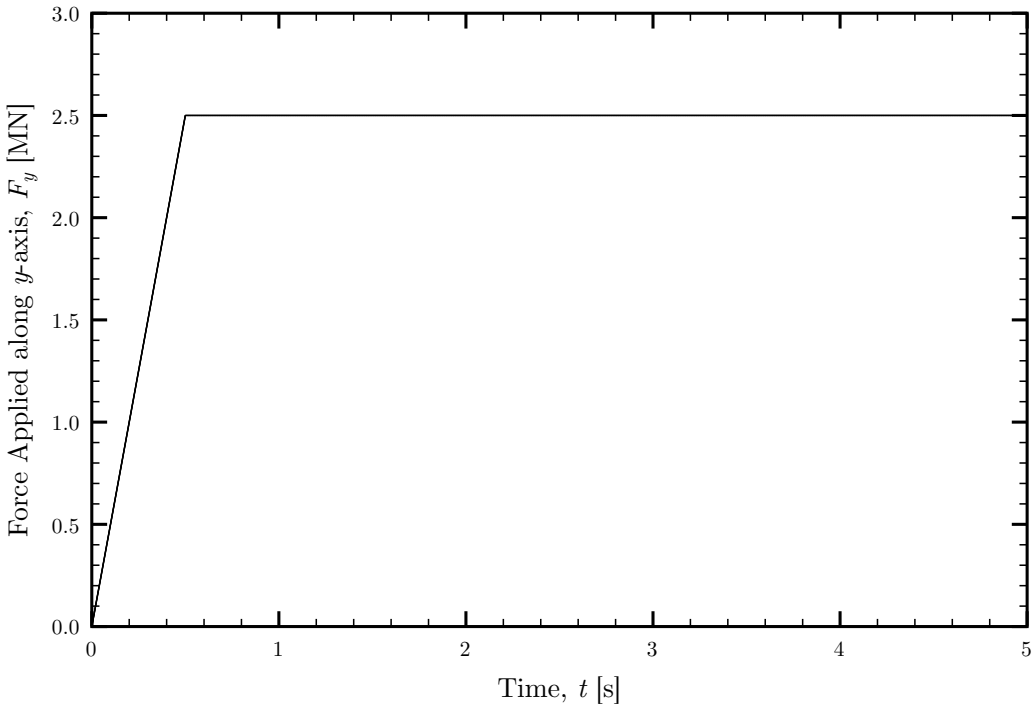

Figure 15. Force applied to twisted beam.

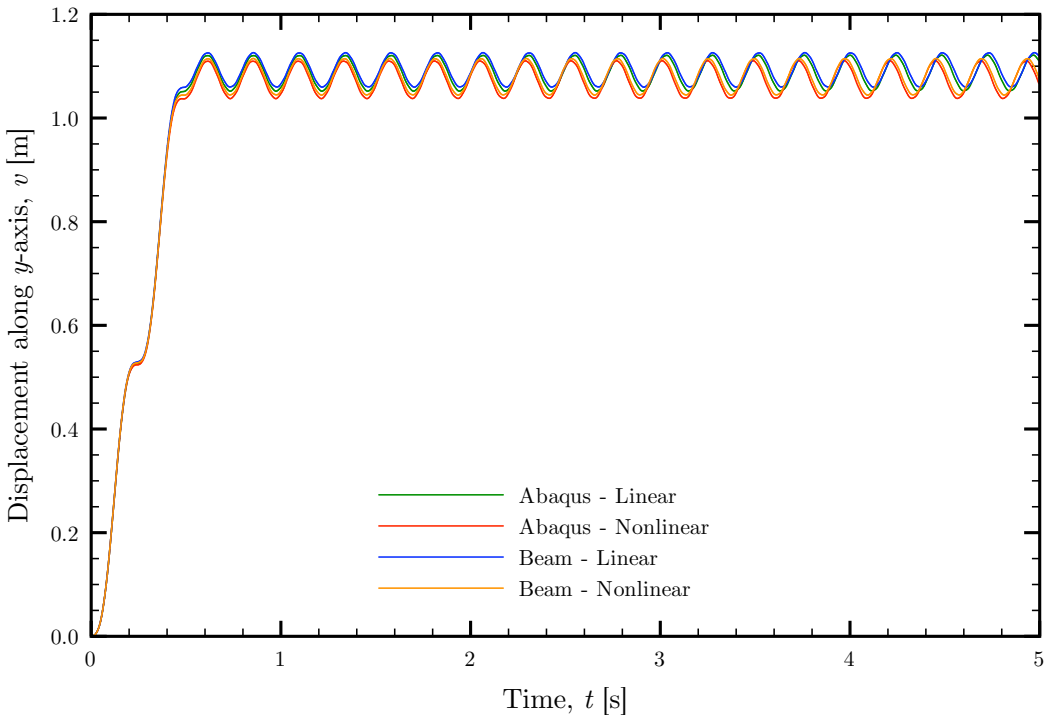

Figure 16. Twisted beam elastic axis displacement along y-axis at $s = L$.

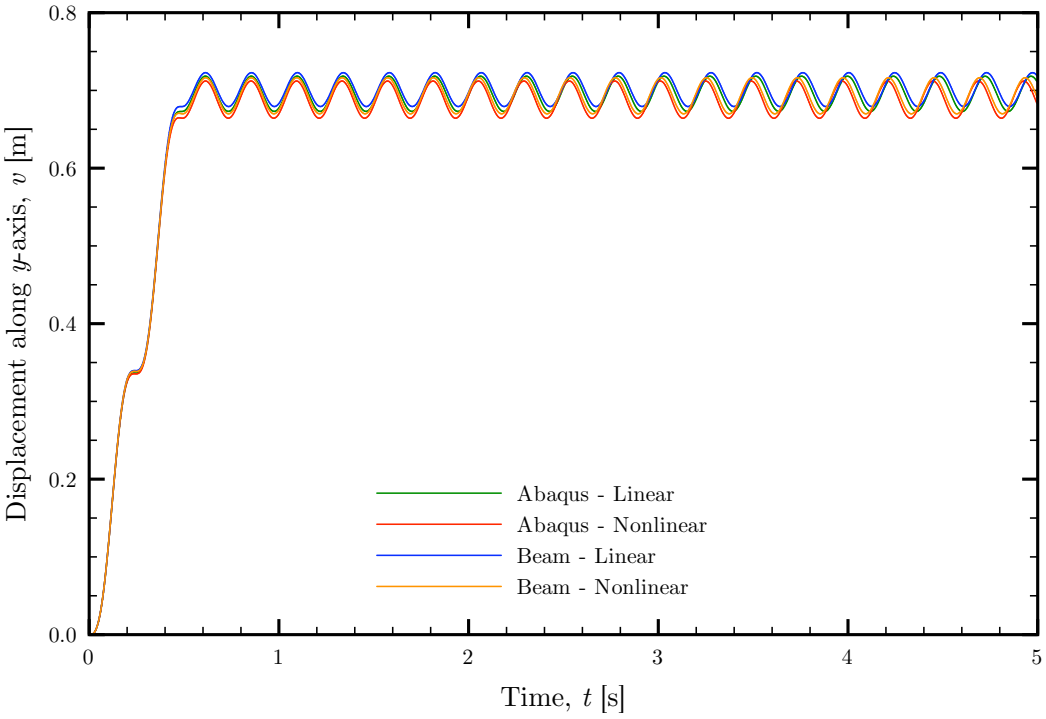

Figure 17. Twisted beam elastic axis displacement along y-axis at $s = \frac{3}{4}L$.

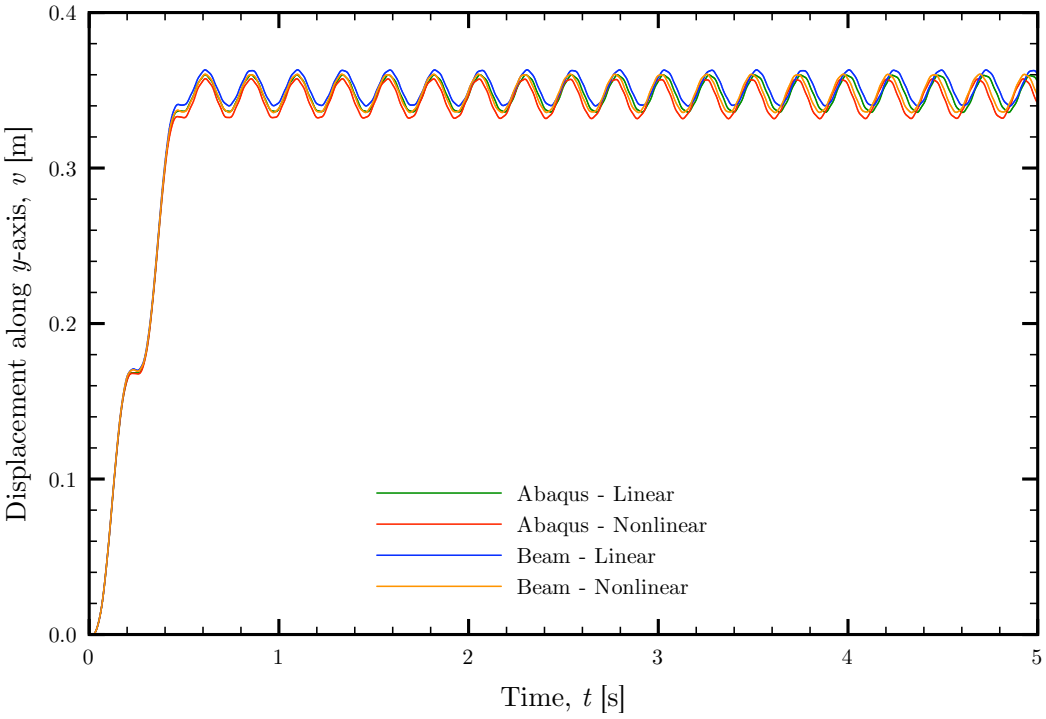

Figure 18. Twisted beam elastic axis displacement along y-axis at $s = \frac{1}{2}L$.

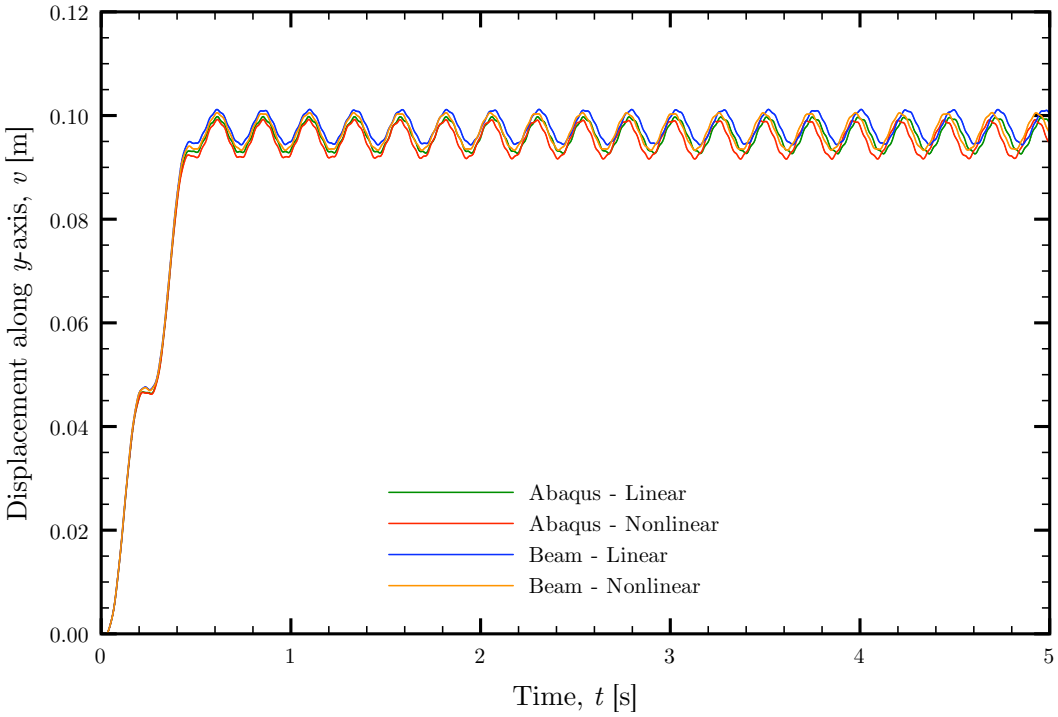

Figure 19. Twisted beam elastic axis displacement along y-axis at $s = \frac{1}{4}L$.

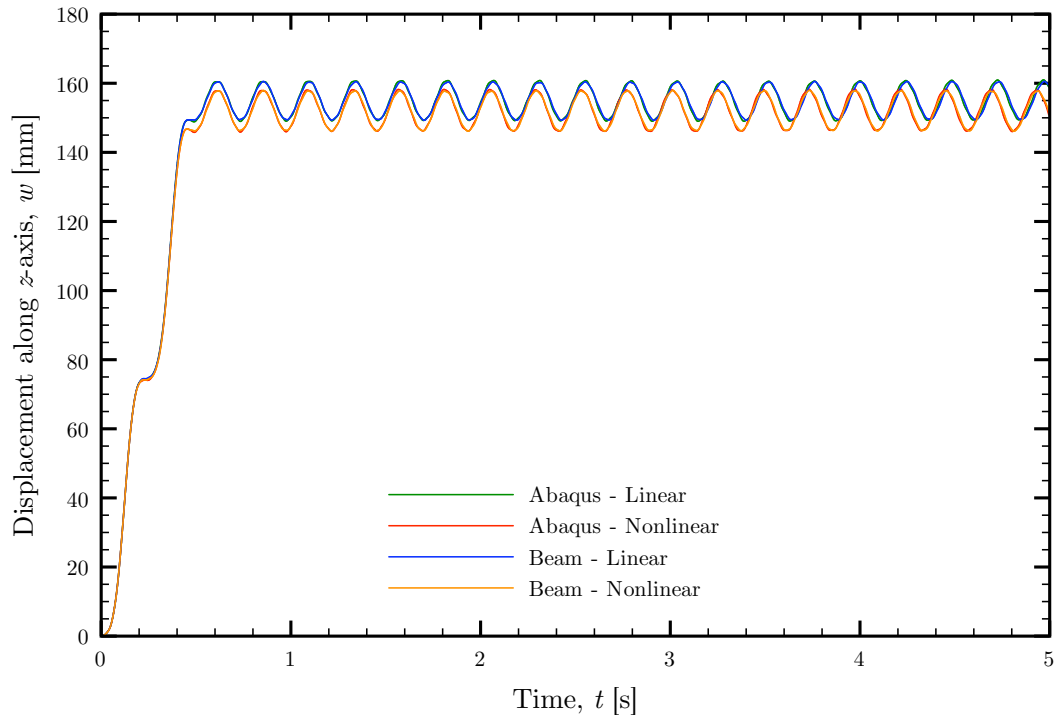

Figure 20. Twisted beam elastic axis displacement along z-axis at $s = L$.

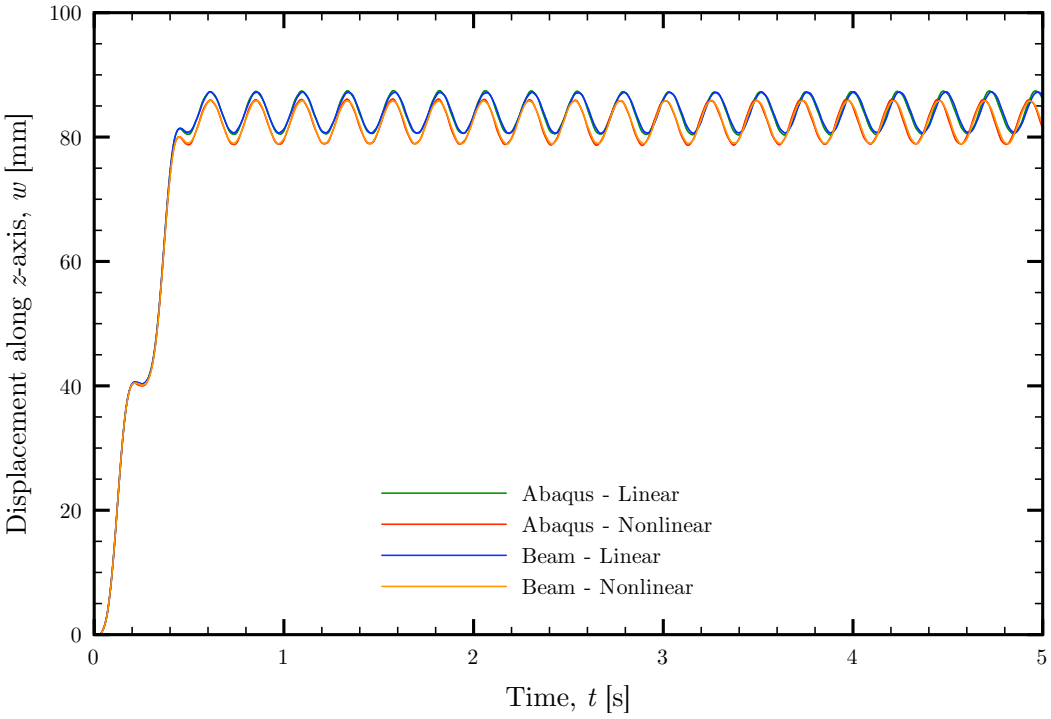

Figure 21. Twisted beam elastic axis displacement along z-axis at $s = \frac{3}{4}L$.

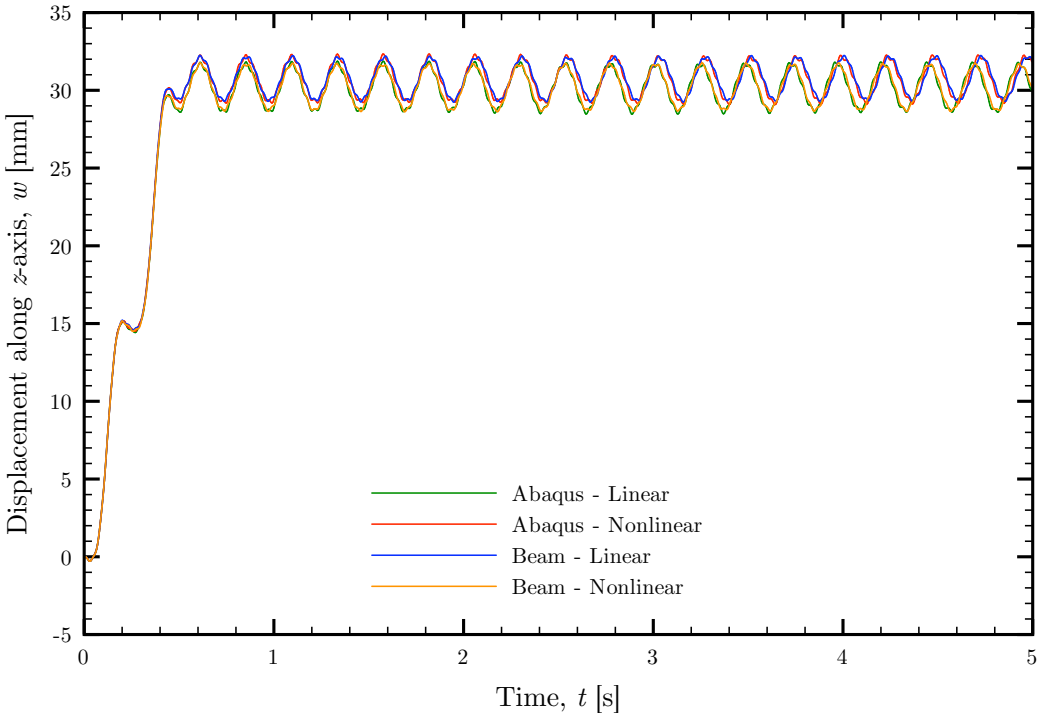

Figure 22. Twisted beam elastic axis displacement along z-axis at $s = \frac{1}{2}L$.

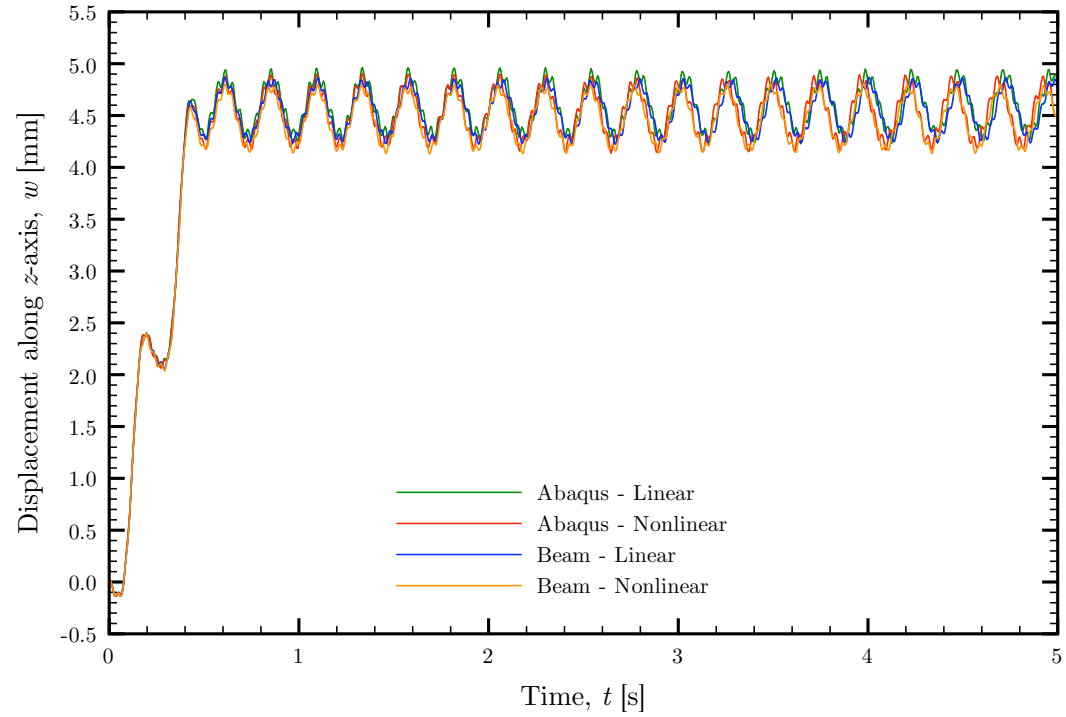

Figure 23. Twisted beam elastic axis displacement along z-axis at $s = \frac{1}{4}L$.

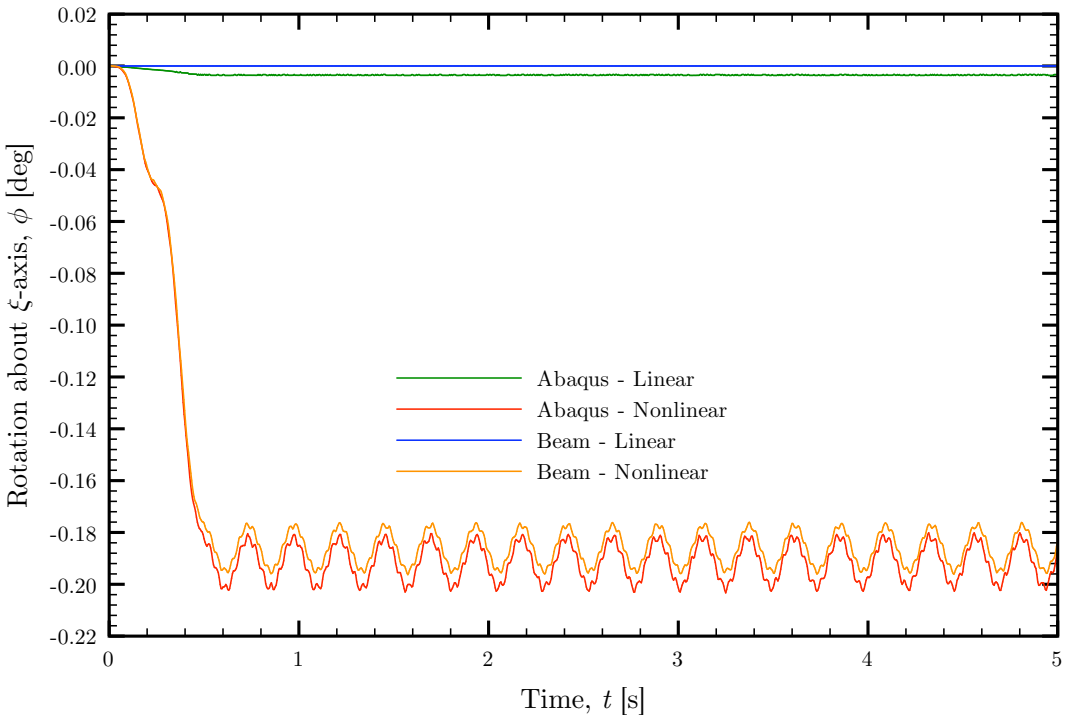

Figure 24. Twisted beam rotation about ξ-axis at $s = L$.

Table XII. Twisted beam computational time.

Method	Time
Abaqus - Linear	77 min
Abaqus - Nonlinear	299 min
Beam - Linear	10 min
Beam - Nonlinear	16 min

3. Case 3: A Composite Beam

The final beam used as a forced-response test case is a lengthwise-uniform composite beam. The beam consists of aluminum alloy 6061-T6 and a fabricated material that has the same Young's modulus and modulus of rigidity as the aluminum alloy but with half the density. Three quarters of the beam are the fabricated material, while the remaining quarter is aluminum. The beam is shown in Figure 25.

This beam is selected because it provides an example of a beam for which the mass and elastic centers of each cross section are offset in both dimensions. Furthermore, the principal bending and mass axes are orientated differently with respect to each other and to the reference coordinate system. Additionally, the constant Young's modulus and Poisson's ratio across the cross section facilitates calculation of an accurate value for the torsional stiffness. The beam is 100-m long with a 6 m $\times$ 4 m cross section. The properties of the composite beam are presented in Table XIII.

Table XIII. Properties of fabricated composite beam.

Parameter	Value
$e_\eta(s)$	0.2 m
$e_\zeta(s)$	-0.3 m
$m(s)$	4.0650×10^4 kg/m
$j_\xi(s)$	1.76150×10^5 kg m^2/m
$j_\eta(s)$	1.21950×10^5 kg m^2/m
$j_\zeta(s)$	0.54200×10^5 kg m^2/m
$j_{\eta\zeta}(s)$	0.12195×10^5 kg m^2/m
$D_\xi(s)$	1.95686×10^{12} N m^2
$D_\eta(s)$	5.04×10^{12} N m^2
$D_\zeta(s)$	2.24×10^{12} N m^2
$D_{\eta\zeta}(s)$	0 N m^2

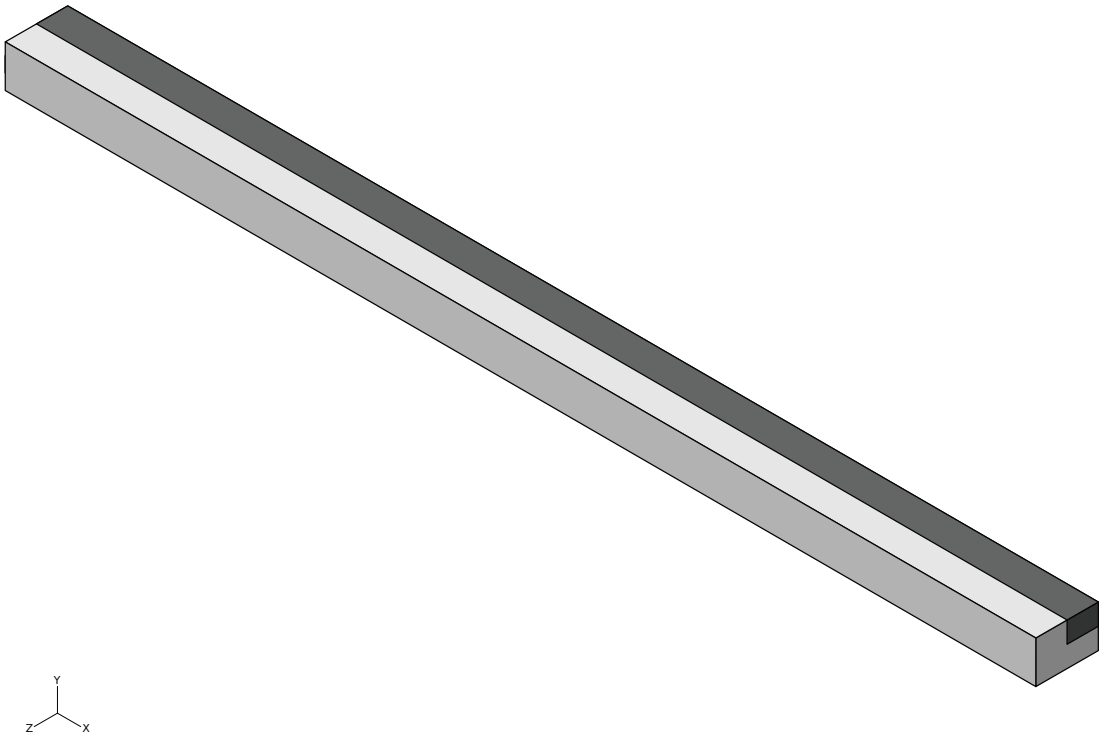

Figure 25. Fabricated composite beam.

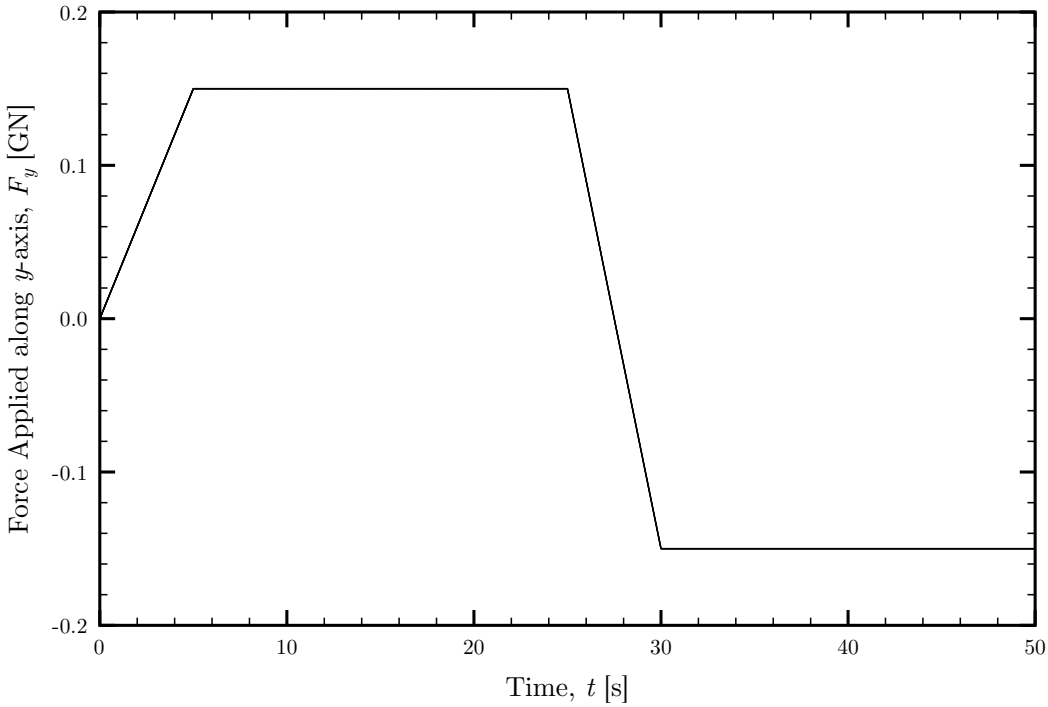

Figure 26. Force applied to composite beam.

This beam is discretized in Abaqus using 2400 (100×4×6) quadratic elements, and the time-dependent force plotted in Figure 26 is applied to the node at the intersection of the elastic axis and the free end. In Abaqus, this simulation spans 50 seconds with 5×10^{-2}-second time steps.

The beam model uses five shape functions for each of the three degrees of freedom. The time step is 10^{-3} seconds, and the beam is discretized with 200 elements.

Figures 27, 28, 29, and 30 respectively plot the time history of the displacement in the y-direction of the nodes along the elastic axis at the free end, three quarters of the length, half of the length, and one quarter of the length. Additionally, the angle about the deformed elastic axis the cross section rotates at the free end is shown in Figure 31. These plots show the results from Abaqus using linear and nonlinear geometric models as well as those from the linear and nonlinear versions of the beam model.

In Figures 27-31, the difference between the linear and nonlinear models is evident in both the amplitudes and the frequencies. The beam models continue to compare favorably with the Abaqus counterparts, and the computation time is shown in Table XIV.

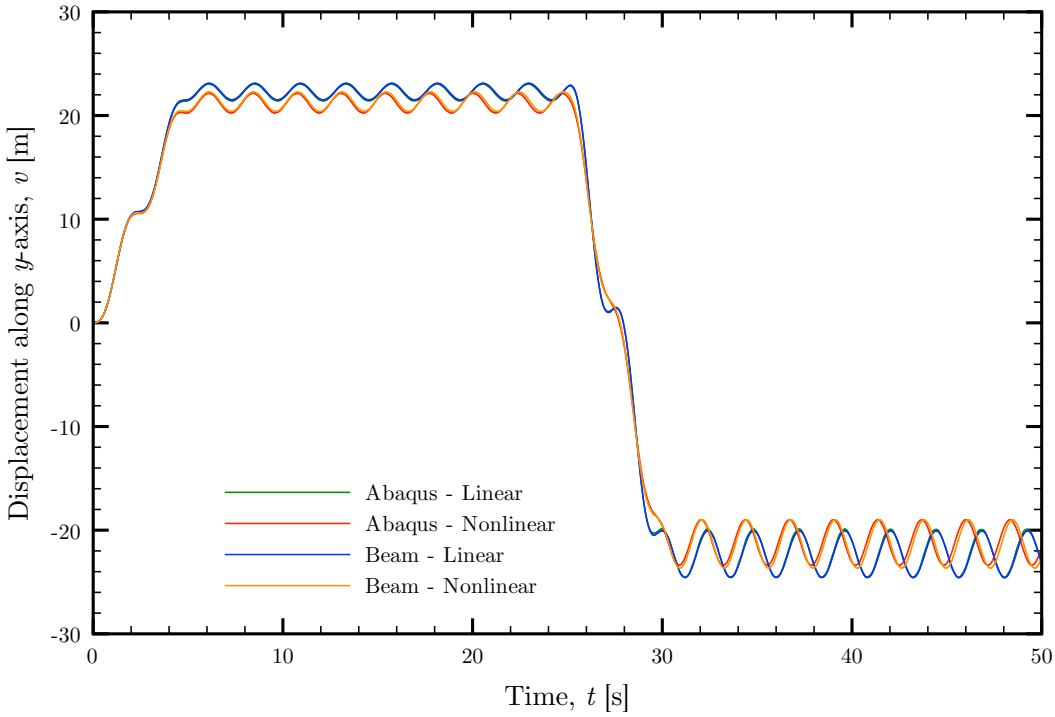

Figure 27. Composite beam elastic axis displacement along y-axis at $s = L$.

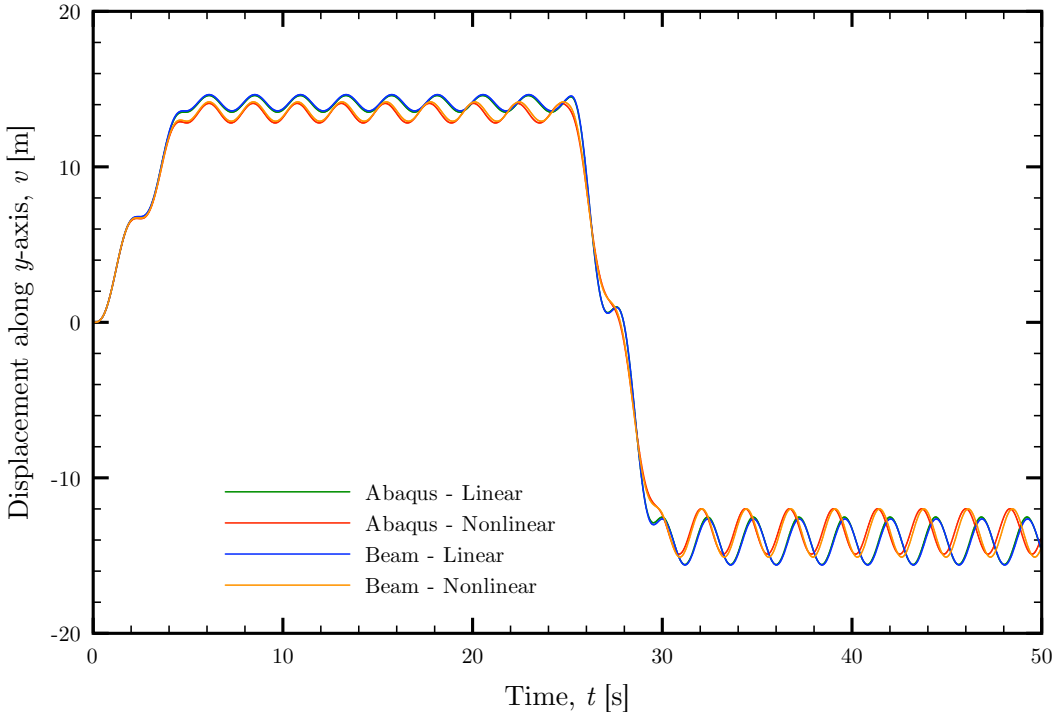

Figure 28. Composite beam elastic axis displacement along y-axis at $s = \frac{3}{4}L$.

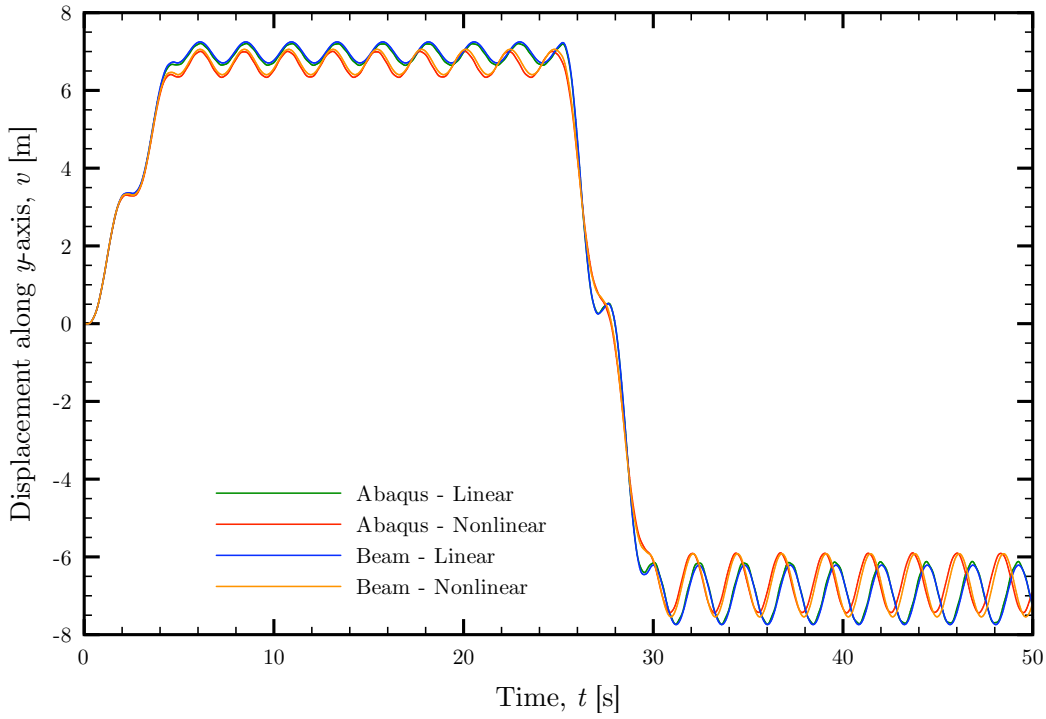

Figure 29. Composite beam elastic axis displacement along y-axis at $s = \frac{1}{2}L$.

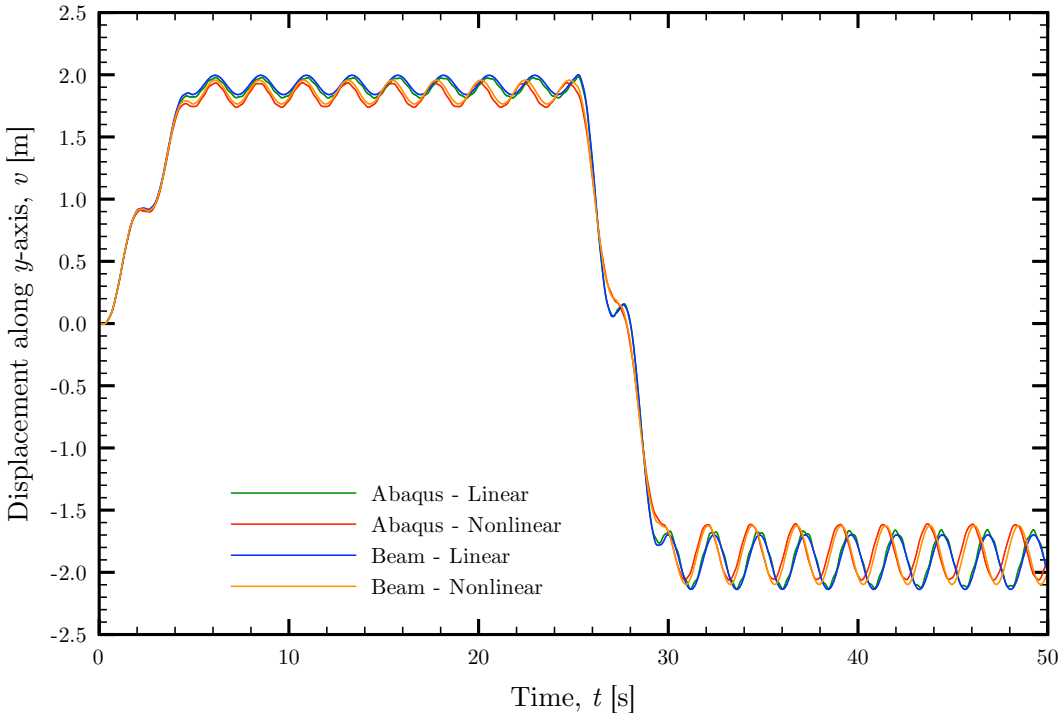

Figure 30. Composite beam elastic axis displacement along y-axis at $s = \frac{1}{4}L$.

Table XIV. Composite beam computational time.

Method	Time
Abaqus - Linear	66 min
Abaqus - Nonlinear	237 min
Beam - Linear	9 min
Beam - Nonlinear	17 min

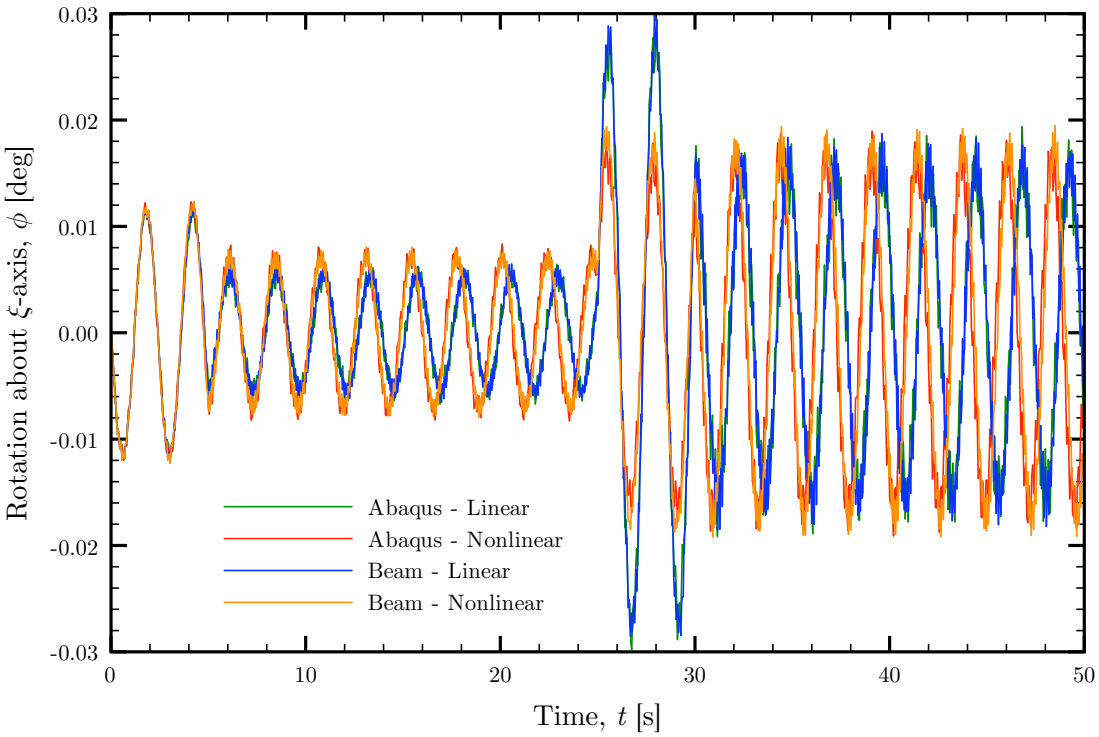

Figure 31. Composite beam rotation about ξ-axis at $s = L$.

CHAPTER VI

APPLICABILITY TO SWEPT WINGS

A. Introduction

The nonlinear beam model can also be extended to wings with moderate sweep for which the elastic axes are straight when undeformed [1, pp. 604-613]. For this approximation to yield meaningful results, the wing cannot be heavily swept or of a low aspect ratio as warping at the fixed end would invalidate the rigid cross section assumption.

B. Definition of Parameters

For the case of the swept wing, the fixed end of the structural model is located at the fixed end of the elastic axis and is normal to the elastic axis as seen in Figure 32. Likewise, the free end is located at the free end of the elastic axis and is normal to the elastic axis. The beam reference axes are rotated about the aerodynamic y-axis by $-\Lambda_{ea}$. Correspondingly, beam properties are given in the beam reference frame instead of the aerodynamic reference frame.

C. Validity

To demonstrate the effect of sweep on the fidelity of the beam model, the first eight frequencies of two swept cases are compared with the unswept representation. Both cases consider an aluminum alloy 6061-T6 structure for which the length of the elastic axis is 10 m. The unswept representation for each case is a 10-m long beam with a 1 m $\times$ 0.2 m rectangular cross section and is depicted in Figure 33. The first case

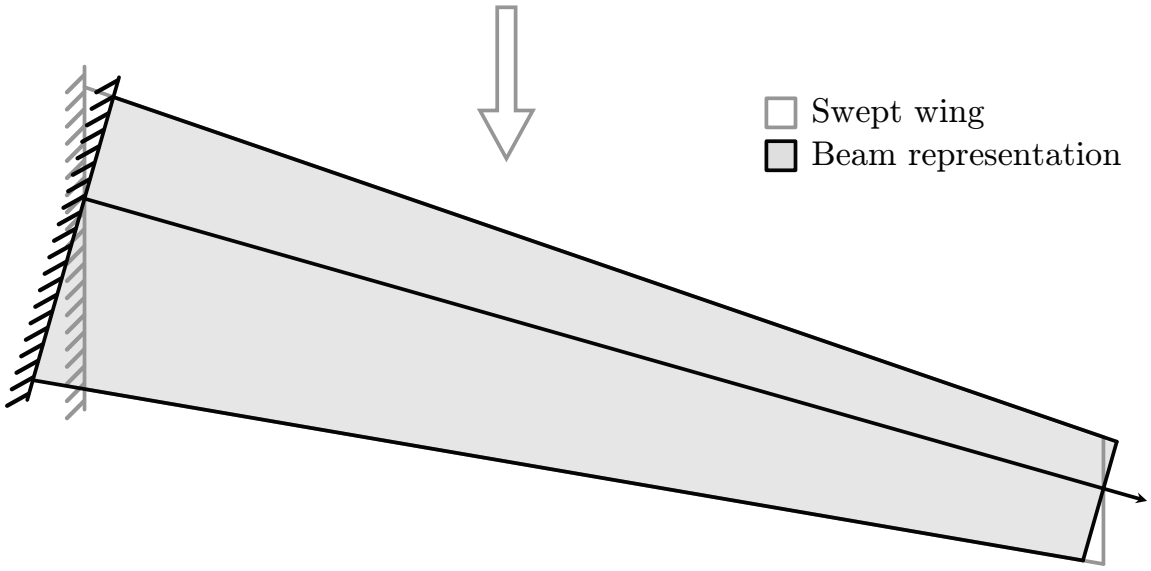

Figure 32. Beam representation of swept wing.

features an elastic axis with a sweep angle of 20°. For the second case, the sweep angle is increased to 45°.

The two swept cases are modeled in Abaqus, while the unswept representation is modeled using both Abaqus and the beam model. The finite element model of the unswept representation uses 13,104 quadratic three-dimensional continuum elements ($182 \times 4 \times 18$), and the beam model uses five shape functions for each of the three independent degrees of freedom.

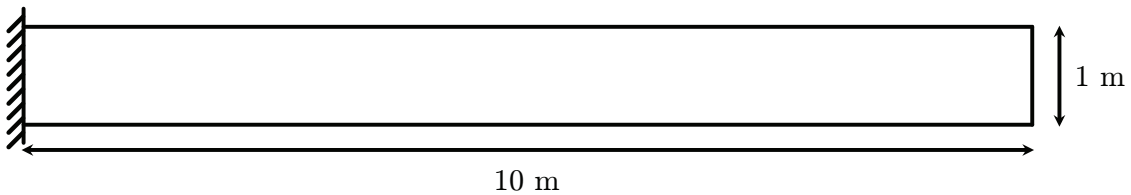

Figure 33. Unswept representation of swept structures.

1. Case 1: 20° Swept Structure

The first case consists of a 20° swept structure as shown in Figure 34. This structure is discretized in Abaqus using 13,832 quadratic three-dimensional continuum elements ($182 \times 4 \times 19$), and the first eight natural frequencies are calculated.

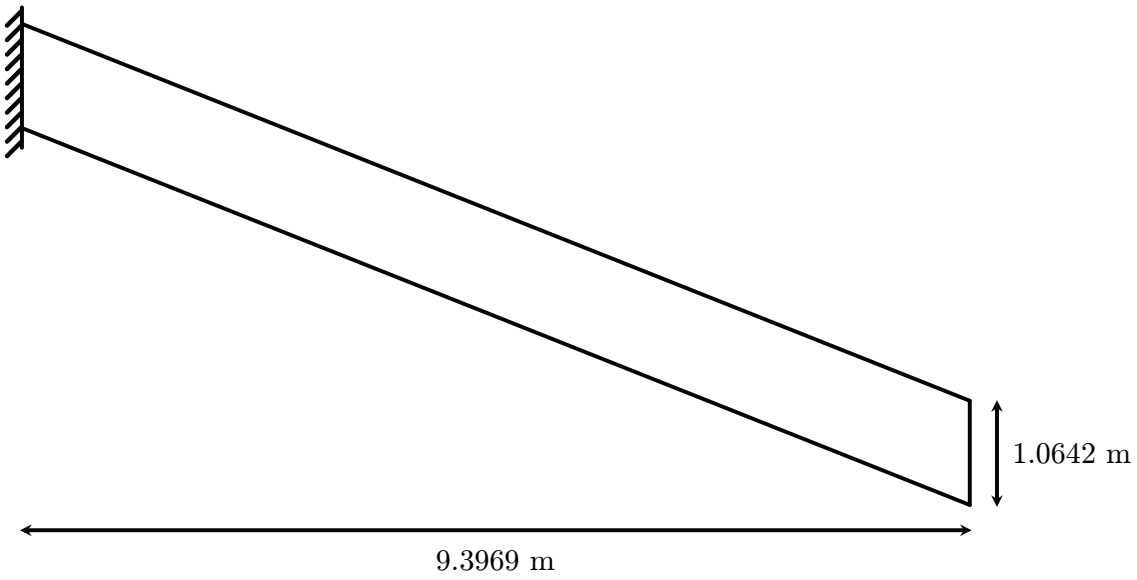

Figure 34. 20° swept structure.

Table XV lists the frequencies of the 20° swept structure calculated by Abaqus. Additionally, the frequencies of the unswept structure calculated by Abaqus and the beam model are included as well as the error relative to the frequencies of the 20° swept structure.

Though the error associated with the beam model of the unswept representation is greater than that of the finite element model of the unswept representation, the results remain reasonable within 4% of the finite element model of the 20° swept structure.

Table XV. First eight frequencies of 20° swept structure.

Mode	Swept FEM [Hz]	Unswept FEM [Hz]	FEM Error [%]	Unswept Beam [Hz]	Beam Error [%]
1	1.6671	1.6524	0.882	1.6420	1.50
2	8.2207	8.1645	0.684	8.2130	0.0941
3	10.410	10.335	0.720	10.288	1.17
4	29.014	28.869	0.500	28.395	2.13
5	29.340	29.221	0.406	28.791	1.87
6	49.244	48.941	0.615	51.168	3.91
7	56.751	56.397	0.624	56.369	0.673
8	87.420	88.056	0.728	85.186	2.56

2. Case 2: 45° Swept Structure

The second case extends the sweep angle of the structure to 45° and is shown in Figure 35. This structure is discretized in Abaqus using 17,500 quadratic three-dimensional continuum elements ($175 \times 4 \times 25$), and the first eight natural frequencies are calculated once more.

The frequencies of the 45° swept structure calculated by Abaqus are tabulated in Table XVI. Additionally, the frequencies of the unswept structure calculated by Abaqus and the beam model are included as well as the error relative to the frequencies of the 45° swept structure. The error has increased significantly compared to the 20° case; however, the values remain reasonable considering the amount of sweep, and the error associated with the beam model is less than 6%.

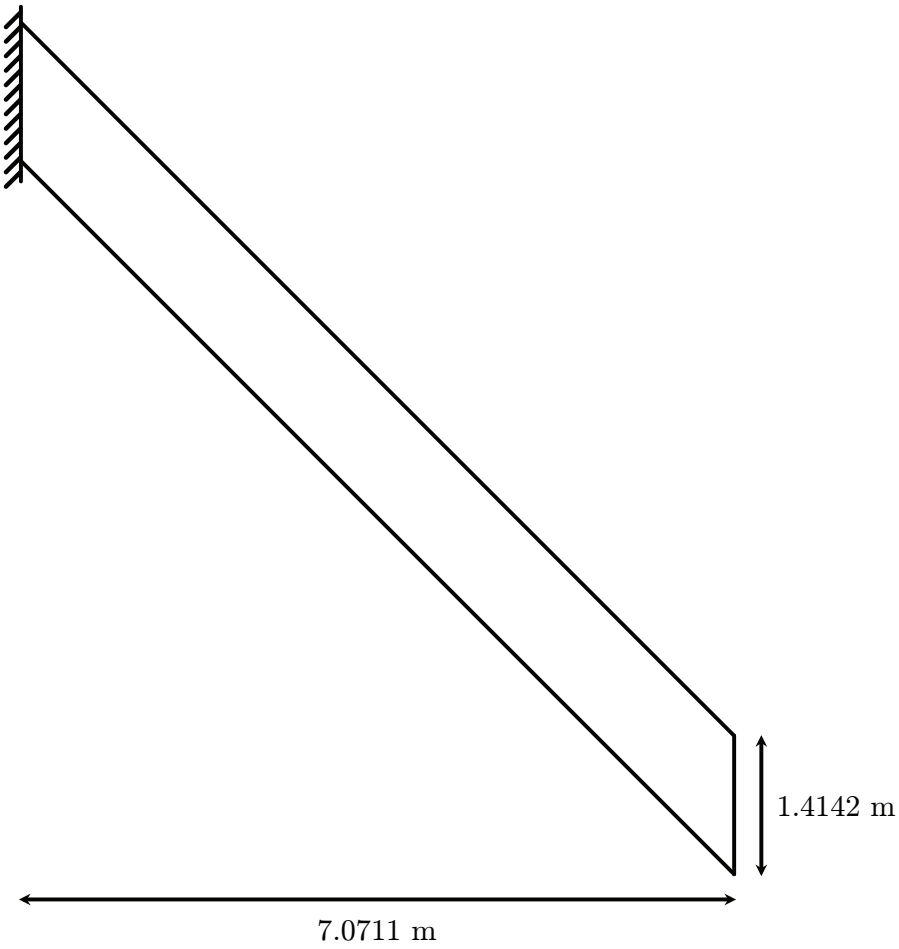

Figure 35. 45° swept structure.

Table XVI. First eight frequencies of 45° swept structure.

Mode	Swept FEM [Hz]	Unswept FEM [Hz]	FEM Error [%]	Unswept Beam [Hz]	Beam Error [%]
1	1.7413	1.6524	5.11	1.6420	5.70
2	8.5252	8.1645	4.23	8.2130	3.66
3	10.781	10.335	4.14	10.288	4.57
4	29.410	28.869	1.84	28.395	3.45
5	30.408	29.221	3.90	28.791	5.32
6	50.801	48.941	3.66	51.168	0.723
7	58.390	56.397	3.41	56.369	3.46
8	86.613	88.056	1.67	85.186	1.65

CHAPTER VII

RESULTS

A. A Comparison between Quadratic and Cubic Nonlinearities

In deriving the nonlinear equations of motion, the order must be consistently selected so as to accurately model the motion of the beam while avoiding an unnecessary computational burden. Therefore, quadratic and cubic models are generally the candidates of choice. In this section, the difference between the two orders is shown, confirming the importance of retaining cubic nonlinearities.

1. Quadratic Nonlinear Matrices

Neglecting the cubic terms of the nonlinear matrices presented in equations (3.9)-(3.11) results in the following nonzero contributions to the nonlinear matrices.

The nonzero submatrices of the nonlinear mass matrix are

$$\begin{aligned}[M_{NL}]_{i,j} = \int_0^L \Bigg\{ & W_i' m e_\zeta \int_0^s w' W_j' d\hat{s} - W_i' m e_\zeta w' W_j \\ & - W_i' w' \int_L^s m e_\zeta W_j' d\hat{s} - 2 W_i' j_{\eta\zeta} \phi W_j' - W_i m e_\zeta w' W_j' \Bigg\} ds \\ & - \left[W_i m e_\zeta \int_0^s w' W_j' d\hat{s} - W_i m e_\zeta w' W_j - 2 W_i j_{\eta\zeta} \phi W_j' \right]_{s=L},\end{aligned}$$

$$\begin{aligned}[M_{NL}]_{i,l+j} = \int_0^L \Bigg\{ & W_i' m e_\zeta \int_0^s v' W_j' d\hat{s} - W_i' m e_\zeta v' W_j \\ & - W_i' w' \int_L^s m e_\eta W_j' d\hat{s} + W_i' \left(-j_\eta \phi + j_\zeta \phi \right) W_j' \Bigg\} ds \\ & - \left[W_i m e_\zeta \int_0^s v' W_j' d\hat{s} - W_i m e_\zeta v' W_j + W_i \left(-j_\eta \phi + j_\zeta \phi \right) W_j' \right]_{s=L},\end{aligned}$$

$$[M_{NL}]_{i,l+m+j} = -\int_0^L W_i m e_\zeta \phi \Phi_j ds,$$

$$\begin{aligned}[M_{NL}]_{l+i,j} = &\int_0^L \Big\{ W_i' m e_\eta \int_0^s w' W_j' d\hat{s} - W_i' v' \int_L^s m e_\zeta W_j' d\hat{s} \\ &- W_i m e_\zeta v' W_j' + W_i' \left(-j_\eta \phi + j_\zeta \phi\right) W_j' \Big\} ds \\ &- \left[W_i m e_\eta \int_0^s w' W_j' d\hat{s} - W_i m e_\zeta v' W_j + W_i \left(-j_\eta \phi + j_\zeta \phi\right) W_j' \right]_{s=L},\end{aligned}$$

$$\begin{aligned}[M_{NL}]_{l+i,l+j} = &\int_0^L \Big\{ W_i' m e_\eta \int_0^s v' W_j' d\hat{s} - W_i' \left[m e_\eta v' + m e_\zeta w' \right] W_j \\ &- W_i' v' \int_L^s m e_\eta W_j' d\hat{s} - W_i \left[m e_\eta v' + m e_\zeta w' \right] W_j' \\ &+ 2 W_i' j_{\eta\zeta} \phi W_j' \Big\} ds - \Big[W_i m e_\eta \int_0^s v' W_j' d\hat{s} \\ &- W_i \left[m e_\eta v' + m e_\zeta w' \right] W_j + 2 W_i j_{\eta\zeta} \phi W_j' \Big]_{s=L},\end{aligned}$$

$$[M_{NL}]_{l+i,l+m+j} = \int_0^L \Big\{ W_i' j_\xi w' \Phi_j - W_i m e_\eta \phi \Phi_j \Big\} ds - \left[W_i j_\xi w' \Phi_j \right]_{s=L},$$

$$[M_{NL}]_{l+m+i,j} = -\int_0^L \Phi_i m e_\zeta \phi W_j ds,$$

$$[M_{NL}]_{l+m+i,l+j} = \int_0^L \Phi_i \Big\{ j_\xi w' W_j' - m e_\eta \phi W_j \Big\} ds.$$

The nonzero submatrices of the nonlinear damping matrix are

$$[C_{NL}]_{i,j} = \int_0^L \left\{ W_i' m e_\zeta \int_0^s \dot{w}' W_j' d\hat{s} - W_i m e_\zeta \dot{w}' W_j' \right\} ds - \left[W_i m e_\zeta \int_0^s \dot{w}' W_j' d\hat{s} \right]_{s=L},$$

$$[C_{NL}]_{i,l+j} = \int_0^L \left\{ W_i' m e_\zeta \int_0^s \dot{v}' W_j' d\hat{s} \right\} ds - \left[W_i m e_\zeta \int_0^s \dot{v}' W_j' d\hat{s} \right]_{s=L},$$

$$[C_{NL}]_{i,l+m+j} = \int_0^L \left\{ - W_i m e_\zeta \dot{\phi} \Phi_j + W_i' \left(-2 j_{\eta\zeta} \dot{w}' - j_\xi \dot{v}' - j_\eta \dot{v}' + j_\zeta \dot{v}' \right) \Phi_j \right\} ds - \left[W_i \left(-2 j_{\eta\zeta} \dot{w}' - j_\xi \dot{v}' - j_\eta \dot{v}' + j_\zeta \dot{v}' \right) \Phi_j \right]_{s=L},$$

$$[C_{NL}]_{l+i,j} = \int_0^L \left\{ W_i' m e_\eta \int_0^s \dot{w}' W_j' d\hat{s} \right\} ds - \left[W_i m e_\eta \int_0^s \dot{w}' W_j' d\hat{s} \right]_{s=L},$$

$$[C_{NL}]_{l+i,l+j} = \int_0^L \left\{ W_i' m e_\eta \int_0^s \dot{v}' W_j' d\hat{s} - W_i \left[m e_\eta \dot{v}' + 2 m e_\zeta \dot{w}' \right] W_j' \right\} ds - \left[W_i m e_\eta \int_0^s \dot{v}' W_j' d\hat{s} \right]_{s=L},$$

$$[C_{NL}]_{l+i,l+m+j} = \int_0^L \left\{ - W_i m e_\eta \dot{\phi} \Phi_j + W_i' \left(2 j_{\eta\zeta} \dot{v}' + j_\xi \dot{w}' - j_\eta \dot{w}' + j_\zeta \dot{w}' \right) \Phi_j \right\} ds - \left[W_i \left(2 j_{\eta\zeta} \dot{v}' + j_\xi \dot{w}' - j_\eta \dot{w}' + j_\zeta \dot{w}' \right) \Phi_j \right]_{s=L},$$

$$[C_{NL}]_{l+m+i,j} = \int_0^L \Phi_i j_{\eta\zeta} \dot{w}' W_j' ds,$$

$$[C_{NL}]_{l+m+i,l+j} = \int_0^L \left\{ - \Phi_i j_{\eta\zeta} \dot{v}' W_j' + \Phi_i \left(j_\xi \dot{w}' + j_\eta \dot{w}' - j_\zeta \dot{w}' \right) W_j' \right\} ds.$$

The nonzero submatrices of the nonlinear stiffness matrix are

$$[K_{NL}]_{i,l+m+j} = \int_0^L \left\{ W_i' D_\xi v'' \Phi_j' + W_i'' \left(-D_\eta v'' + D_\zeta v'' \right) \Phi_j - 2 W_i'' D_{\eta\zeta} w'' \Phi_j \right\} ds,$$

$$[K_{NL}]_{l+i,l+m+j} = \int_0^L \left\{ W_i'' \left(-D_\eta w'' + D_\zeta w'' + 2 D_{\eta\zeta} v'' \right) \Phi_j + W_i'' D_\xi w' \Phi_j' \right\} ds + \left[W_i D_\xi w' \Phi_j'' \right]_{s=L},$$

$$[K_{NL}]_{l+m+i,j} = \int_0^L \left\{ -\Phi_i D_{\eta\zeta} w'' W_j'' + \Phi_i' D_\xi v'' W_j' \right\} ds,$$

$$[K_{NL}]_{l+m+i,l+j} = \int_0^L \Phi_i \left(-D_\eta w'' + D_\zeta w'' + D_{\eta\zeta} v'' \right) W_j'' ds.$$

One of the most significant differences between the quadratic and cubic models is the removal of the diagonal submatrices from the nonlinear stiffness matrix. The implications of the order reduction are seen in the displacement history of the three forced cases used for validation.

2. Quadratic and Cubic Model Response History

As shown in Chapter V, the cubic nonlinear beam model performs well for the forced-response test cases compared to the nonlinear version of Abaqus. In this section, the three forced cases are presented once more to show the difference between the linear-, quadratic-, and cubic-order models.

Figures 36 and 37 show the response of the beam model for the tapered beam when linear, quadratic, and cubic terms are retained. The first- and second-order models are virtually indistinguishable, while the cubic model is noticeably different.

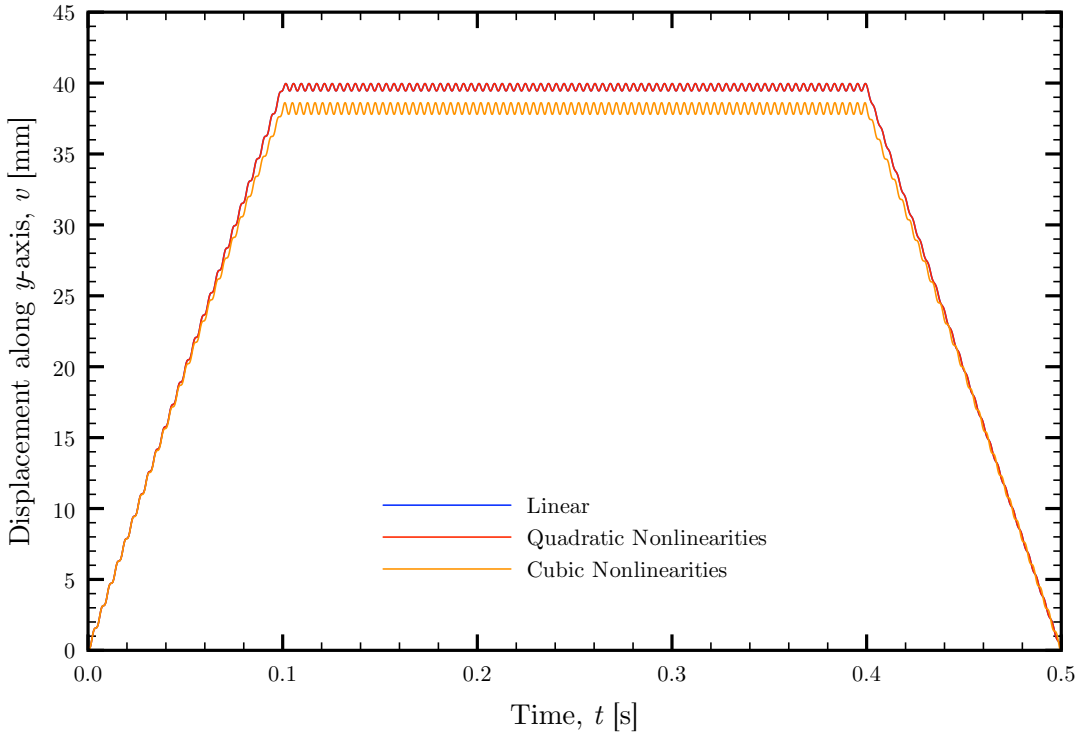

Figure 36. Tapered beam elastic axis displacement along y-axis at $s = L$ for first three orders of beam model.

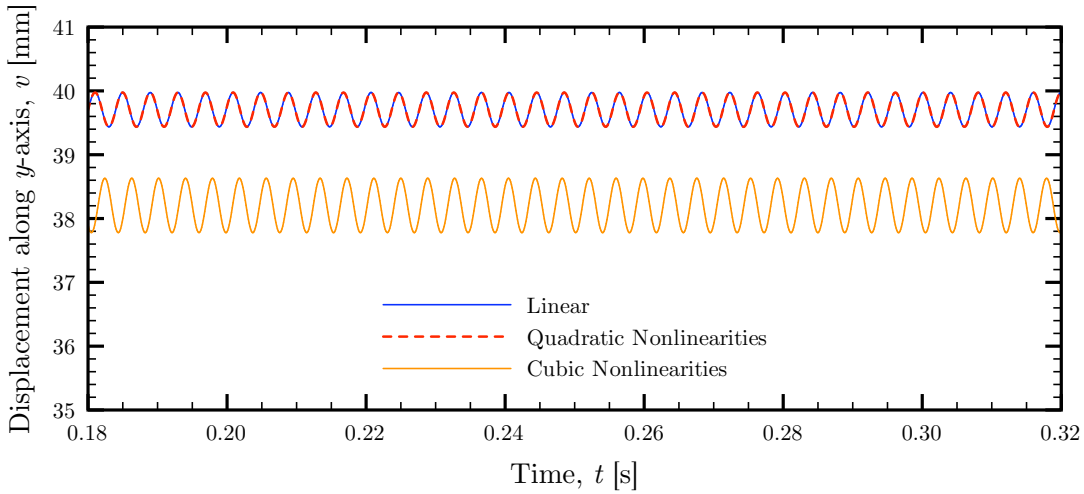

Figure 37. Detailed tapered beam elastic axis displacement along y-axis at $s = L$ for first three orders of beam model.

The response of the twisted beam is presented in Figures 38-42. As with the tapered beam, the quadratic-order beam model is considerably closer to the linear model than to the cubic model for the transverse displacements. However, the quadratic model yields a rotation noticeably greater than that provided by the cubic model. Additionally, there is a slight difference in the frequency of the rotation, resulting in a phase difference that increases in time.

The response of the composite beam is shown in Figures 43-45. The displacement in the y-direction is analogous to that for the previous two cases. Unlike the previous case, the rotational displacement of the quadratic model is much closer to the linear model.

Table XVII lists the computational time of the three orders of the beam model for each of the three beam cases. The additional computational cost that arises in the nonlinear analysis is largely due to the calculation of the time-dependent, nonlinear matrices. Though the quadratic model requires fewer computations than the cubic model, the nonlinear computational burden is disproportional to the increase in fidelity. These results confirm the importance of retaining cubic terms in nonlinear analysis.

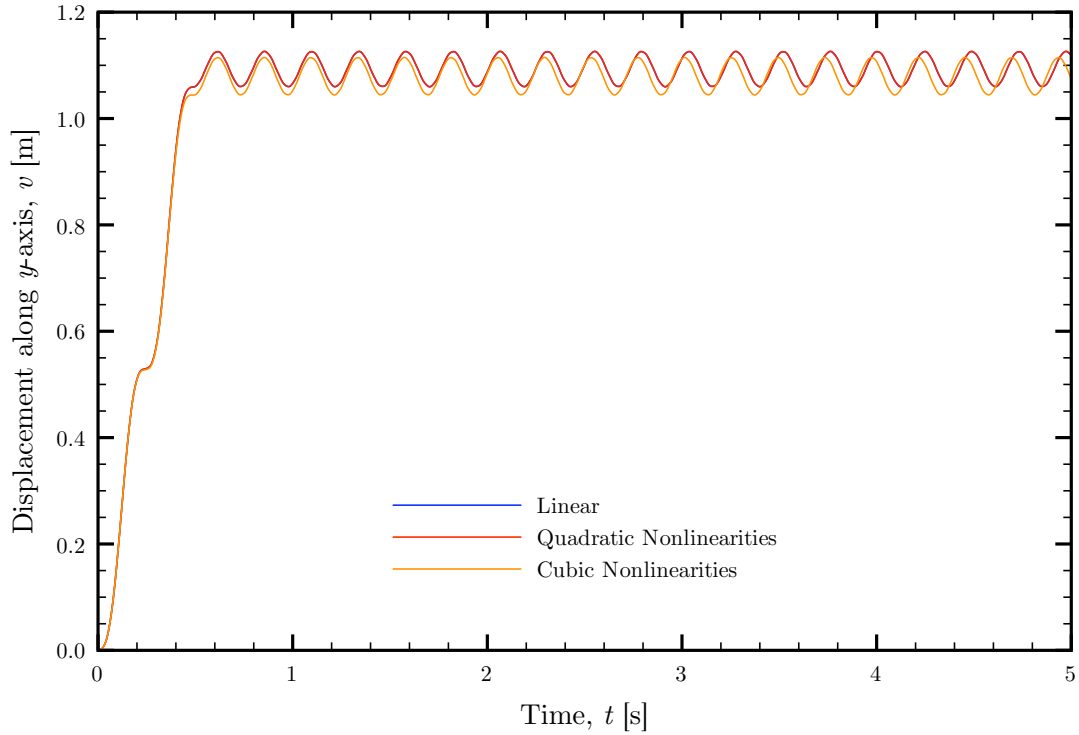

Figure 38. Twisted beam elastic axis displacement along y-axis at $s = L$ for first three orders of beam model.

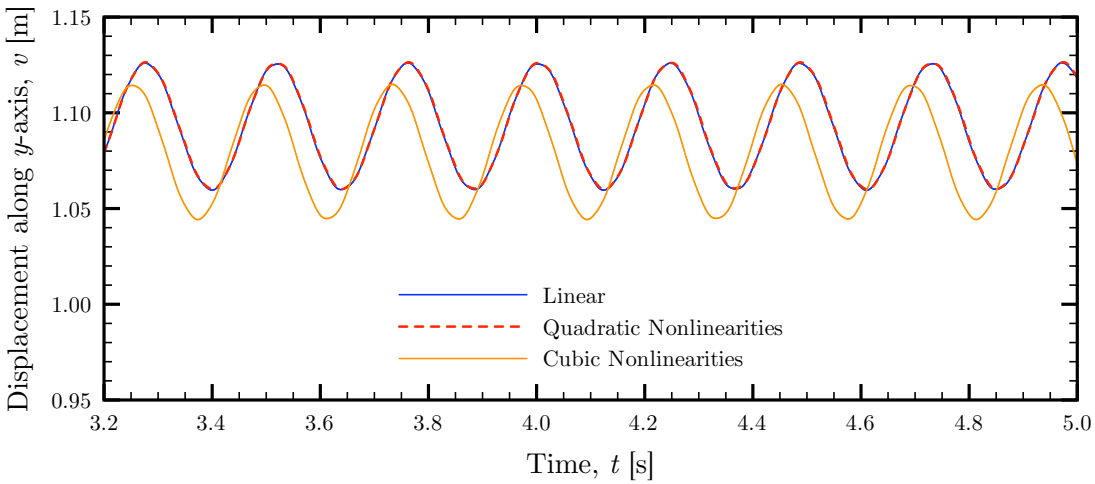

Figure 39. Detailed twisted beam elastic axis displacement along y-axis at $s = L$ for first three orders of beam model.

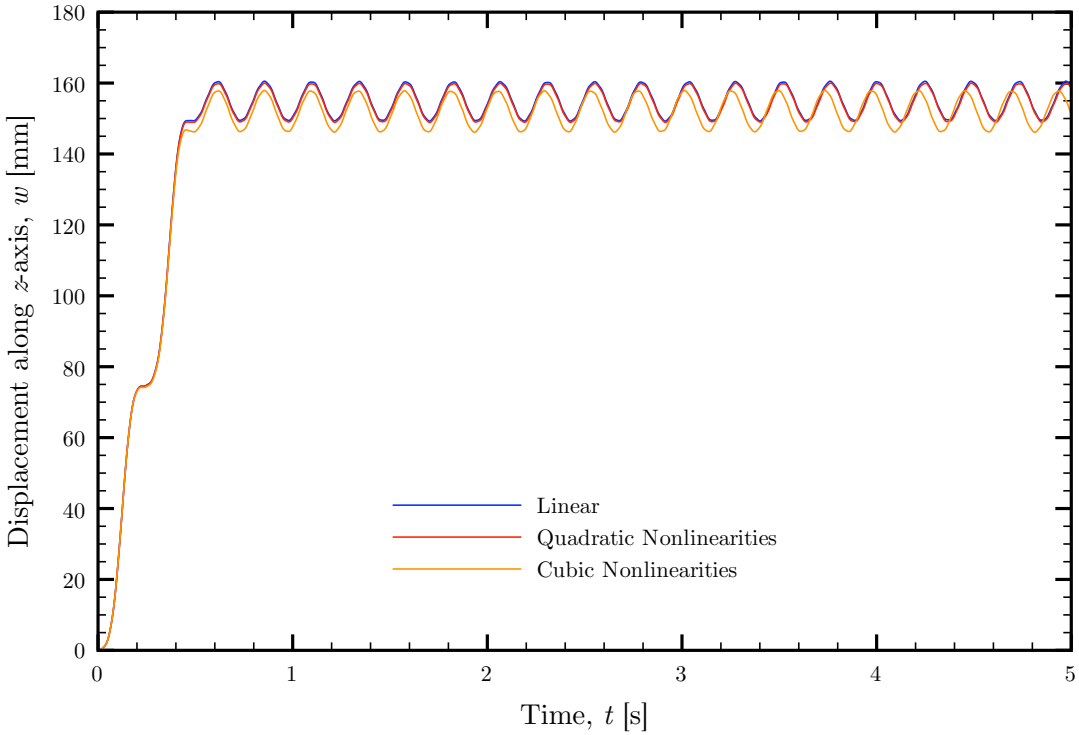

Figure 40. Twisted beam elastic axis displacement along z-axis at $s = L$ for first three orders of beam model.

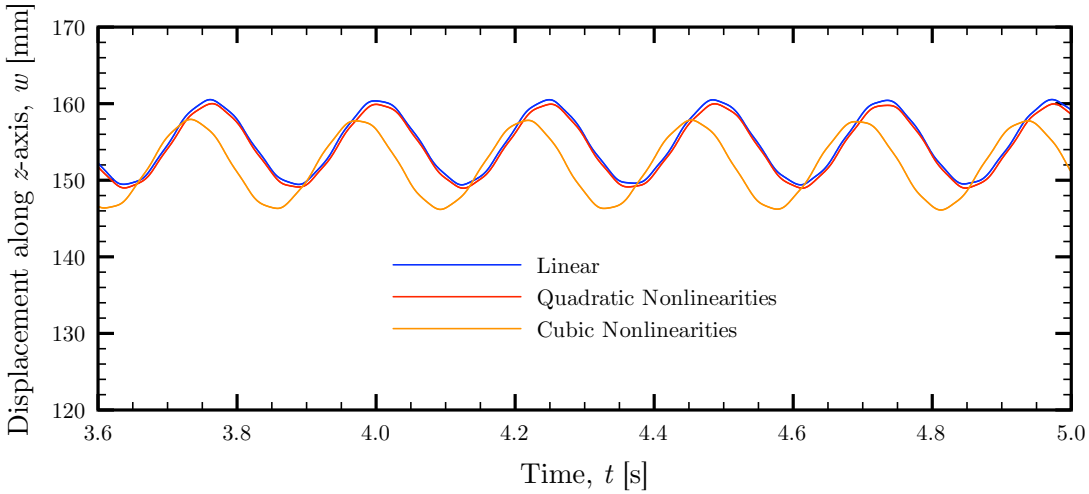

Figure 41. Detailed twisted beam elastic axis displacement along z-axis at $s = L$ for first three orders of beam model.

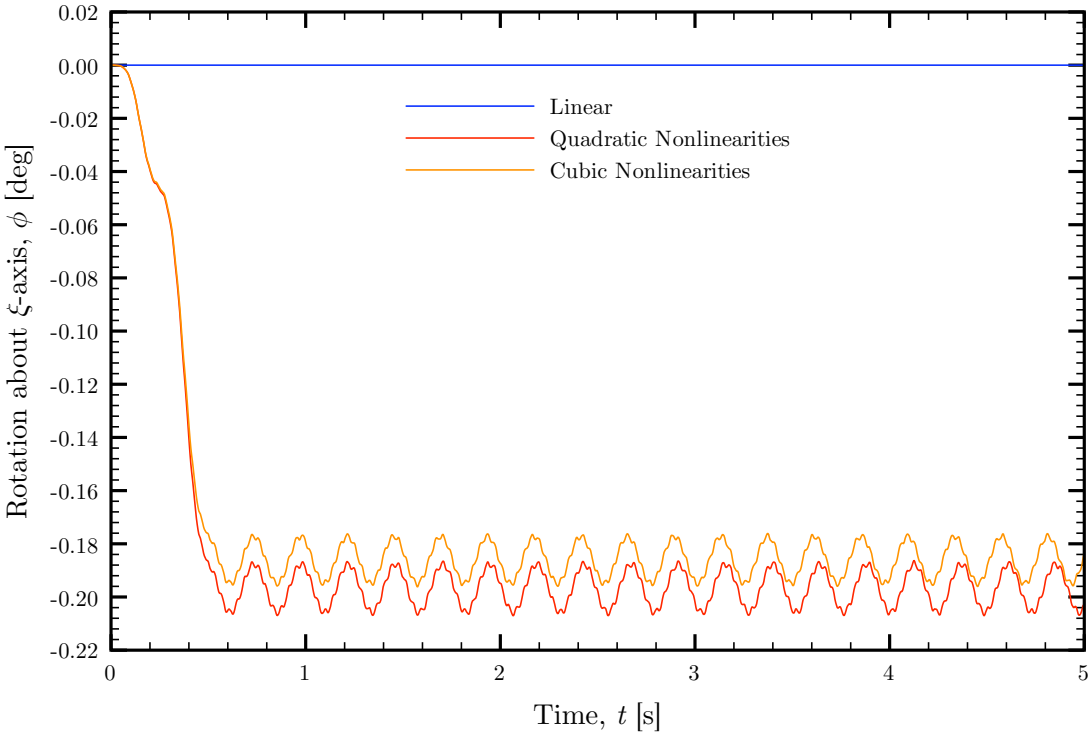

Figure 42. Twisted beam rotation about ξ-axis at $s = L$ for first three orders of beam model.

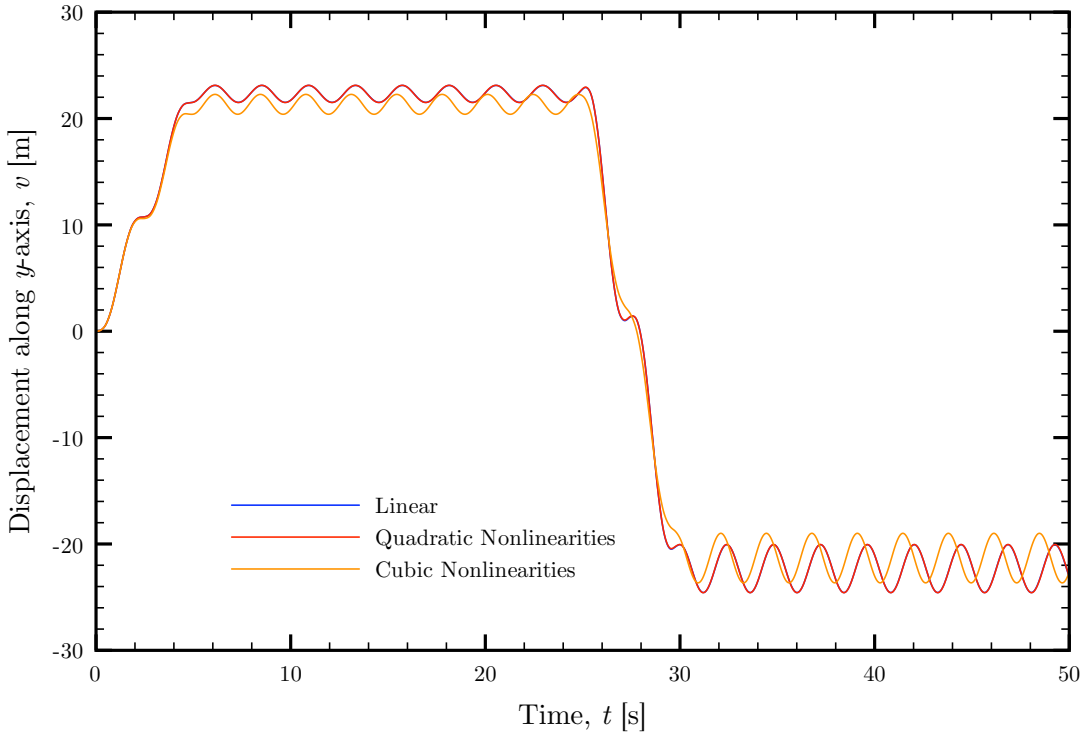

Figure 43. Composite beam elastic axis displacement along y-axis at $s = L$ for first three orders of beam model.

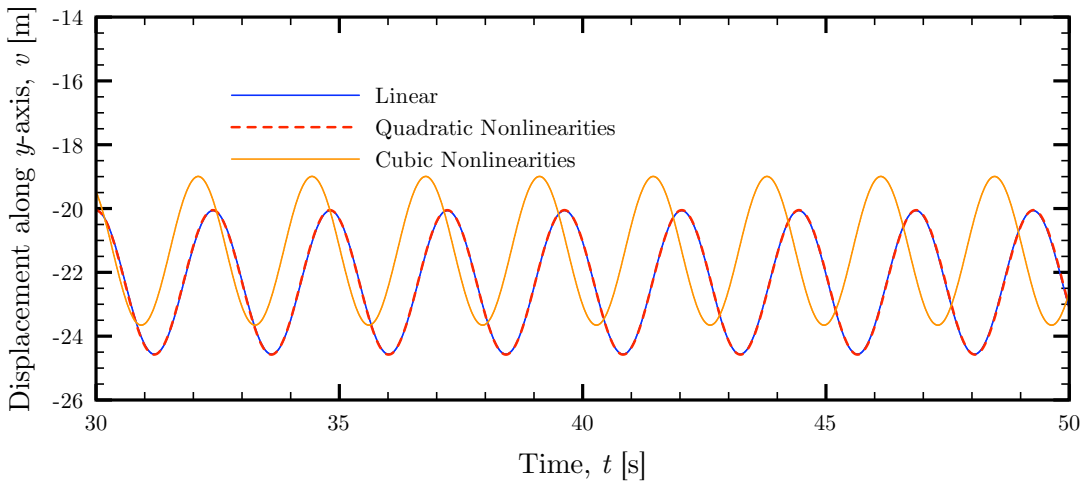

Figure 44. Detailed composite beam elastic axis displacement along y-axis at $s = L$ for first three orders of beam model.

Table XVII. Computational time for first three orders of beam model.

Beam Case	Linear	Quadratic	Cubic
Tapered	8 min	13 min	16 min
Twisted	10 min	15 min	16 min
Composite	9 min	15 min	17 min

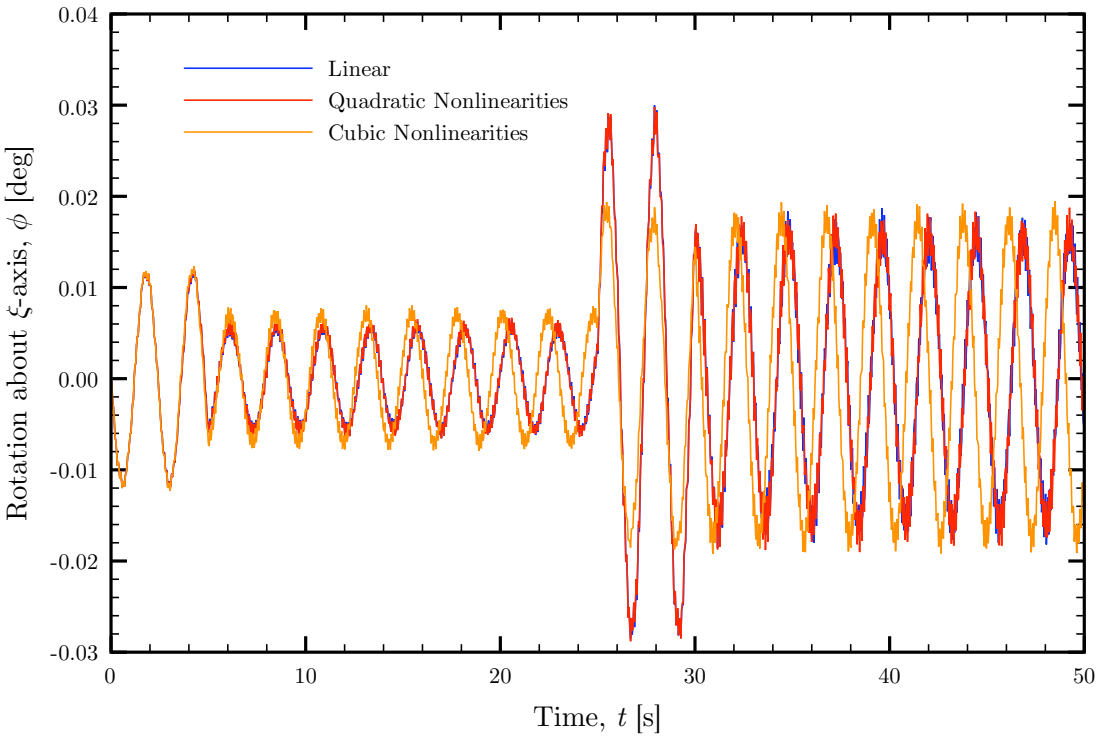

Figure 45. Composite beam rotation about ξ-axis at $s = L$ for first three orders of beam model.

B. General Transport Wing

The beam model can additionally be extended to wings that are more appropriately modeled as plates. The general transport wing, described in Edwards et al. [20], is such an example.

1. Description

The general transport wing is composed of a stepped aluminum plate, which varies in thickness from 0.701 cm at the root to 0.269 cm at the tip. The upper and lower surfaces of the plate are covered in end-grain balsa wood. The elastic axis is located at 40% of the chord aft of the leading edge. A planform view is shown in Figure 46.

2. Beam Representation

The general transport wing is modeled as a homogeneous aluminum beam with a length of 1.409 m. The unswept representation is shown in Figure 47. Due to the material homogeneity, the elastic axis and center of mass axis are collinear. The material homogeneity is not rigorously enforced, however, as the position of the elastic axis relative to the planform is maintained, and this position is not at the geometric center. Additionally, the thickness linearly tapers symmetrically about the elastic axis, varying from a thickness of 0.627 cm at the fixed end to 0.204 cm at the free end.

The remaining properties of the beam are given in Table XVIII. With the exception of the torsional stiffness, D_ξ, all of the properties are consistent with the geometry. Because of the large aspect ratio of the cross section, D_ξ is calculated by taking the product of the modulus of rigidity and the polar moment of inertia and applying a constant reduction factor to account for warping.

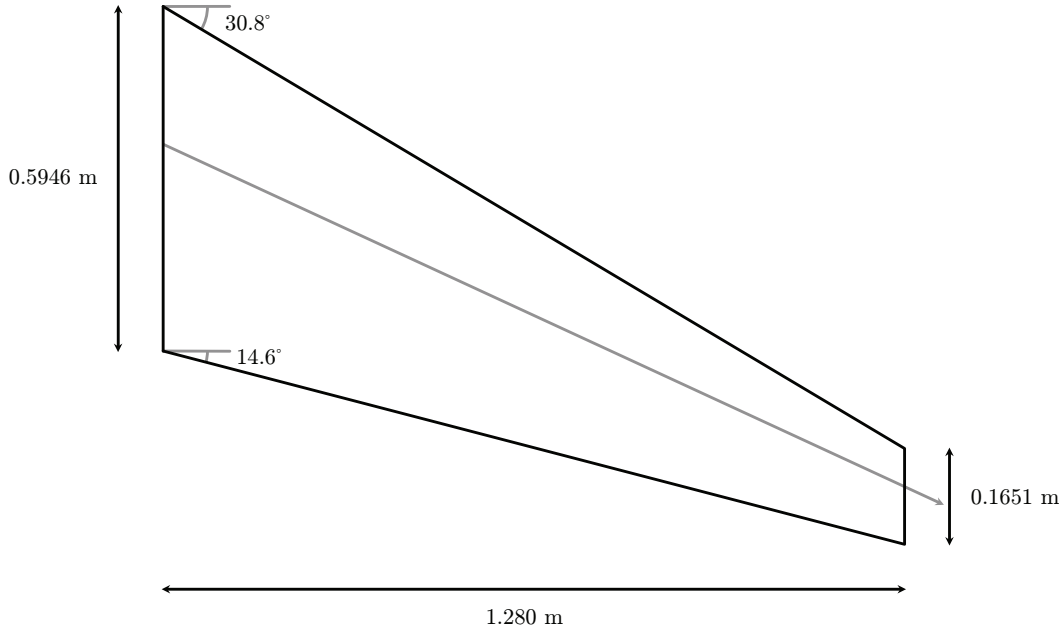

Figure 46. Planform view of general transport wing.

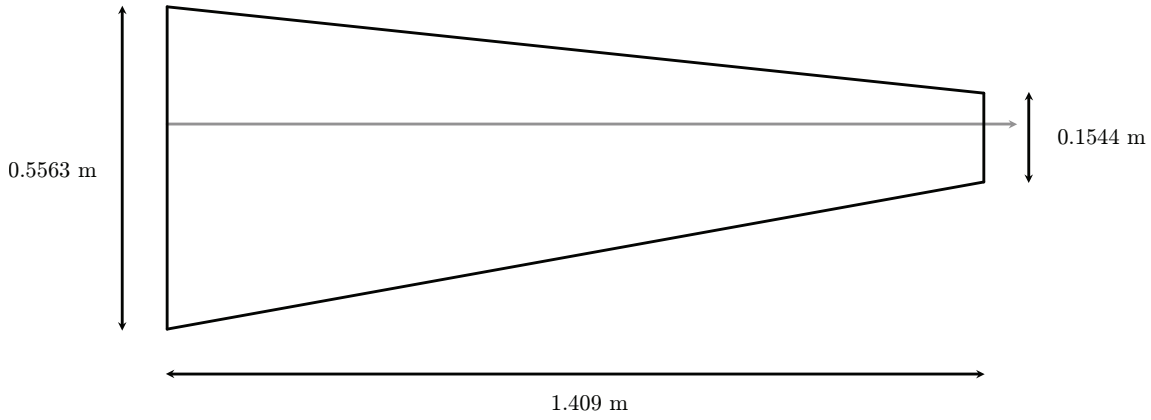

Figure 47. Unswept representation of general transport wing.

Table XVIII. Properties of general transport wing beam model.

Parameter	Value
$m(s)$	$9.4159 - 9.3305s + 2.3087s^2$ kg/m
$j_\xi(s)$	$0.29250 - 0.58964s + 0.44560s^2$
	$-0.14962s^3 + 0.018835s^4$ kg m^2/m
$j_\eta(s)$	$0.29247 - 0.58958s + 0.44556s^2$
	$-0.14961s^3 + 0.018834s^4$ kg m^2/m
$j_\zeta(s)$	$(3.0847 - 6.0086s + 4.3877s^2$
	$-1.4236s^3 + 0.17316s^4) \times 10^{-5}$ kg m^2/m
$D_\xi(s)$	$2220.0 - 4475.2s + 3382.0s^2$
	$-1135.6s^3 + 142.95s^4$ N m^2
$D_\eta(s)$	$(7.4742 - 15.067s + 11.387s^2$
	$-3.8234s^3 + 0.48128s^4) \times 10^6$ N m^2
$D_\zeta(s)$	$788.32 - 1535.5s + 1121.3s^2$
	$-363.80s^3 + 44.251s^4$ N m^2

3. Natural Frequencies

The natural frequencies of the beam model are calculated and compared with those obtained through experiment by Edwards et al. [20] at the NASA Langley Research Center. In the beam model, 3 shape functions are used for bending along the plane of the planform, 7 shape functions are used for bending out of the plane of the planform, and 5 shape functions are used for torsional motion. These frequencies are listed in Table XIX, in which B refers to out-of-plane bending and T refers to torsional motion.

Table XIX. First eight frequencies of general transport wing.

Mode	Experimental [Hz]	Beam Representation [Hz]	% Error
1 (1B)	4.072	4.074	0.0498
2 (2B)	14.043	13.953	0.643
3 (1T)	31.757	31.837	0.252
4 (3B)	32.591	32.221	1.13
5 (2T)	57.791	57.203	1.02
6 (4B)	61.887	59.438	3.96
7 (3T)	90.871	85.027	6.43
8 (5B)	97.57	97.26	0.311

The frequencies of the beam model compare favorably with those obtained through experiment, considering the large cross-sectional aspect ratio that is better addressed through a plate model.

C. Goland Wing

The Goland wing was conceived in 1945 by Martin Goland as a benchmark for flutter analysis [21]. The semi-span is 20 ft, the chord is 6 ft, and the elastic and mass axes are respectively located at 33% and 43% of the chord aft of the leading edge. The planform of the Goland wing is shown in Figure 48, and the properties are listed in Table XX. The contribution of the other mass moments of inertia are assumed negligible by Goland [21], as is the ability for the wing to bend out of the x-z plane. Therefore, only the linear contribution to the beam model is used.

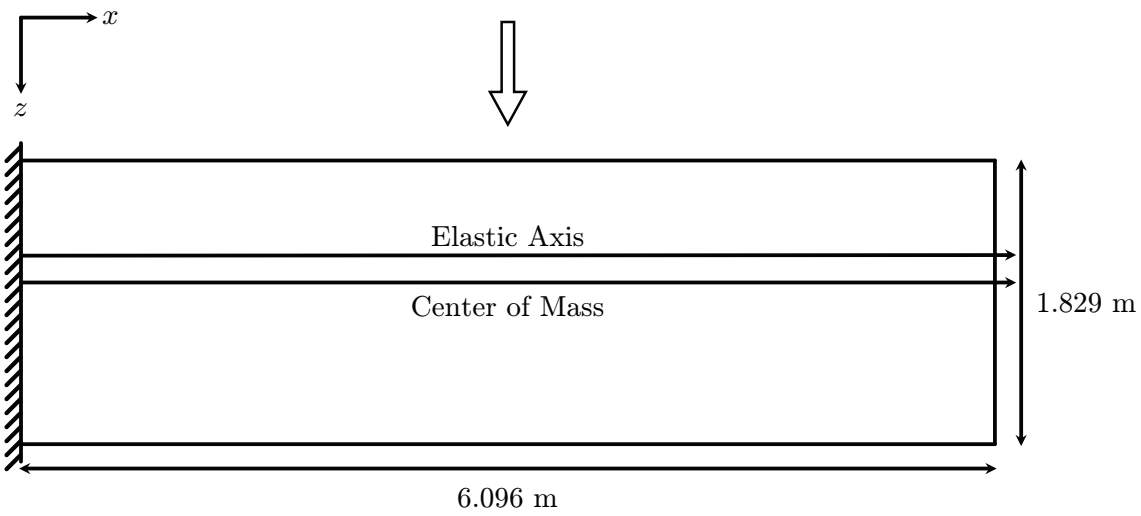

Figure 48. Planform view of Goland wing.

With these simplifying assumptions, the linear equations of motion become:

$$m\ddot{w} - me_\zeta\ddot{\phi} + D_\zeta w'''' = L_A, \tag{7.1}$$

$$j_\xi\ddot{\phi} - me_\zeta\ddot{w} - D_\xi\phi'' = M_A. \tag{7.2}$$

Table XX. Properties of Goland wing.

Parameter	Value
L	6.096 m
c	1.829 m
$e_\zeta(s)$	0.1829 m
$m(s)$	35.72 kg/m
$j_\xi(s)$	8.643 kg m^2/m
$D_\xi(s)$	9.876×10^5 N m^2
$D_\zeta(s)$	9.773×10^6 N m^2

1. Classical Flutter Analysis with Theodorsen Aerodynamics

To gain initial insight, the flutter condition is calculated using the two-degree-of-freedom flutter analysis presented in Bisplinghoff et al. [1, pp. 532-545] and Hodges and Pierce [2, pp. 124-130] that models one translational and one rotational degree of freedom for a rigid section.

The two degrees of freedom are assumed simply harmonic at the flutter condition with the same frequency, though not necessarily in phase. The determinant of the two underlying equations of motion is set to zero to ensure a nontrivial solution. The flutter speed and frequency are varied to satisfy the characteristic equation, while maintaining real values [1, pp. 532-545], [2, pp. 124-130].

Compressibility effects as well as those due to the finite length of the wing are neglected. The unsteady aerodynamic model used is that devised by Theodorsen

[22], [1, pp. 251-281]:

$$L_A = 2\pi\rho_\infty V_\infty bC(k)\left[-\dot{w} + V_\infty(\alpha+\phi) + b\left(\frac{1}{2}-a\right)\dot{\phi}\right] + \pi\rho_\infty b^2\left[-\ddot{w} + V_\infty\dot{\phi} - ba\ddot{\phi}\right], \tag{7.3}$$

$$M_A = 2\pi\rho_\infty V_\infty b^2\left(a+\frac{1}{2}\right)C(k)\left[-\dot{w} + V_\infty(\alpha+\phi) + b\left(\frac{1}{2}-a\right)\dot{\phi}\right] + \pi\rho_\infty b^2\left[-ba\ddot{w} - V_\infty b\left(\frac{1}{2}-a\right)\dot{\phi} - b^2\left(\frac{1}{8}+a^2\right)\ddot{\phi}\right]. \tag{7.4}$$

In equations (7.3) and (7.4), k is the reduced frequency, $\frac{b\omega}{V_\infty}$, b is the semichord, ab is the distance of the elastic axis aft of the semichord, and α is the angle between the freestream and the undeformed chord.

$C(k)$ is Theodorsen's function, a complex-valued function that accounts for lift deficiency and phase offset. Consequently, the terms in (7.3) and (7.4) multiplied by Theodorsen's function are the unsteady circulatory contribution, while the remaining terms are the inertial contribution of the effective mass, with the exception of the term containing the velocity, V_∞, which is circulatory [3, p. 210]. Theodorsen's function is defined by

$$C(k) = F(k) + iG(k) = \frac{H_1^{(2)}(k)}{H_1^{(2)}(k) + iH_0^{(2)}(k)}.$$

The Hankel functions of the second kind, $H_n^{(2)}$, are expressed in terms of Bessel functions of the first and second kind [1, pp. 271-272], [23, pp. 358-428]:

$$H_n^{(2)} = J_n - iY_n.$$

Theodorsen's function is plotted in Figure 49.

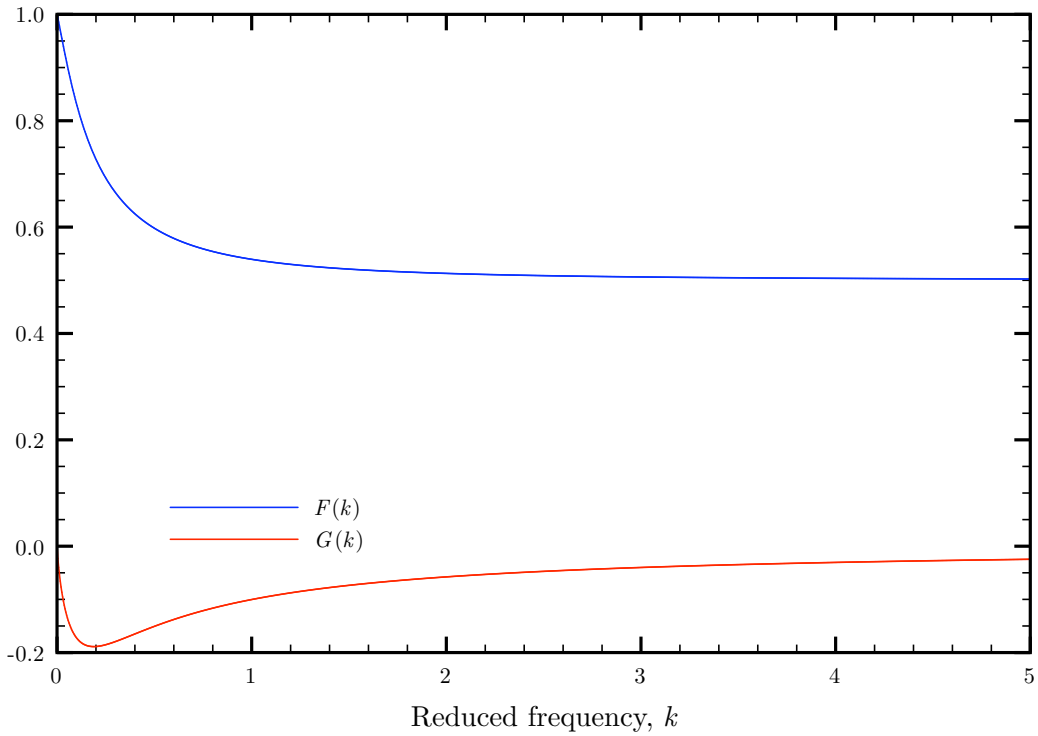

Figure 49. Theodorsen's function, $C(k) = F(k) + iG(k)$.

Classical flutter analysis yields a flutter speed of 131 m/s and a flutter frequency of 71.8 rad/s.

2. The Use of Wagner's Function

Theodorsen's function is adequate when performing analysis in the frequency domain; however, a time domain-based model for unsteady aerodynamics is required for the beam model.

The lift and moment due to an airfoil that undergoes an impulsively initiated

motion is [3, pp. 206-210]

$$\begin{aligned} L_A(t) = {} & 2\pi\rho_\infty V_\infty^2 b\alpha\Phi(\tau) \\ & + 2\pi\rho_\infty V_\infty b\int_0^t \Phi(\tau-\tau_0)\left[V_\infty\dot{\phi} - \ddot{w} + b\left(\frac{1}{2}-a\right)\ddot{\phi}\right]dt_0 \\ & + \pi\rho_\infty b^2\left[-\ddot{w} + V_\infty\dot{\phi} - ba\ddot{\phi}\right], \end{aligned}$$

$$\begin{aligned} M_A(t) = {} & 2\pi\rho_\infty V_\infty^2 b^2\left(a+\frac{1}{2}\right)\alpha\Phi(\tau) \\ & + 2\pi\rho_\infty V_\infty b^2\left(a+\frac{1}{2}\right)\int_0^t \Phi(\tau-\tau_0)\left[V_\infty\dot{\phi} - \ddot{w} + b\left(\frac{1}{2}-a\right)\ddot{\phi}\right]dt_0 \\ & + \pi\rho_\infty b^2\left[-ba\ddot{w} - V_\infty b\left(\frac{1}{2}-a\right)\dot{\phi} - b^2\left(\frac{1}{8}+a^2\right)\ddot{\phi}\right], \end{aligned}$$

where τ is the distance traveled in semichords:

$$\tau = \frac{V_\infty t}{b}.$$

$\Phi(\tau)$ is Wagner's function, for which the exact definition is

$$\Phi(\tau) = 1 - \int_0^\infty \frac{1}{\left(x^2 e^{x\tau}\left[K_0(x) - K_1(x)\right]^2 + \pi^2\left[I_0(x) + I_1(x)\right]^2\right)}dx.$$

I_n and K_n are, respectively, modified Bessel functions of the first and second kind [23, pp. 358-428]. Wagner's function is shown in Figure 50.

Jones's approximation to Wagner's function is used [3, pp. 207-208]:

$$\Phi(\tau) \approx 1 - 0.165e^{-0.041\tau} - 0.335e^{-0.32\tau}.$$

As α is assumed infinitesimal, the unsteady circulatory contribution to the force

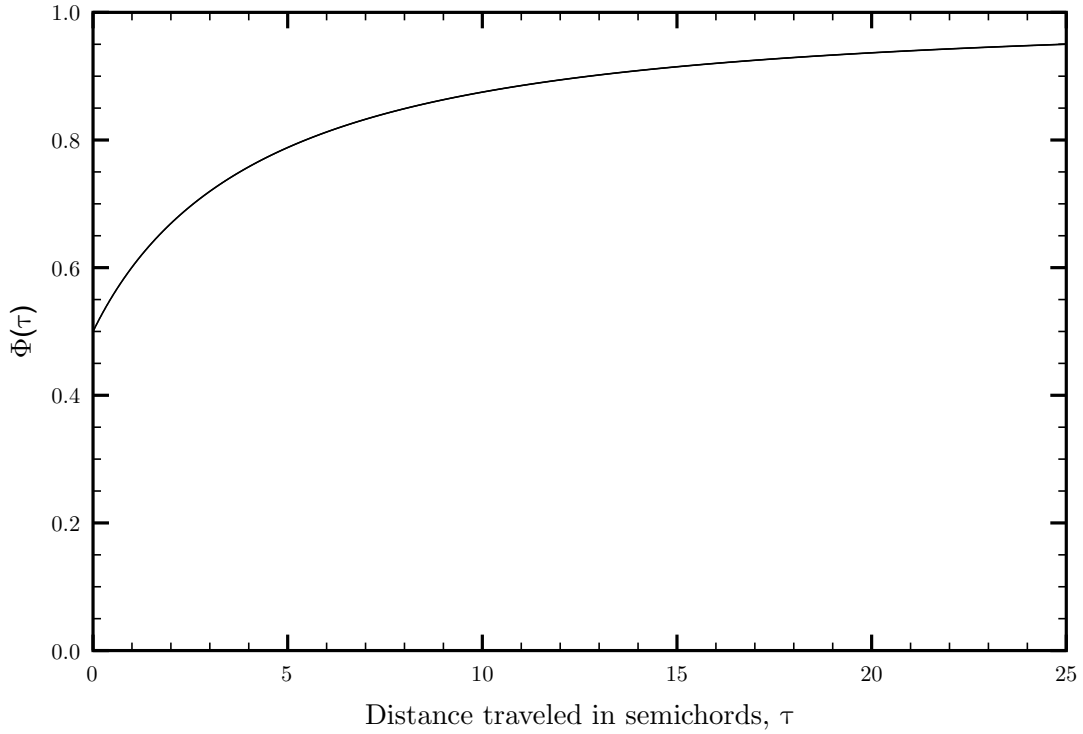

Figure 50. Wagner's function, $\Phi(\tau)$.

vector is

$$\{F_L\}_{l+i} = \int_0^L W_i L_c ds,$$
$$\{F_L\}_{l+m+i} = \int_0^L \Phi_i M_c ds,$$

or

$$\begin{aligned}\{F_L\}_{l+i} = & 2\pi\rho_\infty V_\infty^2 b\alpha \int_0^L W_i ds \\ & + 2\pi\rho_\infty V_\infty^2 b \int_0^t \Phi(\tau-\tau_0) \sum_{a=1}^{n} \dot{\phi}_a \int_0^L W_i(s)\Phi_a(s) ds\, dt_0 \\ & + 2\pi\rho_\infty V_\infty b \int_0^t \Phi(\tau-\tau_0) \sum_{a=1}^{m} \ddot{w}_a \int_0^L W_i(s) W_a(s) ds\, dt_0 \\ & + 2\pi\rho_\infty V_\infty b^2 \left(\frac{1}{2}-a\right) \int_0^t \Phi(\tau-\tau_0) \sum_{a=1}^{n} \ddot{\phi}_a \int_0^L W_i(s)\Phi_a(s) ds\, dt_0,\end{aligned}$$

$$\begin{aligned}\{F_L\}_{l+m+i} = & 2\pi\rho_\infty V_\infty^2 b^2 \left(\frac{1}{2}+a\right) \alpha \int_0^L \Phi_i ds \\ & + 2\pi\rho_\infty V_\infty^2 b^2 \left(\frac{1}{2}+a\right) \int_0^t \Phi(\tau-\tau_0) \sum_{a=1}^{n} \dot{\phi}_a \int_0^L \Phi_i(s)\Phi_a(s) ds\, dt_0 \\ & + 2\pi\rho_\infty V_\infty b^2 \left(\frac{1}{2}+a\right) \int_0^t \Phi(\tau-\tau_0) \sum_{a=1}^{m} \ddot{w}_a \int_0^L \Phi_i(s) W_a(s) ds\, dt_0 \\ & + 2\pi\rho_\infty V_\infty b^3 \left(\frac{1}{4}-a^2\right) \int_0^t \Phi(\tau-\tau_0) \sum_{a=1}^{n} \ddot{\phi}_a \int_0^L \Phi_i(s)\Phi_a(s) ds\, dt_0.\end{aligned}$$

The spatial integrals only need to be computed once. Additionally the non-circulatory, inertial contribution is distributed into a linear mass matrix, while the remaining circulatory terms are placed in a linear damping matrix. The nonzero submatrices of which are

$$\begin{aligned}[M_A]_{l+i,l+j} &= \pi\rho_\infty b^2 \int_0^L W_i W_j ds, \\ [M_A]_{l+i,l+m+j} &= \pi\rho_\infty b^3 a \int_0^L W_i \Phi_j ds, \\ [M_A]_{l+m+i,l+j} &= \pi\rho_\infty b^3 a \int_0^L \Phi_i W_j ds, \\ [M_A]_{l+m+i,l+m+j} &= \pi\rho_\infty b^4 \left(\frac{1}{8}+a^2\right) \int_0^L \Phi_i \Phi_j ds,\end{aligned}$$

and

$$[C_A]_{l+i,l+m+j} = -\pi\rho_\infty V_\infty b^2 \int_0^L W_i \Phi_j ds,$$
$$[C_A]_{l+m+i,l+m+j} = \pi\rho_\infty V_\infty b^3 \left(\frac{1}{2} - a\right) \int_0^L \Phi_i \Phi_j ds.$$

Three cases are examined using the Wagner aerodynamic model. For each of these cases, the linear beam model is used with five shape functions for each of the three independent degrees of freedom. Additionally, the angle of attack is 0.1°, the time step is 10^{-4} seconds, and 200 elements are used for discretization.

a. Limit Cycle Oscillation Case

The flutter speed and frequency are found to be 136.5 m/s and 69.4 rad/s. These are within 2% of the exact solution to (7.1) and (7.2) calculated by Goland [21, 24], using Theodorsen aerodynamics, to be 137.2 m/s and 70.7 rad/s. The transverse displacement and rotation about the elastic axis are shown in Figures 51 and 52, respectively. A phase plane plot is included in Figure 53, confirming cycler convergence with time, which increases in a clockwise manner.

b. Unstable Case

When the speed is increased beyond the flutter speed to 150 m/s, the oscillations become divergent. Figures 54 and 55 show an exponential growth in the amplitude of the oscillations, which is illustrated by the phase plane plot in Figure 56 that grows with respect to time.

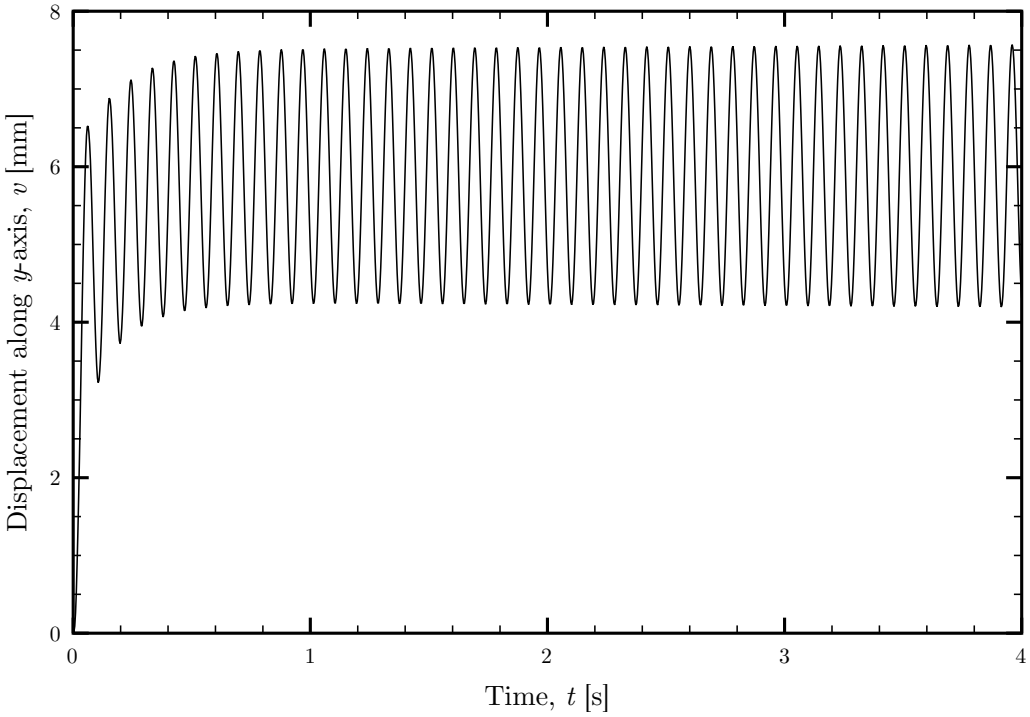

Figure 51. Goland wing elastic axis tip displacement along y-axis for $V_\infty = 136.5$ m/s.

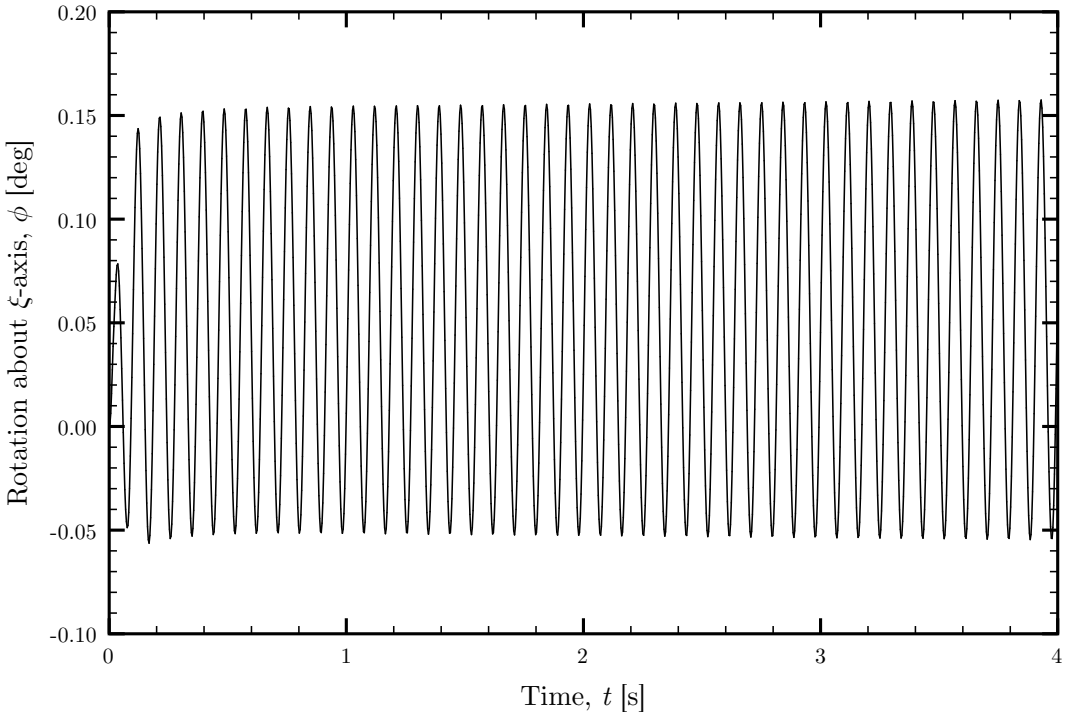

Figure 52. Goland wing rotation about ξ-axis at $s = L$ for $V_\infty = 136.5$ m/s.

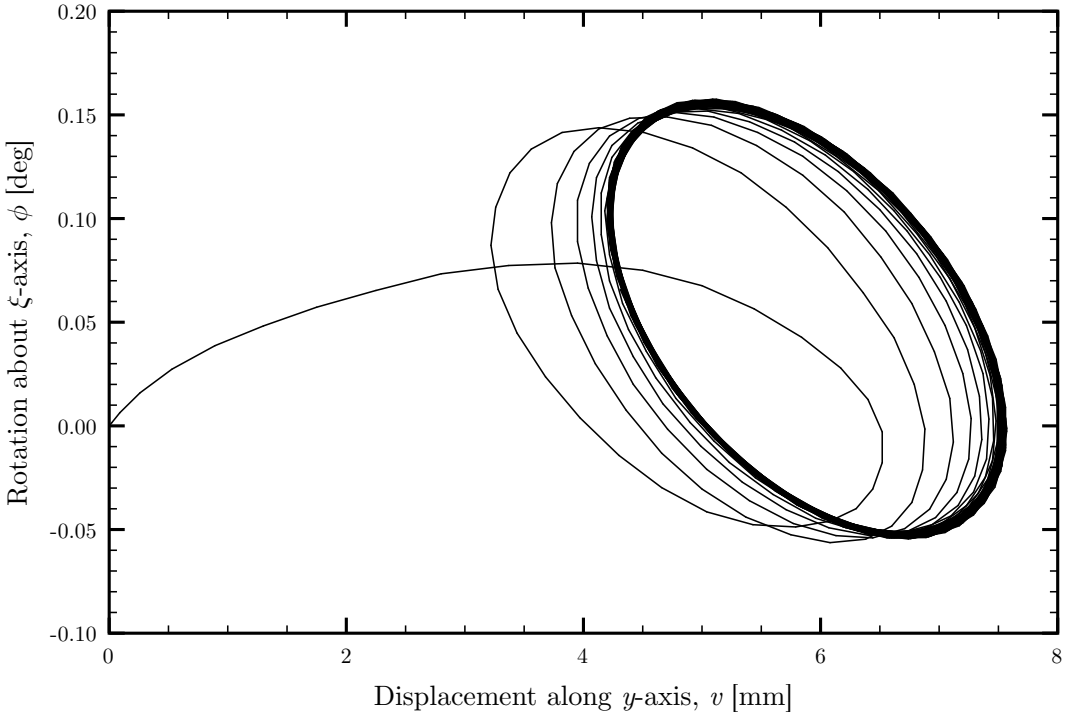

Figure 53. Goland wing phase plane plot for $V_\infty = 136.5$ m/s.

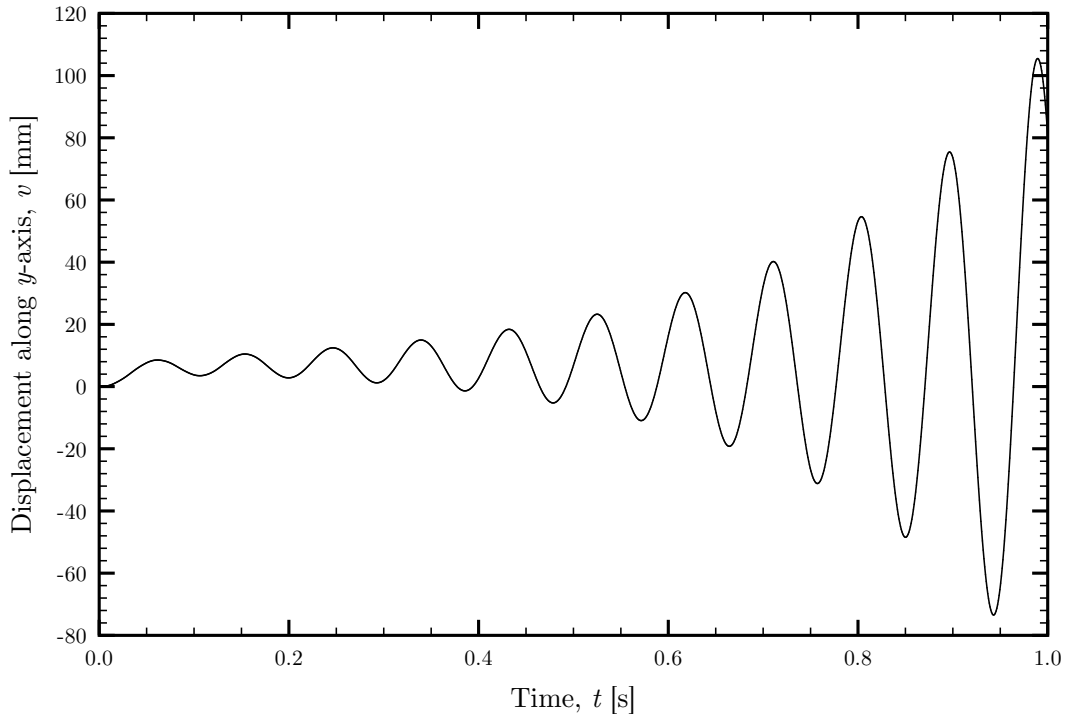

Figure 54. Goland wing elastic axis tip displacement along y-axis for $V_\infty = 150$ m/s.

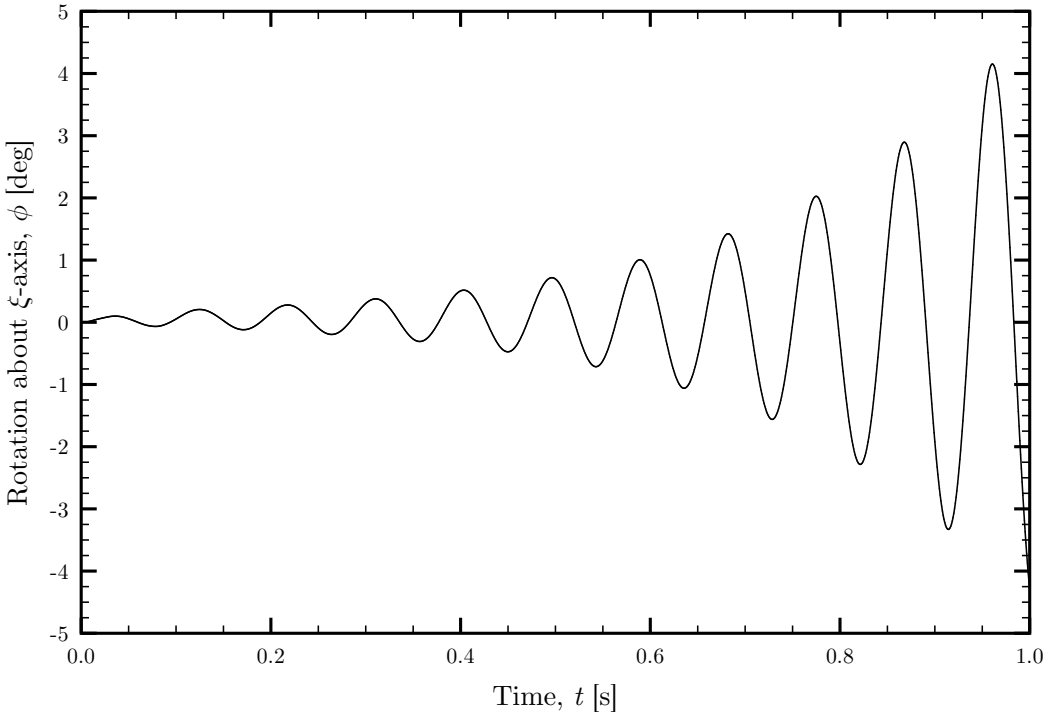

Figure 55. Goland wing rotation about ξ-axis at $s = L$ for $V_\infty = 150$ m/s.

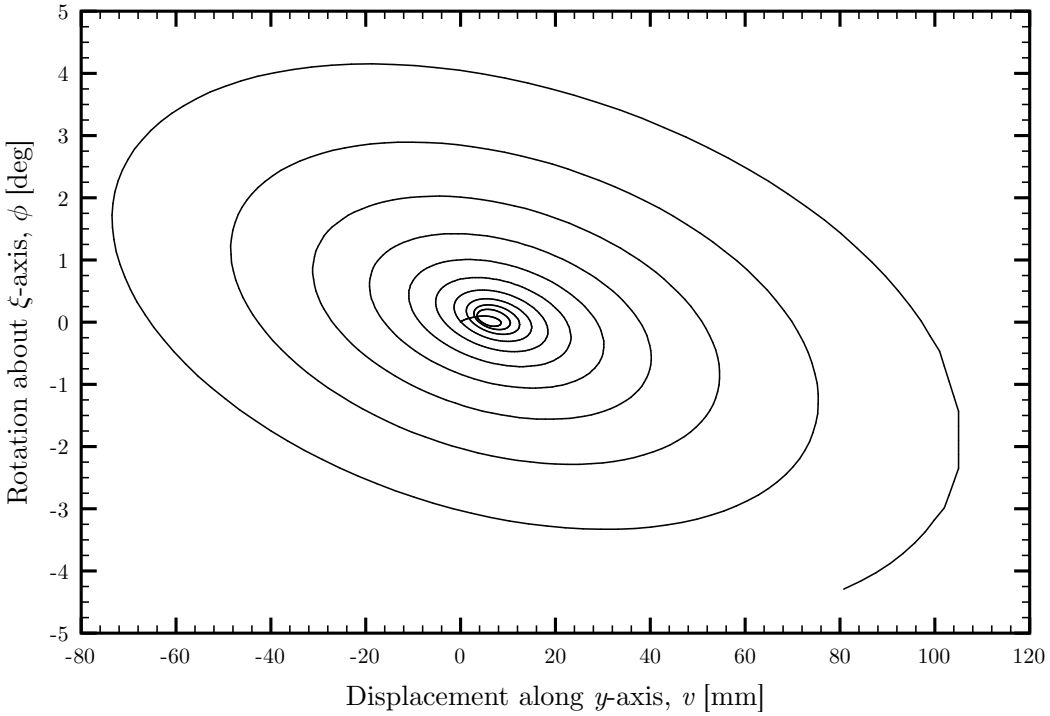

Figure 56. Goland wing phase plane plot for $V_\infty = 150$ m/s.

c. Stable Case

Below the flutter speed at 120 m/s, the oscillations dampen. Figures 57 and 58 show an exponential decay in the amplitude of the oscillations, which is confirmed by the phase plane plot in Figure 59 that converges with respect to time.

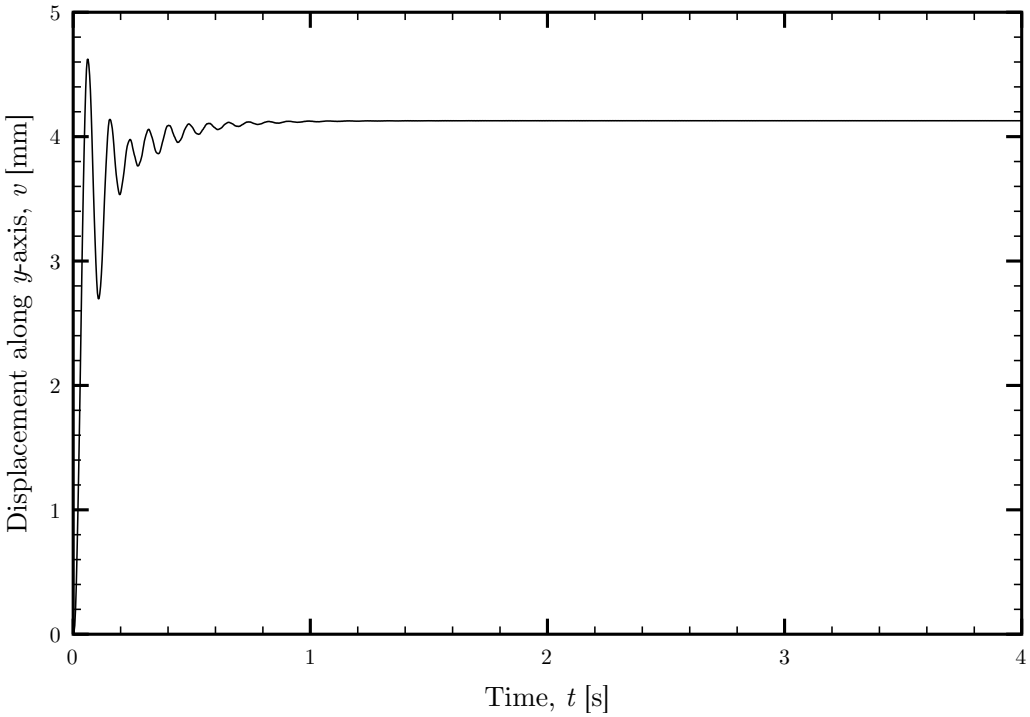

Figure 57. Goland wing elastic axis tip displacement along y-axis for $V_\infty = 120$ m/s.

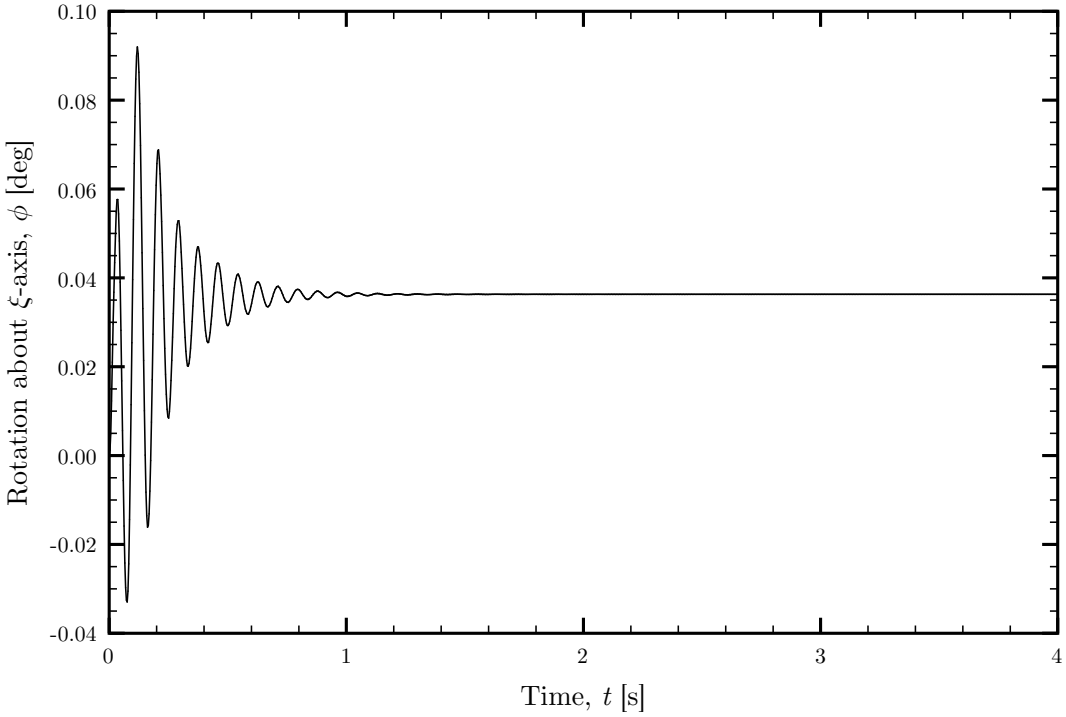

Figure 58. Goland wing rotation about ξ-axis at $s = L$ for $V_\infty = 120$ m/s.

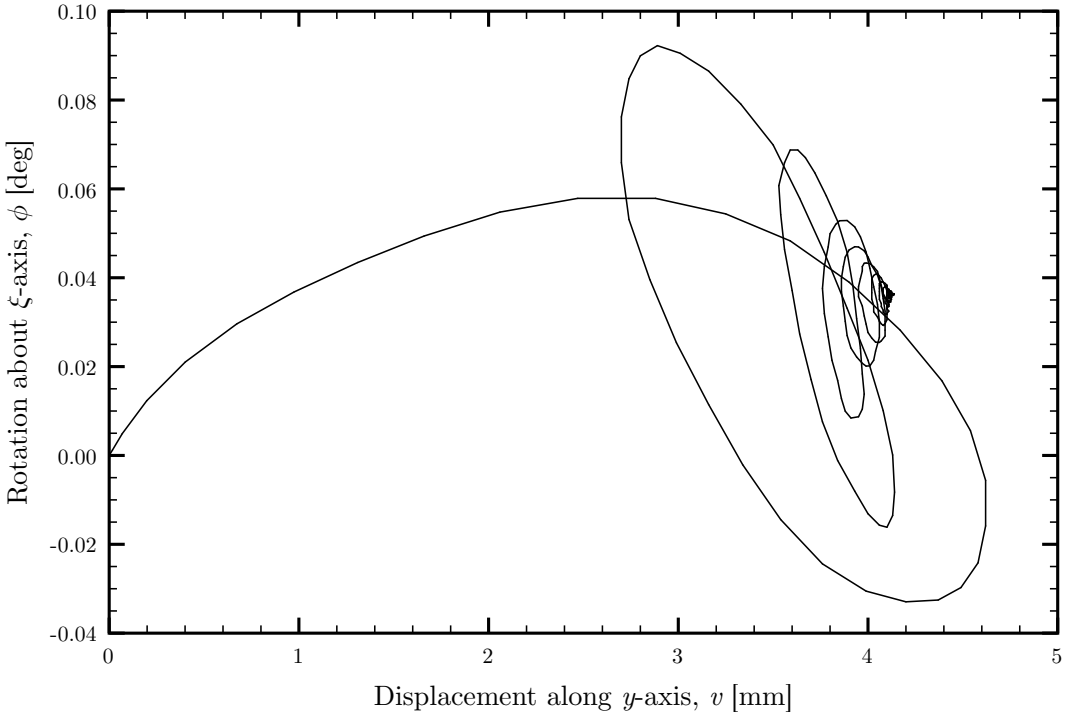

Figure 59. Goland wing phase plane plot for $V_\infty = 120$ m/s.

CHAPTER VIII

CONCLUSIONS

A. Summary

Aerospace structures with large aspect ratio, such as airplane wings, rotorcraft blades, wind turbine blades, and jet engine fan and compressor blades, are particularly susceptible to aeroelastic instabilities. Fortunately, this large aspect ratio permits these structures to be modeled accurately and efficiently as cantilevered beams.

In this thesis, the nonlinear equations of motion are derived for an inextensional, non-uniform cantilevered beam with a straight elastic axis. Along the elastic axis, the cross-sectional center of mass can be offset in both dimensions, and the principal bending and centroidal axes can each be rotated uniquely. The Galerkin method is used, permitting arbitrary and abrupt variations along the length that require no knowledge of the spatial derivatives of the beam properties. Additionally, these equations consistently retain all third-order nonlinearities that account for flexural-flexural-torsional coupling and extend the validity of the equations for large deformations.

Solution to the arising partial differential equations of motion is expedited through the use of shape functions that reduce the system to a set of ordinary differential equations in time. Fidelity is preserved by using an ample amount of shape functions to reflect the shape of the structure at any instant.

The method and implementation are validated through comparison with finite element analysis, and extension to swept wings is discussed.

Finally, a comparison is made between different orders of the beam model, ranging from linear to cubic, and aeroelastic results are shown and compared with those

in the literature.

B. Concluding Remarks

The beam model accurately calculates natural frequencies and linear and nonlinear responses that agree favorably with those obtained through finite element analysis, while taking one to two orders of magnitude less time.

When performing nonlinear beam analysis, the advantage of retaining cubic terms, in addition to quadratic terms, is clear. Generally, the quadratic model provides results similar to the linear model while requiring a disproportionate computational burden.

The beam model can be extended to swept wings; however, one must exercise discretion so as to not underestimate the effects of warping. Nonetheless, the beam model can provide efficient and reasonable results for swept wings.

The aeroelastic applications of the beam model yield a structurally efficient and accurate model in which the bulk of the cost lies in the aerodynamic computations.

REFERENCES

[1] R. L. Bisplinghoff, H. Ashley, R. L. Halfman, Aeroelasticity, Dover Publications, Inc., Mineola, NY, 1996.

[2] D. H. Hodges, G. A. Pierce, Introduction to Structural Dynamics and Aeroelasticity, Cambridge University Press, New York, 2002.

[3] Y. C. Fung, An Introduction to the Theory of Aeroelasticity, Dover Publications, Inc., Mineola, NY, 1993.

[4] M. R. M. Crespo da Silva, C. C. Glynn, Nonlinear flexural-flexural-torsional dynamics of inextensional beams. I. Equations of motion, The Journal of Structural Mechanics 6 (1978) 437–448.

[5] M. R. M. Crespo da Silva, Non-linear flexural-flexural-torsional-extensional dynamics of beams-I. Formulation, International Journal of Solids and Structures 24 (1988) 1225–1234.

[6] D. H. Hodges, E. H. Dowell, Nonlinear Equations of Motion for the Elastic Bending and Torsion of Twisted Nonuniform Rotor Blades, Technical Report NASA-TN-D-7818, National Aeronautics and Space Administration, 1974.

[7] D. H. Hodges, R. A. Ormiston, D. A. Peters, On the Nonlinear Deformation Geometry of Euler-Bernoulli Beams, Technical Report NASA TP-1566, National Aeronautics and Space Administration, 1980.

[8] T. W. Strganac, P. G. Cizmas, C. Nichkawde, J. Gargoloff, P. S. Beran, Aeroelastic analysis for future air vehicle concepts using a fully nonlinear methodology, in: 46th AIAA/ASME/ASCE/AHS/ASC Structures, Structural Dynamics and Materials Conference, Austin, Texas, 2005, pp. 1–34.

[9] K. Kim, Nonlinear Aeroelastic Analysis of Aircraft Wing-with-Store Configurations, Ph.D. thesis, Texas A&M University, 2004.

[10] R. J. Roark, W. C. Young, R. G. Budynas, Roark's Formulas for Stress and Strain, seventh edition, McGraw-Hill, Inc., New York, 2002.

[11] A. E. H. Love, A Treatise on the Mathematical Theory of Elasticity, fourth edition, Dover Publications, Inc., Mineola, NY, 1944.

[12] L. Meirovitch, Analytical Methods in Vibrations, Macmillian, New York, 1967.

[13] R. Haberman, Applied Partial Differential Equations with Fourier Series and Boundary Value Problems, fourth edition, Pearson Education, Inc., Upper Saddle River, NJ, 2004.

[14] M. R. M. Crespo da Silva, C. C. Glynn, Nonlinear flexural-flexural-torsional dynamics of inextensional beams. II. Forced motions, The Journal of Structural Mechanics 6 (1978) 449–461.

[15] C. F. Gerald, P. O. Wheatley, Applied Numerical Analysis, seventh edition, Pearson Education, Inc., Boston, MA, 2004.

[16] SIMULIA, Abaqus Version 6.7 Documentation, Providence, RI, 2009.

[17] S. S. Rao, Mechanical Vibrations, fourth edition, Pearson Education, Inc., Upper Saddle River, NJ, 2004.

[18] F. P. Beer, E. R. Johnston, Jr., J. T. DeWolf, Mechanics of Materials, fourth edition, McGraw-Hill Higher Education, Boston, MA, 2006.

[19] A. C. Ugural, S. K. Fenster, Advanced Stength and Applied Elasticity, Elsevier, New York, 1981.

[20] J. W. Edwards, C. V. Spain, D. F. Keller, R. W. Moses, Transport wing flutter model transonic limit cycle oscillation test, Journal of Aircraft 46 (2009) 1104–1113.

[21] M. Goland, The flutter of a uniform cantilever wing, Journal of Applied Mechanics 12 (1945) A197–A208.

[22] T. Theodorsen, General Theory of Aerodynamic Instability and the Mechanism of Flutter, Technical Report 496, NASA, 1934.

[23] M. Abramowitz, I. A. Stegun, Handbook of Mathematical Functions with Formulas, Graphs, and Mathematical Tables, Dover Publications, Inc., Mineola, NY, 1964.

[24] M. J. Patil, D. H. Hodges, C. E. S. Cesnik, Nonlinear aeroelastic analysis of complete aircraft in subsonic flow, Journal of Aircraft 37 (2000) 753–760.

APPENDIX A

HAMILTON'S PRINCIPLE

The extended form of Hamilton's principle is

$$\delta I = \delta \int_{t_1}^{t_2} (\mathcal{T} + \mathcal{W})\, dt = 0.$$

Noting that

$$\begin{aligned} \mathcal{L} &= \mathcal{T} - \mathcal{V}, \\ \mathcal{W} &= \mathcal{W}_c + \mathcal{W}_{nc}, \\ \delta\mathcal{V} &= -\delta\mathcal{W}_c, \end{aligned}$$

Hamilton's principle can be rewritten as [12]

$$\delta I = \delta \int_{t_1}^{t_2} (\mathcal{L} + W_{nc})\, dt = 0,$$

where

$$\delta\mathcal{W}_{nc} = \delta\mathcal{W}_B + \int_0^L (Q_u\delta u + Q_v\delta v + Q_w\delta w + Q_\phi\delta\phi)\, ds.$$

This leads to

$$\delta I = \int_{t_1}^{t_2} \left\{ \delta\mathcal{L} + \delta\mathcal{W}_B + \int_0^L (Q_u\delta u + Q_v\delta v + Q_w\delta w + Q_\phi\delta\phi)\, ds \right\} dt = 0, \qquad \text{(A.1)}$$

which, upon accounting for the inextensionality constraint, becomes

$$\begin{aligned} \delta I = \int_{t_1}^{t_2} \Bigg\{ & \int_0^L \left(\delta l + \delta \left[\frac{1}{2}\lambda \left(1 - (1+u')^2 + v'^2 + w'^2 \right) \right] \right) ds \\ & + \delta\mathcal{W}_B + \int_0^L (Q_u\delta u + Q_v\delta v + Q_w\delta w + Q_\phi\delta\phi)\, ds \Bigg\} dt = 0. \end{aligned} \qquad \text{(A.2)}$$

The variations of l, θ, and ψ are

$$\begin{aligned}
\delta l = \quad & \frac{\partial l}{\partial \dot{u}}\delta\dot{u} + \frac{\partial l}{\partial \dot{v}}\delta\dot{v} + \frac{\partial l}{\partial \dot{w}}\delta\dot{w} + \frac{\partial l}{\partial \psi}\delta\psi + \frac{\partial l}{\partial \dot{\psi}}\delta\dot{\psi} + \frac{\partial l}{\partial \psi'}\delta\psi' \\
& + \frac{\partial l}{\partial \theta}\delta\theta + \frac{\partial l}{\partial \dot{\theta}}\delta\dot{\theta} + \frac{\partial l}{\partial \theta'}\delta\theta' + \frac{\partial l}{\partial \phi}\delta\phi + \frac{\partial l}{\partial \dot{\phi}}\delta\dot{\phi} + \frac{\partial l}{\partial \phi'}\delta\phi', \\
\delta\theta = \quad & \frac{\partial \theta}{\partial u'}\delta u' + \frac{\partial \theta}{\partial v'}\delta v' + \frac{\partial \theta}{\partial w'}\delta w', \\
\delta\psi = \quad & \frac{\partial \psi}{\partial u'}\delta u' + \frac{\partial \psi}{\partial v'}\delta v'.
\end{aligned}$$

The variation of the cross-sectional Lagrangian is then written as

$$\begin{aligned}
\delta l = \quad & \frac{\partial l}{\partial \dot{u}}\delta\dot{u} + \frac{\partial l}{\partial \dot{v}}\delta\dot{v} + \frac{\partial l}{\partial \dot{w}}\delta\dot{w} + \frac{\partial l}{\partial \psi}\left(\frac{\partial \psi}{\partial u'}\delta u' + \frac{\partial \psi}{\partial v'}\delta v'\right) \\
& + \frac{\partial l}{\partial \dot{\psi}}\left(\frac{\partial^2 \psi}{\partial t \partial u'}\delta u' + \frac{\partial \psi}{\partial u'}\delta\dot{u}' + \frac{\partial^2 \psi}{\partial t \partial v'}\delta v' + \frac{\partial \psi}{\partial v'}\delta\dot{v}'\right) \\
& + \frac{\partial l}{\partial \psi'}\left(\frac{\partial^2 \psi}{\partial s \partial u'}\delta u' + \frac{\partial \psi}{\partial u'}\delta u'' + \frac{\partial^2 \psi}{\partial s \partial v'}\delta v' + \frac{\partial \psi}{\partial v'}\delta v''\right) \\
& + \frac{\partial l}{\partial \theta}\left(\frac{\partial \theta}{\partial u'}\delta u' + \frac{\partial \theta}{\partial v'}\delta v' + \frac{\partial \theta}{\partial w'}\delta w'\right)\delta\theta \\
& + \frac{\partial l}{\partial \dot{\theta}}\left(\frac{\partial^2 \theta}{\partial t \partial u'}\delta u' + \frac{\partial \theta}{\partial u'}\delta\dot{u}' + \frac{\partial^2 \theta}{\partial t \partial v'}\delta v' + \frac{\partial \theta}{\partial v'}\delta\dot{v}' + \frac{\partial^2 \theta}{\partial t \partial w'}\delta w' + \frac{\partial \theta}{\partial w'}\delta\dot{w}'\right) \\
& + \frac{\partial l}{\partial \theta'}\left(\frac{\partial^2 \theta}{\partial s \partial u'}\delta u' + \frac{\partial \theta}{\partial u'}\delta u'' + \frac{\partial^2 \theta}{\partial s \partial v'}\delta v' + \frac{\partial \theta}{\partial v'}\delta v'' + \frac{\partial^2 \theta}{\partial s \partial w'}\delta w' + \frac{\partial \theta}{\partial w'}\delta w''\right) \\
& + \frac{\partial l}{\partial \phi}\delta\phi + \frac{\partial l}{\partial \dot{\phi}}\delta\dot{\phi} + \frac{\partial l}{\partial \phi'}\delta\phi'.
\end{aligned}$$

Expanding (A.2) and performing integration by parts to express the integrand in terms of the variations δu, δv, δw, and $\delta\phi$ yields

$$
\begin{aligned}
\delta I = \int_{t_1}^{t_2}\int_0^L \Bigg\{ & \left[-\frac{\partial^2 l}{\partial s\partial\psi}\frac{\partial\psi}{\partial u'} - \frac{\partial l}{\partial\psi}\frac{\partial^2\psi}{\partial s\partial u'} + \frac{\partial^3 l}{\partial t\partial s\partial\dot{\psi}}\frac{\partial\psi}{\partial u'} + \frac{\partial^2 l}{\partial t\partial\dot{\psi}}\frac{\partial^2\psi}{\partial s\partial u'}\right]\delta u \\
& + \left[\frac{\partial^3 l}{\partial s^2\partial\psi'}\frac{\partial\psi}{\partial u'} + \frac{\partial^2 l}{\partial s\partial\psi'}\frac{\partial^2\psi}{\partial s\partial u'} - \frac{\partial^2 l}{\partial s\partial\theta}\frac{\partial\theta}{\partial u'} - \frac{\partial l}{\partial\theta}\frac{\partial^2\theta}{\partial s\partial u'}\right]\delta u \\
& + \left[\frac{\partial^3 l}{\partial t\partial s\partial\dot{\theta}}\frac{\partial\theta}{\partial u'} + \frac{\partial^2 l}{\partial t\partial\dot{\theta}}\frac{\partial^2\theta}{\partial s\partial u'} + \frac{\partial^3 l}{\partial s^2\partial\theta'}\frac{\partial\theta}{\partial u'} + \frac{\partial^2 l}{\partial s\partial\theta'}\frac{\partial^2\theta}{\partial s\partial u'}\right]\delta u \\
& + \left[-\frac{\partial^2 l}{\partial s\partial\psi}\frac{\partial\psi}{\partial v'} - \frac{\partial l}{\partial\psi}\frac{\partial^2\psi}{\partial s\partial v'} + \frac{\partial^3 l}{\partial t\partial s\partial\dot{\psi}}\frac{\partial\psi}{\partial v'} + \frac{\partial^2 l}{\partial t\partial\dot{\psi}}\frac{\partial^2\psi}{\partial s\partial v'}\right]\delta v \\
& + \left[\frac{\partial^3 l}{\partial s^2\partial\psi'}\frac{\partial\psi}{\partial v'} + \frac{\partial^2 l}{\partial s\partial\psi'}\frac{\partial^2\psi}{\partial s\partial v'} - \frac{\partial^2 l}{\partial s\partial\theta}\frac{\partial\theta}{\partial v'} - \frac{\partial l}{\partial\theta}\frac{\partial^2\theta}{\partial s\partial v'}\right]\delta v \\
& + \left[\frac{\partial^3 l}{\partial t\partial s\partial\dot{\theta}}\frac{\partial\theta}{\partial v'} + \frac{\partial^2 l}{\partial t\partial\dot{\theta}}\frac{\partial^2\theta}{\partial s\partial v'} + \frac{\partial^3 l}{\partial s^2\partial\theta'}\frac{\partial\theta}{\partial v'} + \frac{\partial^2 l}{\partial s\partial\theta'}\frac{\partial^2\theta}{\partial s\partial v'}\right]\delta v \\
& + \left[-\frac{\partial^2 l}{\partial s\partial\theta}\frac{\partial\theta}{\partial w'} - \frac{\partial l}{\partial\theta}\frac{\partial^2\theta}{\partial s\partial w'} + \frac{\partial^3 l}{\partial t\partial s\partial\dot{\theta}}\frac{\partial\theta}{\partial w'}\right]\delta w \\
& + \left[\frac{\partial^2 l}{\partial t\partial\dot{\theta}}\frac{\partial^2\theta}{\partial s\partial w'} + \frac{\partial^3 l}{\partial s^2\partial\theta'}\frac{\partial\theta}{\partial w'} + \frac{\partial^2 l}{\partial s\partial\theta'}\frac{\partial^2\theta}{\partial s\partial w'}\right]\delta w \\
& + \left[\frac{\partial l}{\partial\phi} - \frac{\partial^2 l}{\partial t\partial\dot{\phi}} - \frac{\partial^2 l}{\partial s\partial\phi'}\right]\delta\phi - \frac{\partial^2 l}{\partial t\partial\dot{u}}\delta u - \frac{\partial^2 l}{\partial t\partial\dot{v}}\delta v - \frac{\partial^2 l}{\partial t\partial\dot{w}}\delta w \\
& + \left[\lambda'\left(1+u'\right) + \lambda u''\right]\delta u + \left[\lambda' v' + \lambda v''\right]\delta v + \left[\lambda' w' + \lambda w''\right]\delta w \\
& + Q_u\delta u + Q_v\delta v + Q_w\delta w + Q_\phi\delta\phi\Bigg\}\, ds + \left[\frac{\partial l}{\partial\phi'}\delta\phi\right. \\
& - \left(\left[\frac{\partial^2 l}{\partial t\partial\dot{\psi}} + \frac{\partial^2 l}{\partial s\partial\psi'} - \frac{\partial l}{\partial\psi}\right]\frac{\partial\psi}{\partial u'} + \left[\frac{\partial^2 l}{\partial t\partial\dot{\theta}} + \frac{\partial^2 l}{\partial s\partial\theta'} - \frac{\partial l}{\partial\theta}\right]\frac{\partial\theta}{\partial u'} + \lambda\left[1+u'\right]\right)\delta u \\
& - \left(\left[\frac{\partial^2 l}{\partial t\partial\dot{\psi}} + \frac{\partial^2 l}{\partial s\partial\psi'} - \frac{\partial l}{\partial\psi}\right]\frac{\partial\psi}{\partial v'} + \left[\frac{\partial^2 l}{\partial t\partial\dot{\theta}} + \frac{\partial^2 l}{\partial s\partial\theta'} - \frac{\partial l}{\partial\theta}\right]\frac{\partial\theta}{\partial v'} + \lambda v'\right)\delta v \\
& - \left(\left[\frac{\partial^2 l}{\partial t\partial\dot{\theta}} + \frac{\partial^2 l}{\partial s\partial\theta'} - \frac{\partial l}{\partial\theta}\right]\frac{\partial\theta}{\partial w'} + \lambda w'\right)\delta w + \delta\mathcal{W}_B \\
& + \left(\frac{\partial l}{\partial\psi'}\frac{\partial\psi}{\partial v'} + \frac{\partial l}{\partial\theta'}\frac{\partial\theta}{\partial v'} - \left[\frac{\partial l}{\partial\psi'}\frac{\partial\psi}{\partial u'} + \frac{\partial l}{\partial\theta'}\frac{\partial\theta}{\partial u'}\right]\frac{v'}{1+u'}\right)\delta v' \\
& + \left.\left(\frac{\partial l}{\partial\psi'}\frac{\partial\psi}{\partial w'} + \frac{\partial l}{\partial\theta'}\frac{\partial\theta}{\partial w'} - \left[\frac{\partial l}{\partial\psi'}\frac{\partial\psi}{\partial u'} + \frac{\partial l}{\partial\theta'}\frac{\partial\theta}{\partial u'}\right]\frac{w'}{1+u'}\right)\delta w'\right]_{s=0}^{s=L} dt = 0. \qquad \text{(A.3)}
\end{aligned}
$$

Using the notation

$$A_\alpha := \frac{\partial^2 l}{\partial t \partial \dot{\alpha}} + \frac{\partial^2 l}{\partial s \partial \alpha'} - \frac{\partial l}{\partial \alpha} \quad (\alpha = \psi, \theta, \phi),$$

$$H_\alpha := \frac{\partial l}{\partial \psi'}\frac{\partial \psi}{\partial \alpha'} + \frac{\partial l}{\partial \theta'}\frac{\partial \theta}{\partial \alpha'} \qquad (\alpha = u, v, w),$$

(A.3) can be written as

$$\begin{aligned}
\delta I = \int_{t_1}^{t_2}\int_0^L \Bigg\{ & \left[A_\psi \frac{\partial \psi}{\partial u'} + A_\theta \frac{\partial \theta}{\partial u'} + \lambda\left(1+u'\right)\right]' \delta u + \left[A_\psi \frac{\partial \psi}{\partial v'} + A_\theta \frac{\partial \theta}{\partial v'} + \lambda v'\right]' \delta v \\
& + \left[A_\theta \frac{\partial \theta}{\partial w'} + \lambda w'\right]' \delta w - A_\phi \delta\phi - \frac{\partial^2 l}{\partial t \partial \dot{u}}\delta u - \frac{\partial^2 l}{\partial t \partial \dot{v}}\delta v - \frac{\partial^2 l}{\partial t \partial \dot{w}}\delta w \\
& + Q_u \delta u + Q_v \delta v + Q_w \delta w + Q_\phi \delta\phi \Bigg\} ds \\
& + \left[\frac{\partial l}{\partial \phi'}\delta\phi - \left(A_\psi \frac{\partial \psi}{\partial u'} + A_\theta \frac{\partial \theta}{\partial u'} + \lambda\left[1+u'\right]\right)\delta u - \left(A_\psi \frac{\partial \psi}{\partial v'} + A_\theta \frac{\partial \theta}{\partial v'} + \lambda v'\right)\delta v \right. \\
& - \left(A_\theta \frac{\partial \theta}{\partial w'} + \lambda w'\right)\delta w + \delta \mathcal{W}_B + \left(H_v - H_u \frac{v'}{1+u'}\right)\delta v' \\
& \left. + \left(H_w - H_u \frac{w'}{1+u'}\right)\delta w' \right]_{s=0}^{s=L} dt = 0. \qquad \text{(A.4)}
\end{aligned}$$

Equation (A.4) must remain valid for arbitrary values of t_1 and t_2, requiring that

$$\begin{aligned}
\left[A_\psi \frac{\partial \psi}{\partial u'} + A_\theta \frac{\partial \theta}{\partial u'} + \lambda\left(1+u'\right)\right]' &= \frac{\partial^2 l}{\partial t \partial \dot{u}} - Q_u, \\
\left[A_\psi \frac{\partial \psi}{\partial v'} + A_\theta \frac{\partial \theta}{\partial v'} + \lambda v'\right]' &= \frac{\partial^2 l}{\partial t \partial \dot{v}} - Q_v, \\
\left[A_\theta \frac{\partial \theta}{\partial w'} + \lambda w'\right]' &= \frac{\partial^2 l}{\partial t \partial \dot{w}} - Q_w, \\
A_\phi &= Q_\phi.
\end{aligned}$$

These are the equations of motion.

APPENDIX B

TAYLOR SERIES EXPANSIONS

In the following approximations, the inextensionality constraint (2.7) is used to express u' in terms of v' and w', and the result is approximated through a Taylor series expansion.

$$\psi = \tan^{-1}\frac{v'}{1+u'} = \tan^{-1}\frac{v'}{\sqrt{1-v'^2-w'^2}} \approx v'\left(1+\frac{v'^2}{6}+\frac{w'^2}{2}\right)$$

$$\frac{\partial\psi}{\partial u'} = \frac{\partial}{\partial u'}\tan^{-1}\frac{v'}{1+u'} = \frac{-v'}{(1+u')^2+v'^2} = \frac{-v'}{1-w'^2} \approx -v'$$

$$\frac{\partial\psi}{\partial v'} = \frac{\partial}{\partial v'}\tan^{-1}\frac{v'}{1+u'} = \frac{(1+u')}{(1+u')^2+v'^2} = \frac{\sqrt{1-v'^2-w'^2}}{1-w'^2} \approx 1-\frac{v'^2}{2}+\frac{w'^2}{2}$$

$$\theta = \tan^{-1}\frac{-w'}{\sqrt{(1+u')^2+v'^2}} = \tan^{-1}\frac{-w'}{\sqrt{1-w'^2}} \approx -w'\left(1+\frac{w'^2}{6}\right)$$

$$\frac{\partial\theta}{\partial u'} = \frac{\partial}{\partial u'}\tan^{-1}\frac{-w'}{\sqrt{(1+u')^2+v'^2}} = \frac{w'(1+u')}{\sqrt{(1+u')^2+v'^2}} = \frac{w'\sqrt{1-v'^2-w'^2}}{\sqrt{1-w'^2}} \approx w'$$

$$\frac{\partial\theta}{\partial v'} = \frac{\partial}{\partial v'}\tan^{-1}\frac{-w'}{\sqrt{(1+u')^2+v'^2}} = \frac{v'w'}{\sqrt{(1+u')^2+v'^2}} = \frac{v'w'}{\sqrt{1-w'^2}} \approx v'w'$$

$$\frac{\partial\theta}{\partial w'} = \frac{\partial}{\partial w'}\tan^{-1}\frac{-w'}{\sqrt{(1+u')^2+v'^2}} = -\sqrt{(1+u')^2+v'^2} = -\sqrt{1-w'^2} \approx -1+\frac{w'^2}{2}$$

$$u' = \sqrt{1-v'^2-w'^2}-1 \approx -\frac{1}{2}\left(v'^2+w'^2\right)$$

$$u \approx -\frac{1}{2}\int_0^s \left(v'^2+w'^2\right)d\hat{s}$$

VITA

Brian Andrew Freno was born in San Diego, California. He completed his Bachelor of Science degree in Aerospace Engineering at Texas A&M University in 2008 with a minor in Mathematics. Subsequently, Brian remained at Texas A&M University, where he earned his Master of Science degree in Aerospace Engineering in 2010.

While an undergraduate, Brian spent two summers interning in the Aerodynamics Department at Lockheed Martin Missiles and Fire Control in Orlando, Florida. Prior to his internships at Lockheed Martin, he spent two summers interning at Standard Aero in San Antonio, Texas.

Brian's e-mail address is brianfreno@gmail.com, and his address is

Texas A&M University

Department of Aerospace Engineering

H.R. Bright Building, Ross Street - TAMU 3141

College Station, TX 77843-3141